Journal of Natural Gas Science and Engineering 3 (2011) 423–459

Contents lists available at ScienceDirect

Journal of Natural Gas Science and Engineering

journal homepage: www.elsevier.com/locate/jngse

Invited Review

Natural gas to synthesis gas – Catalysts and catalytic processes

K. Aasberg-Petersen, I. Dybkjær*, C.V. Ovesen, N.C. Schjødt, J. Sehested, S.G. Thomsen

Haldor Topsøe A/S, Nymøllevej 55, 2800 Lyngby, Denmark

ARTICLE INFO

Article history:
Received 9 February 2011
Received in revised form
25 March 2011
Accepted 28 March 2011

Keywords:
Natural gas
Synthesis gas
Catalysts
Steam reforming
Oxidative reforming
Autothermal reforming
Shift conversion

ABSTRACT

Natural gas is a dominating feedstock for the production of several bulk chemicals such as ammonia, methanol, and dimethyl ether (DME), and for the increasingly important production of synthetic liquid fuels by Fischer–Tropsch synthesis (FT synthesis) and similar processes.

A major step in the conversion of natural gas to products is the production of synthesis gas with the desired composition – ranging from the 3:1 mixture of hydrogen and nitrogen used for production of ammonia to the 1:1 mixture of hydrogen and carbon monoxide preferred for production of DME.

Catalysts and catalytic processes are important in the production of synthesis gas from natural gas. As an example, production of ammonia synthesis gas may in modern plants involve up to 8 separate catalytic process steps.

In the article, relevant catalytic technologies are reviewed with emphasis on the present status and possible future developments. The relevant technologies are:

- Final feed gas purification
- Adiabatic prereforming
- Fired tubular reforming
- Heat exchange steam reforming
- Adiabatic, oxidative reforming, mainly autothermal reforming (ATR) and secondary reforming
- Other reforming technologies such as Catalytic Partial Oxidation (CPO) and Ceramic Membrane Reforming (CMR).
- Conversion of carbon monoxide to carbon dioxide by the shift reaction
- Final purification of synthesis gas, mainly removal of nitrogen compounds and removal of carbon oxides by methanation.

After the discussion of the individual catalysts and catalytic process steps, applications are illustrated by summary descriptions of complete process concepts for production of ammonia, methanol, and hydrocarbons by low temperature FT synthesis (GTL). In a final section, future trends in the area are briefly discussed.

© 2011 Published by Elsevier B.V.

1. Introduction

Natural gas is an important ingredient in the global energy pool (Economides, 2009), not the least for power production. However, natural gas is also a dominating feedstock for the production of several bulk chemicals such as ammonia, methanol, and dimethyl ether (DME), and for the increasingly important production of synthetic liquid fuels by Fischer–Tropsch synthesis (FT synthesis) and similar processes. Recent developments in the natural gas market, such as production from unconventional sources like coal bed methane and shale gas (NaturalGas) and in the longer time frame probably also gas hydrates (Makogon, 2010), serve to maintain the importance of natural gas also in the future.

A major step in the conversion of natural gas to products is the production of synthesis gas with the desired composition – ranging from the 3:1 mixture of hydrogen and nitrogen used for production of ammonia to the 1:1 mixture of hydrogen and carbon monoxide preferred for production of dimethyl ether. Catalysts and catalytic

* Corresponding author. Tel.: +45 45272329.
E-mail address: id@topsoe.dk (I. Dybkjær).

1875-5100/$ – see front matter © 2011 Published by Elsevier B.V.
doi:10.1016/j.jngse.2011.03.004

processes are important in the production of synthesis gas from natural gas. As an example, production of ammonia synthesis gas may in modern plants involve up to 8 separate catalytic process steps. The processes have all been known and applied in industry for decades. However, continued research and development efforts applying more and more sophisticated tools, see e.g. Knözinger et al., 2008; Clausen et al., 2006; Nørskov et al., 2009; Creemer et al., 2005; Molenbroek et al., 2009, have resulted in improved catalysts and processes, leading to improved overall efficiency and environmental performance, and there are no signs that this will not continue in the future.

In the following, relevant catalytic technologies will be reviewed with emphasis on the present status and possible future developments. The technologies to be discussed are:

- Final feed gas purification
- Adiabatic prereforming
- Fired tubular reforming
- Heat exchange steam reforming
- Adiabatic, oxidative reforming, mainly autothermal reforming (ATR) and secondary reforming
- Other reforming technologies such as Catalytic Partial Oxidation (CPO) and Ceramic Membrane Reforming (CMR).
- Conversion of carbon monoxide to carbon dioxide by the shift reaction
- Final purification of synthesis gas, mainly removal of carbon oxides by methanation and removal of nitrogen compounds.

An impressive amount of literature is available on these technologies. Examples discussing several different concepts and containing further references may be found in (Rostrup-Nielsen, 1994; Dybkjær, 1995a,b, 2003; Madsen, 1998; Aasberg-Petersen et al., 2001, 2004; Rostrup-Nielsen, 2002; Nitrogen, 2003; Dybkjær et al., 2006).

After the discussion of the individual catalysts and catalytic process steps, the applications will be illustrated by summary descriptions of complete process concepts for production of synthesis gas for production of ammonia, methanol, and hydrocarbons by low temperature FT synthesis (GTL).

2. Final feed gas purification

2.1. Feed gas characteristics and purification requirements

Examples of feed gas specifications for natural gas based synthesis gas units are shown in Table 1.

The most important impurities to be considered in the feedstock purification unit are H_2S and other sulphur compounds, since these compounds are poisons for downstream catalysts. Other impurities, e.g. solids, moisture, and certain trace components such as As and Hg may be present in the raw feedstock. Removal of such impurities is considered outside the scope of this paper. N_2 and CO_2 are often present in minor quantity. N_2 will be an inert with no detrimental effects other than the resulting dilution of the synthesis gas. However, trace amounts of N compounds such as NH_3 and HCN may be formed in the reactors in the synthesis gas preparation section and may have to be removed from the synthesis gas before it is passed to the synthesis section. The effects of CO_2 may be significant and must be taken into account as described in the following paragraphs. Oxygenates may also be present in the feed, e.g. methanol added to the natural gas to avoid hydrate formation. Oxygenates may also be present in recycle gases originating from other sections of the plant.

There is no general value for the desirable concentration of sulphur compounds in the purified gas. However, for certain types of downstream catalysts, both in the synthesis gas preparation section and in the synthesis section, very low concentrations, preferably single digit ppb, are desirable to ensure an acceptable lifetime.

The main challenge in final feed gas purification for use as feed for synthesis gas production is thus to remove essentially all sulphur compounds – type and concentration uncertain and variable – to a concentration preferably below the detection limit of a few ppb.

Table 1
Typical feed gas specifications.

	Natural gas		Associated gas	
	Lean	Heavy	Lean	Heavy
N_2, vol%	3.97	3.66	0.83	0.79
CO_2, vol%	–	–	1.61	1.50
CH_4, vol%	95.70	87.86	89.64	84.84
C_2H_6, vol%	0.33	5.26	7.27	6.64
C_{3+}, vol%	–	3.22	0.65	6.23
Max. total S, vol ppm	20	20	4	4
Hydrogen sulphide, vol ppm (typical)	4	4	3	3
COS, vol ppm (typical)	2	2	n.a.	n.a.
Mercaptans, vol ppm (typical)	14	14	1	1

2.2. Principles of gas desulphurisation

The typical process concept for desulphurisation of natural gas and similar feedstock is a two-step process based on hydrogenation of organic sulphur compounds (HDS) and subsequent adsorption/absorption of H_2S. This process concept has been used industrially for decades and is well documented in the literature, see e.g. Philipson, 1970; Carnell, 1989; Nitrogen, 1971; Hidalgo-Vivas and Cooper, 2003, which gives a description of technologies for sulphur removal from different raw materials including both natural gas and heavier hydrocarbon streams.

A typical layout for desulphurisation of natural gas is shown in Fig. 1.

The feedstock is mixed with a small amount of hydrogen or hydrogen-rich gas, preheated to 350–400 °C, and passed to a first reactor containing a hydrogenation catalyst, typically based on cobalt and molybdenum (CoMo) or nickel and molybdenum (NiMo). After the hydrogenation reactor the gas passes to two sulphur absorbers in series, both typically containing zinc oxide (ZnO), which absorbs the H_2S formed in the hydrogenation reactor.

2.3. Reactions in the hydrogenator

The conversion of organic S-compounds over the hydrogenation catalyst depends on hydrogenolysis (addition of hydrogen over the S–C bond) by reactions such as:

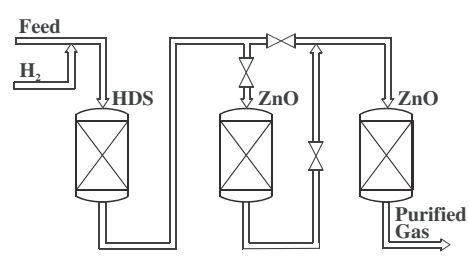

Fig. 1. Typical process flow diagram for desulphurisation of natural gas.

$$R\text{-}SH + H_2 = RH + H_2S \quad (1)$$

$$R\text{-}S\text{-}R_1 + 2H_2 = RH + R_1H + H_2S \quad (2)$$

$$R\text{-}S\text{-}S\text{-}R_1 + 3H_2 = RH + R_1H + 2H_2S \quad (3)$$

$$C_4H_8S\ (\text{tetrahydrothiophene}) + 2H_2 = C_4H_{10} + H_2S \quad (4)$$

$$C_4H_4S\ (\text{thiophene}) + 4H_2 = C_4H_{10} + H_2S \quad (5)$$

All these reactions have very large equilibrium constants in the temperature range relevant for desulphurisation reactors (Nitrogen, 1971). This means that full conversion is achievable for all types of organic sulphur compounds, if sufficient H_2 is present. If no or too little H_2 is present, the sulphur compounds may react by thermal decomposition forming olefins and H_2S. For some compounds this may happen at temperatures prevailing in the preheaters upstream of the hydrogenation reactor. This is undesirable, and H_2 should therefore preferably be added before preheating. If the temperature is too low, the rate of conversion of the organic sulphur compounds may be too low, and some mercaptans or sulphides may pass unconverted through the hydrogenator. At sufficiently high temperature, practically complete conversion to H_2S (and COS) will be ensured.

Oxygenates such as methanol may react with H_2S in the hydrogenator to form organic S-compounds such as mercaptans and sulphides:

$$CH_3OH + H_2S = CH_3SH + H_2O \quad (6)$$

$$2CH_3SH = (CH_3)_2S + H_2S \quad (7)$$

Carbon oxides and carbonyl sulphide (COS) interact with H_2 and steam according to the following reactions:

$$COS + H_2O = CO_2 + H_2S \quad (8)$$

$$CO + H_2O = CO_2 + H_2 \quad (9)$$

Both these reactions will generally be at equilibrium after the hydrogenator. The equilibrium constants are shown in Fig. 2.

In total a potentially rather complicated situation exists. However, as indicated above it may be expected that all the reactions (1)–(9) are active in the hydrogenator and reach a close approach to equilibrium. Calculations show that if this is the case, then the concentration of organic sulphur compounds other than COS will be below 1 ppb at all temperatures below about 450 °C. The equilibrium concentration of COS may be quite high, especially at high temperature and high CO_2 concentration.

2.4. Hydrogenation catalysts

The catalysts used for hydrogenolysis of the organic sulphur compounds are based on either cobalt molybdate (CoMo) or nickel molybdate (NiMo). The catalysts are prepared by impregnation on high-surface-area carriers, usually alumina.

The active phase in the operating catalyst is the so-called Co–Mo–S or Ni–Mo–S phase. The Co–Mo–S phase – and the corresponding Ni–Mo–S phase – is not a well-defined compound. Rather "it should be regarded as a family of structures with a wide range of Co concentrations, ranging from pure MoS_2 up to essentially full coverage of the MoS_2 edges by Co" (cited from p.32 in Topsøe et al. (1996), an authoritative review of hydrotreating catalysts and catalysis).

The hydrogenation catalysts are manufactured and supplied normally in the oxide state and must be converted to the sulphided state to gain full activity. This sulphidation will normally take place by exposing the catalyst as delivered to the normal operating conditions in the plant, i.e. the sulphur for the sulphidation is supplied by the feed and at the concentration at which it is available.

2.5. Reactions in the sulphur absorber

After the hydrogenation reactor the gas will, as explained above, mainly contain sulphur in the form of H_2S. If CO_2 is present in the hydrocarbon feed, significant amounts (several hundred ppb) of COS may also be present.

In the absorption vessel, H_2S reacts with ZnO according to:

$$ZnO + H_2S = ZnS + H_2O \quad (10)$$

The equilibrium constant for this reaction is shown in Fig. 3.

In addition to the bulk phase reaction with H_2S the ZnO also has some activity for reaction (8), COS hydrolysis, and for reaction (9),

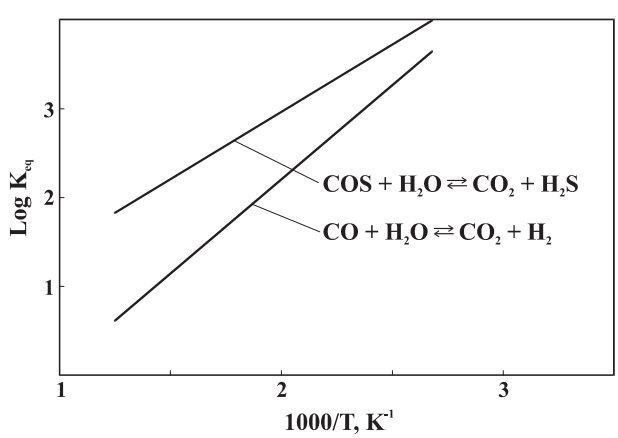

Fig. 2. Equilibrium constants for COS hydrolysis and the shift reaction.

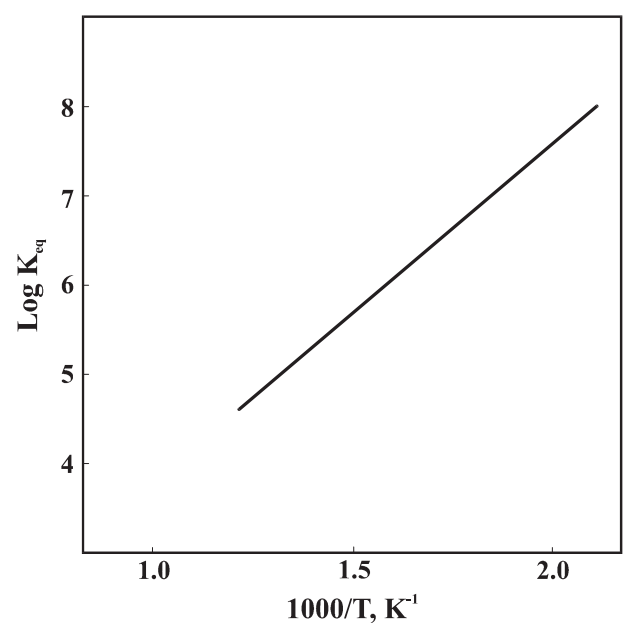

Fig. 3. Equilibrium constant for reaction (10) (Aasberg-Petersen et al., 2004).

the shift reaction. Absorption of H_2S will cause the COS hydrolysis (8) to proceed to full conversion, and COS will thus be completely removed by ZnO operating at the proper temperature. Finally, a certain capacity for chemisorption of H_2S must be taken into account when considering the performance of ZnO in the absorption vessel.

If the feedstock contains carbon dioxide, the reverse of the shift reaction (9) will cause the steam content in the gas to increase. The increased steam content will have an impact on the equilibrium for absorption of H_2S on the ZnO, reaction (10). Fig. 4 shows, as an example, the equilibrium content of H_2S as a function of temperature over ZnO at a CO_2 content in the feedstock of 5% and varying H_2 concentration.

Fig. 5 shows, for the case with 3% H_2 in the feed, the concentrations of CO, CO_2 and H_2 in the equilibrated gas. It is seen that significant amounts of CO may be formed. The possible formation of carbon in downstream equipment due to this presence of CO must be taken into account in the design (Richardson and Drucker, 1998).

From the above it is obvious that there are two ways to reduce the equilibrium level of H_2S and CO over ZnO in cases where CO_2 is present in the feed:

- by reducing the temperature in the HDS section
- by reducing the H_2 recycle

It is noted that the temperature has a greater impact on the equilibrium sulphur content on ZnO than the amount of hydrogen recycle.

However, as previously discussed, both the hydrogen recycle and the temperature play a vital role with regard to the performance of the HDS section. If the hydrogen recycle is reduced, the reaction rate on the hydrogenation catalyst is decreased, and there is a risk that organic sulphur starts to leak. If the temperature is decreased, the hydrogenation reaction rate is again reduced, and the sulphur absorption efficiency of the ZnO becomes lower.

The sulphur uptake in a zinc oxide reactor ideally consists of various zones as illustrated in Fig. 6.

Fig. 6 shows the situation at one particular time. The fronts will gradually move through the ZnO bed towards the outlet, and eventually breakthrough will occur.

Five distinct zones may be identified:

- Zone 1: Bulk saturated. The zinc oxide in this zone is fully saturated with sulphur. The gas phase concentration is constant and equal to the feed gas concentration.
- Zone 2: The bulk absorption front. The zinc oxide has capacity for absorbing the sulphur. The sulphur is transported through the catalyst pellets by means of solid diffusion and pore diffusion until full saturation is achieved. The gas phase concentration drops to the bulk equilibrium level as determined by reaction (10), as described above.

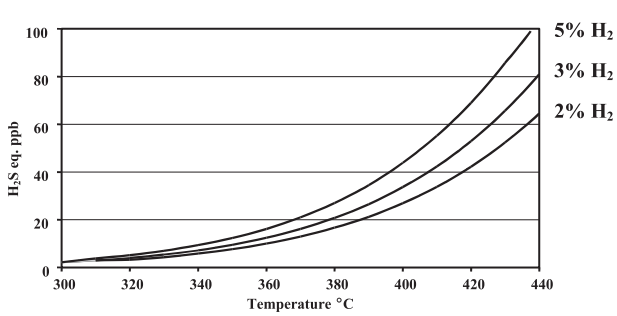

Fig. 4. Equilibrium H_2S, 5% CO_2 in natural gas (Aasberg-Petersen et al., 2004).

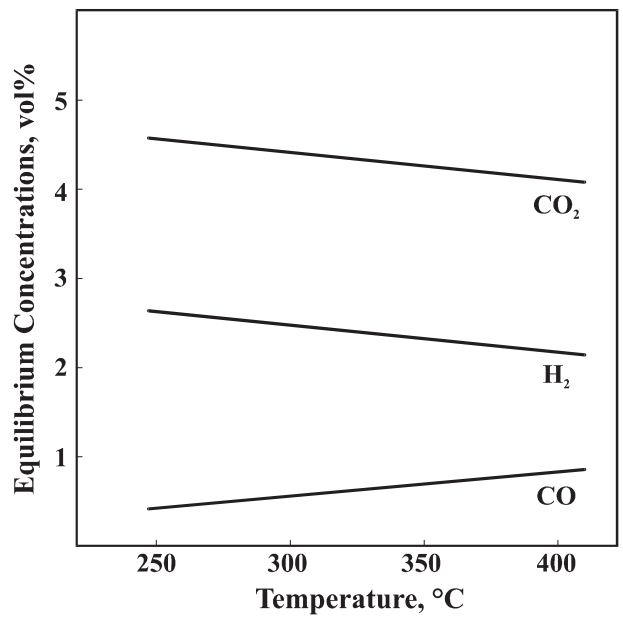

Fig. 5. Equilibrium concentrations of CO, CO_2, and H_2; 3% H_2 and 5% CO_2 in the feed (Aasberg-Petersen et al., 2004).

- Zone 3: Chemisorption saturated. The surface of the zinc oxide is covered with sulphur. The gas phase concentration is constant at the bulk equilibrium level.
- Zone 4: The chemisorption front. In cases with low concentration of H_2S and high concentration of CO_2, the chemisorption front will develop. The H_2S, which escapes zone 2 due to equilibrium according to reaction (10), will be chemisorbed on the fresh catalyst. The gas phase concentration drops to a very low level. In theory, H_2S and COS are removed to sub ppb levels.
- Zone 5: Fresh ZnO. No reactions occur.

If the H_2S concentration in the feed is 'high', and when CO_2 is absent or present in low concentration only, the bulk absorption front will move faster than the chemisorption front, which will then not be visible. There will be only one absorption front, and the gas phase concentration will drop directly from the inlet concentration to the outlet concentration, which will in the ideal case correspond to the immeasurably low chemisorption equilibrium. In such cases the bulk absorption determines the design of the absorption vessel, and the ideal absorption material has the highest possible absorption capacity per volume.

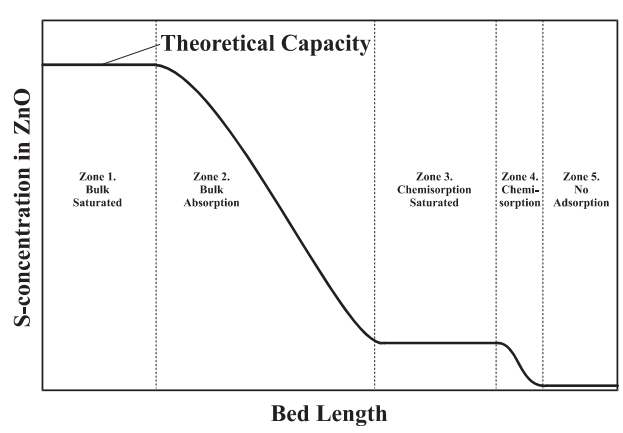

Fig. 6. Ideal sulphur profile in a zinc oxide bed.

However, in cases where low (single digit ppm or lower) concentrations of H_2S (+COS) and/or high CO_2 concentrations (several vol% are not uncommon in natural gas) are present in the feed, the chemisorption front may move faster than the bulk absorption front under normal operating conditions. In such cases the operating temperature may be reduced to the lowest acceptable level (to decrease the equilibrium concentration of H_2S according to reaction (10)), and a ZnO with highest possible chemisorption capacity (highest possible surface area per volume) may be selected. If this is not enough, a special absorption material with high chemisorption capacity, e.g. based on Cu, may be installed downstream of the ZnO to ensure efficient removal of H_2S.

H_2S appears to absorb on ZnO according to a 'core-shell-model' or 'shrinking-core-model' (Carnell and Denny, 1985). However, new research (Fan et al., 2003), as well as industrial feedback, indicates that this simple model cannot adequately describe all situations. Deviations from expected profiles may be seen, especially at a low sulphur concentration and/or high CO_2 concentration in the feed.

2.6. Sulphur absorbents

As mentioned in the preceding paragraphs, ZnO is the universal sulphur absorption material in modern desulphurisation units. It may be supplied in the form of extruded cylindrical pellets, ideally consisting of almost 100% pure ZnO. In order to ensure the highest possible absorption capacity per volume installed absorption material, the highest possible bulk density is desired. However, a certain porosity is required to ensure proper functioning of the material, and this limits the achievable bulk density. At a density of 1.3 kg/l, pure ZnO will absorb about 510 kg/m^3 installed volume at full saturation.

In certain situations it may, as mentioned above, be desirable to optimise not the bulk absorption capacity, but the chemisorption capacity. In such cases the bulk density, and consequently the S-content at full saturation, will be lower. It may also, in certain applications, be advantageous to add promoters to the ZnO, to enhance the ability to absorb COS directly (Jensen and Søndergaard, 1984).

3. Steam reforming

Steam reforming is the conversion of hydrocarbons with steam into a mixture of carbon oxides, hydrogen, methane and unconverted steam. Steam reforming is carried out in several different types of reactors. Each of these may be optimised for specific applications. The main types of reactors are:

- Adiabatic prereformers
- Tubular or primary steam reformers
- Various types of heat exchange reformers

The fundamentals of the steam reforming reactions are described in the Section 3.1. In Section 3.2, reforming catalysts are described along with the reaction mechanisms and the typical reasons for catalyst deactivation. The characteristics of the above-mentioned three types of reactors are described in Sections 3.3–3.5. Finally, metal dusting corrosion, which is a potential problem mainly in heat exchange reforming, is discussed in Section 3.6.

3.1. Fundamentals of steam reforming

The reactions taking place under the steam reforming process are given in Table 2 along with the enthalpy of reaction and the equilibrium constant.

Reactions 1 and 2 in Table 2 are the steam and CO_2 reforming reactions for methane and reaction 3 is the water gas shift reaction, which takes place simultaneously. The water gas shift reaction is fast and is generally considered in equilibrium. Reaction 4 is the steam reforming reaction of higher hydrocarbons. The enthalpy and equilibrium constant is given for steam reforming of n-heptane.

Table 2
Key reactions in steam reforming.

Reaction	Std. enthalpy of reaction ($-\Delta H^o_{298}$, kJ/mol)	Equilibrium constant $\ln K_p = A + B/T$[a]	
		A	B
1. $CH_4 + H_2O \rightleftarrows CO + 3H_2$	−206	30.420	−27,106
2. $CH_4 + CO_2 \rightleftarrows 2CO + 2H_2$	−247	34.218	−31,266
3. $CO + H_2O \rightleftarrows CO_2 + H_2$	41	−3.798	4160
4. $C_nH_m + nH_2O \rightarrow nCO + (n + \frac{m}{2})H_2$	−1175[b]	21,053[b]	−141,717[b]

[a] Standard state: 298 K and 1 bar.
[b] For n-C_7H_{16}.

The steam reforming reactions are strongly endothermic and lead to gas expansion. This means that reaction 1 is favoured at low pressure and high temperature as illustrated in Fig. 7, where the equilibrium conversion is shown as a function of temperature and pressure.

The heat required to convert a 1:2 mixture of methane and steam from 600 °C to equilibrium at 900 °C is 214 kJ/mole CH_4 at 30 bar.

Transition metals from group VIII are found to be active in steam reforming of hydrocarbons, and a number of studies have been carried out to rank their relative activities (Rostrup-Nielsen, 1973; Rostrup-Nielsen and Hansen, 1993; Kikuchi et al., 1974; Qin and Lapszewicz, 1994; Craciun et al., 1998; Yamaguchi and Iglesia, 2010; Jones et al., 2008). Early work by Rostrup-Nielsen on ethane steam reforming (Rostrup-Nielsen, 1973) and later on by methane steam reforming (Rostrup-Nielsen and Hansen, 1993) demonstrated that Ru and Rh are the most active elements, followed by Ni, Ir, Pt, Pd and Re which are less active. Cobalt and iron are also active but oxidise under normal steam reforming conditions (Rostrup-Nielsen, 1973). These findings were supported by studies on methane steam reforming by Kikuchi et al. (1974) in which a similar ranking of the transition metals was found. Interestingly, in recent studies of the activity of group VIII metals, Yamaguchi and Iglesia (2010) found that Pt and Ir are the most active metals over Rh and Ru, with Ru and Ni having almost similar activity. They also found that the activity scales with the dispersion, indicating that the local metal structure is important. The ranking of the group VIII metals was addressed by Jones et al. (2008), who could not reproduce the results by Wei and Inglesia but found similar trends as the early studies. The findings are shown in Fig. 8 in which the measured turnover frequencies as a function of dispersion are given (Jones et al., 2008). They proposed that the different ranking found

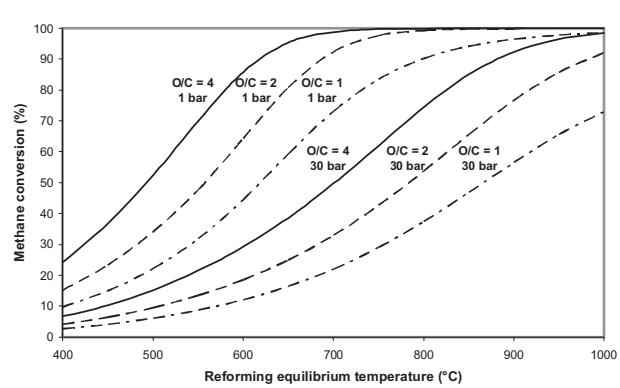

Fig. 7. Steam reforming and methane conversion (O/C: ratio of steam to methane in the feed gas) (Aasberg-Petersen et al., 2004).

by Inglesia et al. was due to deactivation of the small catalyst particles used in their studies.

The experimental findings were supported by first principal calculations of the steam reforming activities of the transition metal catalysts. The basis for the calculations is a detailed understanding of the active sites and reactions mechanism. Based on density functional theory it has been possible to calculate the full reaction pathway of methane steam reforming over terrace site Ni(111) and step site Ni(211) (Bengaard et al., 2002). The energies along the reaction pathway are shown in Fig. 9. This figure shows the energies of the intermediates on the nickel surface and activation barriers separating the intermediates along the reaction path. Steps are much more reactive than the close-packed surface. However, all intermediates are also much stronger bound at steps than on terraces resulting in more free active sites at terraces. There are therefore (at least) two different reaction channels, one with a low activation barrier, which is associated with steps, and another associated with terraces. In both cases the reaction pathway is a stepwise dissociation of methane down to adsorbed carbon and hydrogen where the first reaction is the activated chemisorption of methane to CH_3* and H*. Carbon reacts with adsorbed oxygen formed from water dissociated down to adsorbed oxygen and hydrogen to form carbon monoxide. Hydrogen is formed from recombination of adsorbed hydrogen. By combining scaling relationships for adsorption energies of simple molecules adsorbed on pure metals of fcc(221) step sites with thermodynamic and kinetic analysis, it was possible to establish a model from which the reaction rates could be calculated, which resulted in the 2D volcano curve shown in Fig. 10. Only two independent parameters describe the rate, the adsorption energy of C and the adsorption energy of O. It is seen that the peak of the volcano plot, where the rate is highest, lies close to the region of the adsorption energies on Ni, Rh and Ru. The peak lies in the region where the CO formation and CH_4 adsorption are roughly balanced and there is competition between these two processes. The peak activity is at a slightly lower C adsorption energy than that of the pure metals, which has the highest activity (Ru, Rh and Ni).

This example illustrates that the theoretical calculation tools are so advanced today that it is possible to reproduce experimental findings with great accuracy. These tools will become more and more important in future catalyst research and development.

3.2. Steam reforming catalysis

A steam reforming catalyst should be designed to its specific application. An optimal pre-reforming catalyst differs from an optimal primary steam reforming catalyst. Some general trends exist with respect to active sites, deactivation and poisoning, which will be discussed in the following sections. However the balance between catalytic and physical properties strongly depends on the specific application of the catalyst, which will also be discussed.

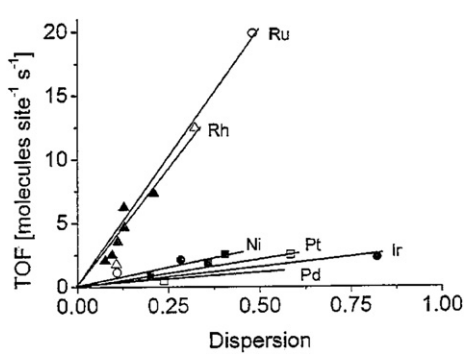

Fig. 8. Reaction rate as a function of dispersion for methane steam reforming (773 K, 0.19 bar CH_4, 0.74 bar H_2O, 0.7 bar H_2) (Jones et al., 2008).

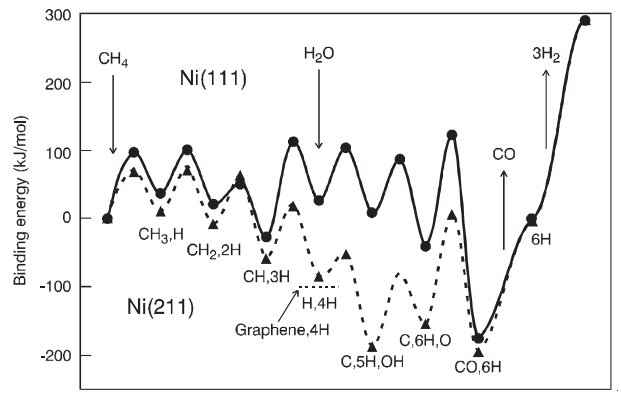

Fig. 9. Calculated energies along the reaction path for steam reforming on the Ni(111) and Ni(211) surfaces. All energies are given relative to a situation in which all reactants are in the gas phase far from the clean surface (Bengaard et al., 2002).

3.2.1. The steam reforming catalysts

As discussed in the previous section, noble metals such as Rh and Ru have the highest activity for steam reforming. However, due to the high price of these metals, they are not used in conventional steam reformers. The preferred choice in industrial steam reforming catalysts is nickel, which has good steam reforming activity and moderate price. Nickel is supported on an oxide carrier, typically Al_2O_3, ZrO_2, $MgAl_2O_4$, $CaO(Al_2O_3)n$, MgO and mixtures thereof to maximise its dispersion. An example of a steam reforming catalyst on nano-scale is given in Fig. 11 showing that the catalyst consists of a huge number of small nickel particles supported on the ceramic carrier. There is an optimum Ni-loading for a given support surface area (Rostrup-Nielsen, 1984) and the Ni-loading of a given catalyst should be optimised accordingly. The active surface area may be calculated from equation (11) when the average nickel particle diameter, d_{Ni} and the Ni-loading X_{Ni} (g/m^3) are known:

$$A_{Ni}\left(\mathrm{m^2\,g^{-1}}\right) = \frac{6800X_{Ni}}{d_{Ni}\left(\text{Å}\right)} \tag{11}$$

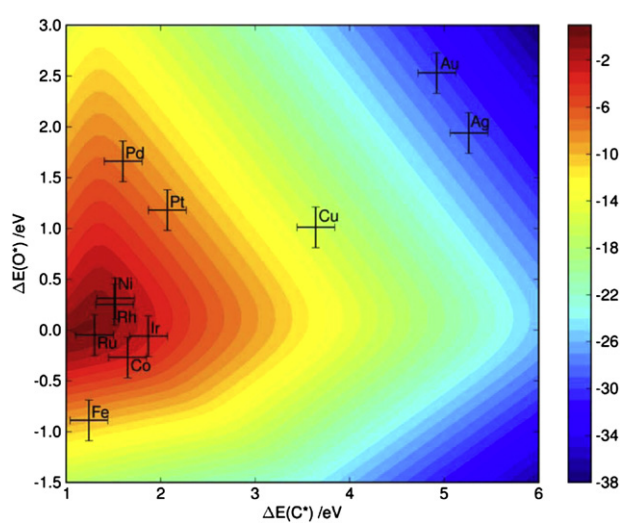

Fig. 10. Two-dimensional volcano curve of the turnover frequency at 773 K and 1 bar pressure at a conversion of 10% as a function of O and C adsorption energy (Jones et al., 2008).

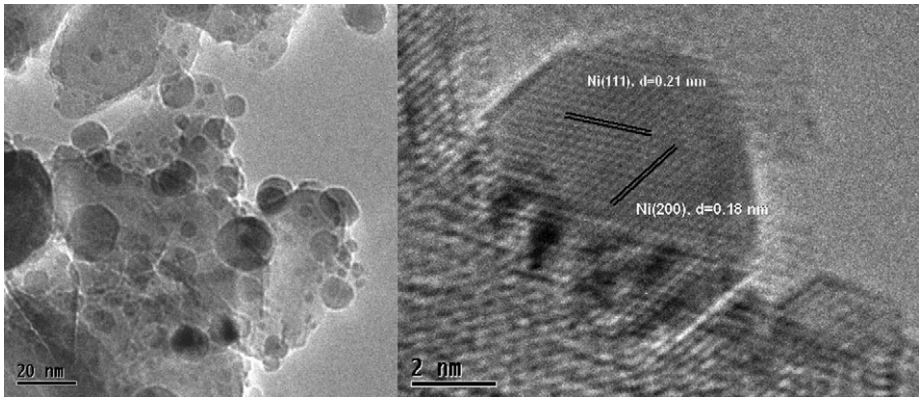

Fig. 11. Nickel supported on an $MgAl_2O_4$ spinel carrier. Recorded at 550 °C and 7 mbar of hydrogen using the in situ electron microscope at Haldor Topsøe A/S.

Equation (11) applies to spherical nickel particles. A_{Ni} is the nickel surface area in $m^2\,g^{-1}$. As discussed in Section 3.1, the steam reforming reaction is structure sensitive with step sites having lower activation energies than terrace sites. The importance of step sites on the reactivity has also been observed in ethane reforming studies over Ni/Al_2O_3 catalysts (Rostrup-Nielsen, 1984). A linear correlation between the reforming activity and the step density as determined by nitrogen adsorption was seen, whereas no correlation between the activity and Ni-surface area was found.

Several factors depending on the specific application influence the requirements of a steam reforming catalyst. The primary function of a prereforming catalyst is to convert higher hydrocarbons in the natural gas into a mixture of methane, carbon dioxide, carbon monoxide and hydrogen. As an added benefit, the prereforming catalyst will adsorb any slip of sulphur from the desulphurisation section. Therefore a high nickel surface area is essential for a prereforming catalyst. Due to the low temperature operation in adiabatic reactors with moderate reactor size, catalyst pellet strength, thermal stability, and pressure drop are less important than in other applications. This allows the use of catalyst pellets of moderate size to be used in prereforming reactors. In tubular reformers, low pressure drop and high heat transfer are essential for good operation. A high heat transfer coefficient minimises the tube wall temperature, thereby reducing the required wall thickness. The pellet size for primary steam reforming catalysts is much larger than for the prereforming catalyst, and the shape is optimised for low pressure drop and high heat transfer.

Catalysts for application in secondary and autothermal reformers are strongly affected by diffusion limitations and the key aspect for this type of catalysts is a strong and stable catalyst carrier that can withstand the high temperatures applied in these processes.

The lifetime of the catalyst will be determined by the operating conditions and feed composition. A number of factors influence the deactivation, such as sintering, poisoning and carbon formation (Rostrup-Nielsen, 1984; Rostrup-Nielsen et al., 2002; Sehested, 2003, 2006; Sehested et al., 2001, 2004, 2006; Rasmussen et al., 2004; Bartholomew, 2001).

3.2.2. Sintering mechanism

Sintering is the growth of small Ni-particles in size and thereby loss in surface area, which will reduce the activity. It is a complex process influenced by several parameters including chemical environment, catalyst structure and composition, and support morphology. Factors that promote sintering include high temperature and high steam partial pressure (Sehested, 2003, 2006; Sehested et al., 2001, 2004, 2006; Rasmussen et al., 2004). The sintering mechanisms have been followed by in situ electron microscopy (Sehested et al., 2001). Sintering of Ni-particles on an $MgAl_2O_4$ support was studied under simulated pre-reforming conditions, i.e. in a 10:1 mixture of steam and hydrogen at 500 °C and 30 bar total pressure. The mechanism for sintering under these conditions was identified as migration and coalescence of nickel particles on the spinel carrier surface (Sehested, 2003; Sehested et al., 2001). Particle movement is associated with diffusion of Ni_2-OH dimers on the nickel surface, which was supported by DFT calculations (Sehested et al., 2004). A simple model was proposed to account for the Ni-particle size growth with time as a function of exposed gaseous environment and temperature (Sehested, 2006). The model shows that the sintering of the Ni-particles is initially fast and will slow down as the Ni-particles grow in size. High partial pressures of steam enhance sintering. The model was experimentally validated up to a sintering temperature of 581 °C. An increase in the sintering rate in H_2O/H_2 atmospheres is seen at temperatures above 600 °C (Fig. 12) (Sehested, 2006). Furthermore, the dependence of H_2-partial pressure is seen to be stronger. This is interpreted as a change in sintering mechanism from particle migration and coalescence to Ostwald ripening via atom migration at the support. For tubular reformers the sintering mechanism in the main part of the reactor will be governed by Ostwald ripening, whereas the migration and coalescence mechanism dominates under prereforming conditions (Sehested, 2006).

3.2.3. Sulphur poisoning

Sulphur is a severe poison for steam reforming catalysts of group VIII metals. Nickel is most susceptible to sulphur poisoning of the group VIII metals as shown by Wise et al. (1985). Sulphur must be removed to a very low level from the feed before it enters the

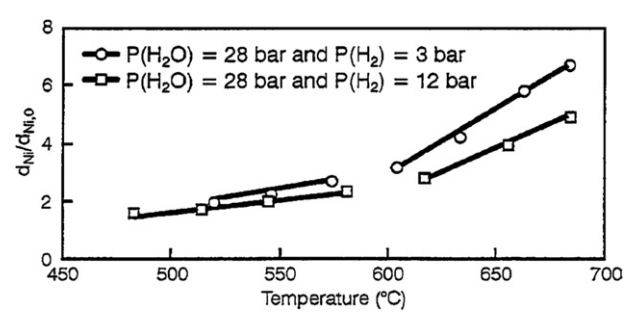

Fig. 12. Relative average nickel particle diameter in a 22 wt% $Ni/MgAl_2O_4$ catalyst after sintering for 700 h plotted as a function of the sintering temperature (Sehested, 2006).

reformer, see Section 2. Under steam reforming conditions all sulphur compounds will be converted into H_2S, which is chemisorbed on the nickel surface through the reaction:

$$H_2S + Ni_{surface} \rightleftarrows Ni_{surface}\text{-}S + H_2$$

The adsorbed sulphur forms a well defined 2-dimentional surface structure with a stoichiometry of approximately 0.5 (Rostrup-Nielsen et al., 2002). This corresponds to a sulphur uptake of 440 μg S per m^2 nickel surface (Rostrup-Nielsen, 1984; Rostrup-Nielsen et al., 2002). The surface coverage of sulphur on nickel depends on the temperature and the partial pressures of H_2S and H_2. It can be estimated from the expression (Rostrup-Nielsen et al., 2002):

$$\theta_s = 1.45 - 9.53 \times 10^{-5} \cdot T + 4.17 \times 10^{-5} \cdot T \ln(P_{H_2S}/P_{H_2}) \quad (12)$$

This expression is not valid for θ_s close to zero and close to one. For nickel at 500 °C, $\theta_s = 0.5$ corresponds to the ratio of partial pressures $H_2S/H_2 = 1.6 \times 10^{-12}$ (Rostrup-Nielsen et al., 2002). This means that sulphur is quantitatively withheld until saturation. The uptake of sulphur correlates with the Ni-surface area. The low H_2S equilibrium pressure is also reflected in the sulphur uptake of a catalyst pellet as illustrated in Fig. 13. A sharp sulphur profile is seen and only the interior of the pellet furthest away from the exterior surface and the holes are unpoisoned. The poisoning by sulphur takes place as shell poisoning due to pore diffusion. The average coverage of sulphur in the particle will be lower than in the shell and it may take years before the chemisorption front has moved to the centre of the particle (Christensen, 1996).

Sulphur has a strong impact on the reaction rate of the reforming catalyst and will decrease the rate significantly (Rostrup-Nielsen, 1984). It was shown that the intrinsic activity of a catalyst decreases rapidly with the coverage of unpoisoned sites in the third power as expressed below:

$$r_i(\theta_s) = (1 - \theta_s)^3 \cdot r_0 \quad (13)$$

where r_0 is the activity of the unpoisoned catalyst.
Other poisons reported are arsenic, lead, phosphorous, silica and alkali metals (Rostrup-Nielsen, 1984). Silica may substantially reduce the activity of the catalyst by acting as a pore mouth poison (Christensen and Rostrup-Nielsen, 1996). The alkali metals reduce the reaction rates in some cases by orders of magnitude.

3.2.4. Carbon formation

Carbon formation is a challenge in steam reforming processes. The potential for carbon formation is highest when the steam-to-carbon ratio is low or under CO_2 reforming. In steam reforming processes, carbon formation is avoided through proper design of the catalyst and steam reforming process.

The reactions leading to carbon formation are given in Table 3.

Reaction (1) in Table 3 is commonly referred to as "the Boudouard reaction", reaction (2) as "CO reduction", and reaction (3) as "methane cracking". Reaction (4) describes how hydrocarbons polymerise into long-chain hydrocarbons. The reaction product is often referred to as "encapsulating carbon" or "gum". Different types of carbon may be formed by the carbon forming reactions as illustrated in Fig. 14, i.e. whisker carbon, encapsulating carbon also called gum and pyrolytic carbon (Rostrup-Nielsen, 1984; Rostrup-Nielsen et al., 2002; Sehested, 2006).

Whisker carbon formation is the most destructive form of carbon. It is characterised by long filamentous nanofibres formed from the decomposition of carbon monoxide, methane or higher hydrocarbons on the Ni-particles in gas mixtures where the steam-to-hydrocarbon ratio is too low and the temperature above a certain limit. Carbon whiskers grow by the reaction of hydrocarbons at one side of the nickel particle and nucleation of carbon as a whisker on the other side of the nickel particle. Continued growth may cause catalyst disintegration and increase the pressure drop. The carbon whisker has a higher energy than graphite (Rostrup-Nielsen, 1984). This means that operation under conditions at which thermodynamics predict formation of graphite may be feasible without carbon formation of the catalyst. The carbon limit also depends upon the crystal size of the nickel particle. Smaller nickel crystals are more resistant towards carbon formation. The temperature at the onset of whisker carbon formation was approximately 100 °C higher for the catalyst with small nickel crystals (around 7 nm) than for that with large crystals (around 100 nm) (Rostrup-Nielsen et al., 2002).

Encapsulating carbon (gum) may be formed in reforming of heavy feeds with a high content of aromatic compounds. The risk of forming gum is also enhanced at low temperature, low steam-to-carbon ratio and high final boiling point of the hydrocarbon mixture. Encapsulating carbon is a thin film of a few atom layers of graphite, which covers the nickel particles and leads to deactivation of the catalyst.

Pyrolytic carbon refers to the thermal cracking of hydrocarbons and is formed from the exposure of higher hydrocarbons to high temperatures, typically above 600 °C (Rostrup-Nielsen, 1984). In tubular reformers the formation of pyrolytic carbon is seen as reddish zones known as 'hot bands' on the walls of the tubes. The pyrolytic carbon is a result of carbon formed by thermal cracking of higher hydrocarbons, often related to loss of catalyst activity due to sulphur poisoning.

Detailed insight into the mechanism of carbon formation has emerged from a combination of in situ electron microscopy studies and density functional calculations (Helveg et al., 2004; Abild-Pedersen et al., 2006; Saadi et al., 2010). Adsorbed atomic carbon is much more stable at steps than at terrace sites (Fig. 9), and steps are therefore much better nucleation sites for carbon. When carbon atoms cover step sites, a single graphite layer can grow from the step as illustrated in Fig. 15A. After a graphene island has nucleated,

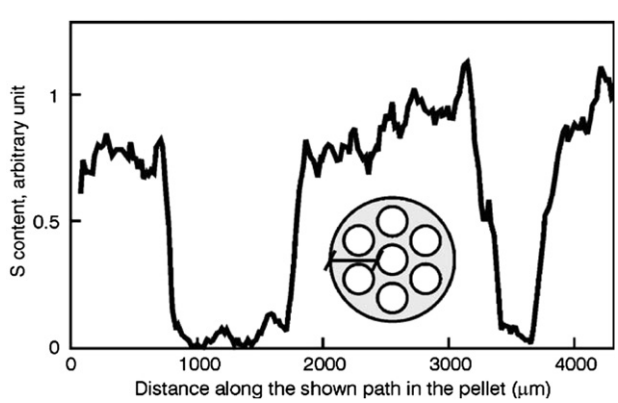

Fig. 13. Sulphur uptake profile of a severely sulphur poisoned seven-hole reforming catalyst (Sehested, 2006).

Table 3
Reactions in steam reforming leading to carbon formation.

Reaction	Std. enthalpy of reaction ($-\Delta H^o_{298}$, kJ/mol)
1. $2CO \rightleftarrows C + CO_2$	172
2. $CO + H_2 \rightleftarrows C + H_2O$	131
3. $CH_4 \rightleftarrows C + 2H_2$	−75
4. $C_nH_m \rightarrow$ 'carbonaceous deposits'	–

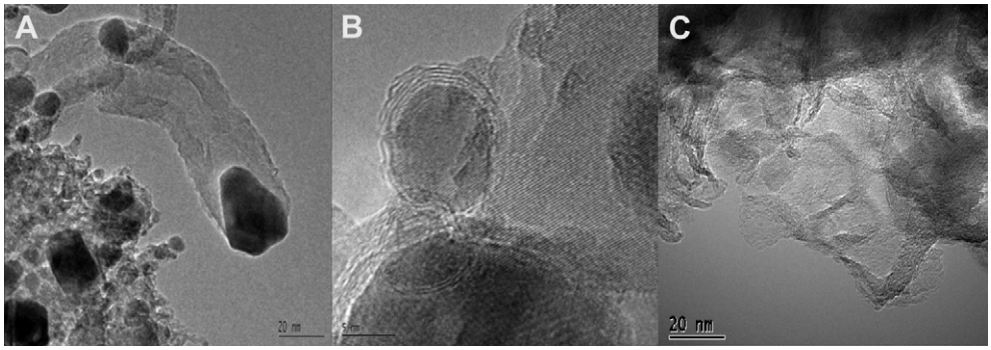

Fig. 14. Electron microscopy images of whisker carbon (A), encapsulating carbon gum (B) and pyrolytic carbon on the $MgAl_2O_4$ carrier (C) of a $Ni/MgAl_2O_4$ reforming catalysts (Sehested, 2006).

the growth may continue by surface or bulk transport of carbon atoms or carbon containing fragments to the island. In this case gum has formed. Alternatively new layers may nucleate below the first graphene layer and grow by addition of carbon atoms. This growth is accompanied by surface transport of nickel to the free nickel surface resulting in the growth of carbon whiskers from the Ni particle (Fig. 15B and C). Step sites thus play an important role both in having a higher turnover frequency of the steam reforming reaction but also in carbon formation. Potassium, sulphur and gold are known to retard carbon formation (Bengaard et al., 2002; Rostrup-Nielsen et al., 2002). DFT calculations have shown that these species are preferentially located at step sites, thus explaining their retarding effect on carbon formation.

3.2.5. Reaction kinetics

Steam reforming of methane and higher hydrocarbons (reactions (1) and (4) in Table 2) are relatively fast reactions which make it difficult to obtain intrinsic kinetics (Rostrup-Nielsen, 1984; Rostrup-Nielsen et al., 2002). Furthermore the large negative heat of reaction also makes it difficult to obtain isothermal measurements. These aspects require studies on crushed diluted catalyst particles or metal foil and preferably at low temperatures (<600 °C). The lack of back diffusion in laboratory scale reactors also requires addition of hydrogen to the inlet gas to avoid oxidation of the catalyst. Furthermore, the reaction is accompanied by the water gas shift reaction which generally is considered to be fast under steam reforming conditions (Rostrup-Nielsen, 1984). Many studies have aimed at establishing the reaction order of methane (Yamaguchi and Iglesia, 2010; Rostrup-Nielsen et al., 2002; Zeppieri et al., 2010), and there is general consensus that the reaction order of methane is close to one. This is consistent with activated methane adsorption being the rate limiting step. The reaction order of water and hydrogen are more debated. The total pressure dependence under conditions close to industrial operation is reported to be slightly negative (Rostrup-Nielsen et al., 2002). Overall activation energies are found to be in the range of 100–120 kJ/mol (Rostrup-Nielsen, 1984).

A comprehensive study of the kinetics of the methane steam reforming over a Ni-based catalyst was performed by Xu and Froment (1989). A detailed Langmuir Hinshelwood based model in which the water gas shift reaction (reaction (3) in Table 2) was included was proposed. Methane reforming to CO and CO_2 was treated as two separate reactions accompanied by the water gas shift reaction:

$$\mathrm{A}: \quad CH_4 + H_2O \leftrightarrow CO + 3H_2$$

$$r_1 = \frac{k_1 P_{CH_4} P_{H_2O}}{P_{H_2}^2 Z^2}(1-\beta)$$

$$\mathrm{B}: \quad CO + H_2O \leftrightarrow CO_2 + H_2$$

$$r_2 = \frac{k_2 P_{CO} P_{H_2O}}{P_{H_2}^2 Z^2}(1-\beta)$$

$$\mathrm{C}: \quad CH_4 + 2H_2O \leftrightarrow CO_2 + 4H_2$$

$$r_3 = \frac{k_3 P_{CH_4} P_{H_2O}^2}{P_{H_2}^{3.5} Z^2}(1-\beta)$$

$$Z = 1 + K_{CO}P_{CO} + K_{H_2}P_{H_2} + K_{CH_4}P_{CH_4} + K_{H_2O}\frac{P_{H_2O}}{P_{H_2}}$$

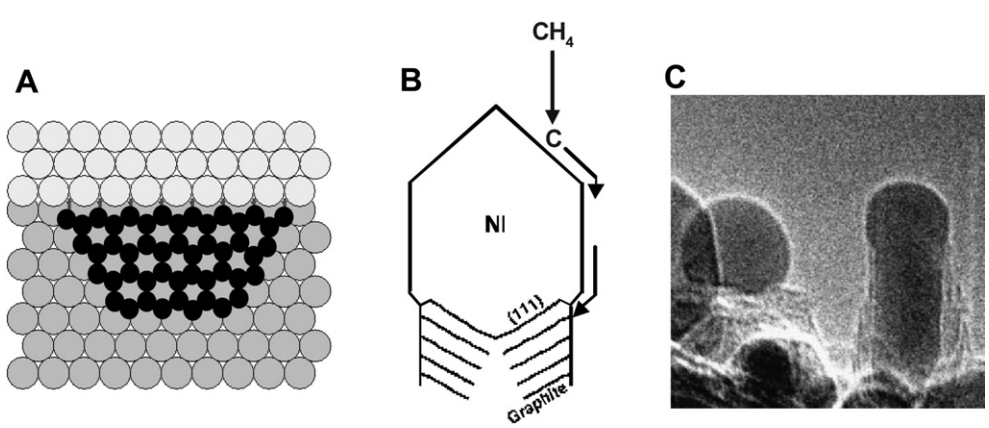

Fig. 15. Schematic illustration of the process by which carbon whiskers are formed at the nickel particle during steam reforming. (A) Illustration of a graphene island nucleated from a Ni(211) step at a Ni(111) surface (Bengaard et al., 2002). (B) Schematic illustration of whisker formation. (C) In situ electron microscopic picture of 'lift off' for a nickel particle from the carrier due to whisker carbon formation (Helveg et al., 2004).

where k_i is the rate constant for reaction i and K_I the equilibrium constant for reaction i. Because the three reactions are not independent, it was necessary to combine the three rate equations into two expressing the rate of methane conversion and CO_2 formation:

$$r_{CH_4} = r_1 + r_3$$
$$r_{CO_2} = r_2 + r_3$$

The advantage of this model is that it includes the water gas shift kinetic in the model and thus can be used for design. The model predicts a decreasing reaction order of water with temperature ($K_{H_2O} = 1.77 \times 10^5 \exp(-88.68/RT)$) reflected in an increase in the coverage of oxygen atoms. This implies a negative heat of adsorption of water which is in contrast to fundamental studies of water adsorption (Rostrup-Nielsen et al., 2002). Avetisov et al. (2010) have recently reanalysed the model proposed by Xu and Froment and expanded the model to be more consistent with microkinetic insight into the steam reforming reaction.

Hou and Hughes (2001) considered the same reactions as Froment in establishing an intrinsic kinetic model of methane steam reforming also over a Ni-based catalyst. Surface reaction of adsorbed intermediates was considered to be rate controlling steps. The kinetic model differs from the model by Froment, which was assigned to the use of a different catalyst.

The microkinetic approach has also been applied by Jones et al. (Jones et al., 2008; Jakobsen et al., 2010a,b) as discussed in Section 3.1 where a kinetic model for the group VIII metals based on the reaction pathway in Fig. 9 is proposed. Two reactions were considered rate limiting: the activated chemisorption of methane to CH_3^* and H^* and the reaction of adsorbed carbon and oxygen to form carbon monoxide. For noble metals the CO formation step is the kinetically controlling step at low temperature. At high temperature and for less noble metals, the dissociative chemisorption of methane becomes the kinetically controlling step. This explains some of the controversy found in the literature concerning reaction orders since these will be dependent on the applied reaction conditions.

The group of Vlachos (Maestri et al., 2009) have also applied the microkinetic approach and formulated a complete model based on 82 elementary reactions which can describe methane conversion to syngas over Rh/Al_2O_3. A hierarchical data-driven methodology is found to be essential with respect to experimental data analysis in this approach for obtaining reliable predictive kinetic models. The microkinetic approach was also used by the group of Deutschmann (Schädel et al., 2009) for describing the steam reforming of methane, ethane, propane, butane and natural gas over an Rh-based catalyst. The model is based on 42 elementary reactions and gives a good description of the reaction of both single component feed and mixtures hereof.

In industrial size reactors the heat and mass transfer limitations are significant. For normal steam reforming catalysts, the effectiveness factor is far less than 10% because of transport restrictions. The mass transport restrictions are related mainly to intra particle diffusion with bulk diffusion dominating at the high pressure in a reformer, whereas heat transfer restrictions are located in the gas film. The strong endothermic reaction results in a temperature drop of about 5–10 °C over the gas film.

This means that the activity is roughly proportional to the external surface area.

3.2.6. Physical properties

In order to ensure good performance and a long lifetime of the catalyst in the plant, optimal physical properties of the catalyst are just as important as optimal catalytic properties (Aasberg-Petersen et al., 2004; Rostrup-Nielsen, 1984). Key aspects to consider are pore size distribution and pellet shape, size and mechanical strength. The pore size distribution must be optimised for large surface area and good access to the active sites. The pellet shape is important with respect to packing density in the reactor and thereby the void fraction. The pressure drop over the reactor strongly depends on the void fraction: the higher the pellet diameter the lower is the pressure drop. In adiabatic prereformers the pressure drop is low and a small pellet size can be used to minimise mass transfer limitations. In tubular reformers the pressure drop can be large and a compromise between pellet size and void fraction is made. The result is catalyst pellets with large external diameters and high void fraction achieved by rings or cylinders with several holes. The shape of the catalyst is also important with respect to ensuring a high heat transfer. This is important in tubular reformers where a high heat transfer coefficient results in a lower tube wall temperature, thereby increasing the lifetime of the tubes. A catalyst pellet with high external surface is also desirable to maximise the effective activity. Good mechanical pellet strength is of importance since deterioration of the pellets will increase the pressure drop in the reactor, may create hot spots and eventually require shutdown and reload of the reactor. This means that the catalyst support material must be stable under process conditions and under the conditions during start-up and shutdown of the plant. The initial catalyst pellet strength should be high, but also the strength under operating conditions should be high. Fig. 16 shows two typical shapes of commercial reforming catalyst.

3.3. Adiabatic prereforming

An adiabatic prereformer may be installed upstream of a fired tubular reformer, a heat exchange reformer or an autothermal reformer. The adiabatic prereformer converts higher hydrocarbons in the feedstock into a mixture of methane, steam, carbon oxides and hydrogen according to the reactions in Table 2. All higher hydrocarbons are quantitatively converted by reaction (4) assuming sufficient catalyst activity (Christensen, 1996). This is accompanied by the equilibration of the exothermic shift (3) and methanation (the reverse of methane steam reforming (1)) reactions. Finally, the prereformer also removes any trace of sulphur present in the feed stream, thus preventing poisoning of downstream catalysts.

Heating of non-converted reformer hydrocarbon feedstock to high temperature may result in thermal reactions of higher hydrocarbons into non-saturated compounds and carbon. This may eventually lead to carbon formation on catalysts and/or fouling of heat exchangers. Removal of the higher hydrocarbons by prereforming allows a higher preheat temperature resulting in higher plant efficiency and a smaller tubular reformer. In the case of autothermal reforming, the increased preheat temperature made possible by use of prereforming results in a significant reduction in the oxygen consumption.

Fig. 16. Examples of commercial reforming catalyst. A cylindrical shaped prereforming catalyst of 4.5 × 4.5 mm size and a seven-hole cylindrical shaped primary steam reforming catalyst of 16 × 11 mm size.

3.3.1. Reactor and catalyst characteristics and operating conditions

The prereforming reactor is an adiabatic vessel with specially designed reforming catalysts based on nickel. The operating conditions depend on the type of feedstock and the application. The inlet temperature is between 350 °C and 550 °C. The low operating temperature requires a catalyst with high surface area to obtain sufficient activity and resistance to poisoning especially by sulphur. The optimal shape of the catalyst particle depends on the specific application and on the plant capacity. In many cases catalyst particles of a cylindrical shape in a size of 3–5 mm are used (Christensen, 1996). This particle provides a large surface area for access of the gas into the pore system. The pressure drop over the prereformer is often low for small or medium-scale plants even with such particles giving low void. For large-scale plants, a shape-optimised catalyst will be an advantage, and particles in the form of cylinders with one or several axial holes are usually the preferred choice for minimum pressure drop and high activity (Christensen, 1996).

In Fig. 17 the temperature profile in an adiabatic prereformer with natural gas feed at high steam-to-carbon (H_2O/C) ratio in an ammonia plant is illustrated.

The selection of the operating conditions in the prereformer is in many cases dictated by the limits of carbon formation on the catalyst. For a given feedstock and pressure, the adiabatic prereformer must be operated within a certain temperature window. The formation of a whisker type of carbon will occur above the upper temperature limit. Operation below the lower temperature limit may result either in a polymeric type of carbon formation (gum) or lack of sufficient catalyst activity. The formation of carbon on the catalyst is further discussed in Section 3.2.4.

Deactivation of the prereformer catalyst may occur during operation. The cause is typically sulphur, but gum formation may also play a role as discussed earlier. The deactivation of the catalyst can be observed as a progressive movement of the temperature profile as illustrated in Figs. 15 and 17. The resistance to deactivation is an important aspect in the design of adiabatic prereformers.

The assessment of the performance of an adiabatic prereformer during operation is used to determine the actual rate of deactivation and the optimal time for changing the catalyst (Christensen and Rostrup-Nielsen, 1996). This can be done by monitoring a number of parameters. It is important to follow the content of higher hydrocarbons as an increase in concentration may indicate loss of activity. The approach to equilibrium of the methane steam reforming reaction at the reactor exit is also a parameter which can be used to monitor the performance. The approach to equilibrium is expressed by a temperature difference defined as:

$$T_R = T(\text{exit catalyst}) - T(Q_R), \quad Q_R = \frac{P_{CO}P_{H_2}^3}{P_{CH_4}P_{H_2O}} \tag{14}$$

in which $T(Q_R)$ is the equilibrium temperature corresponding to an equilibrium constant equal to the reaction quotient Q_R.

The approach to equilibrium and the content of higher hydrocarbons in the prereformer exit are generally close to zero and constant throughout the operation period of the prereformer. In many cases a graphical deactivation plot is used to assess the performance of the prereformer (Christensen and Rostrup-Nielsen, 1996). The deactivation plot shows the length of the reaction front as a function of operation time. The method is illustrated in Fig. 18.

The temperature difference between the outlet and the inlet is calculated. The axial position ($z90$) at which 90% of the temperature difference has been obtained is plotted versus time. A steep slope indicates a high rate of deactivation. The inverse slope of the deactivation plot is known as the resistance number defined as the amount of feed required to deactivate 1 g of catalyst. A large resistance number indicates slow deactivation.

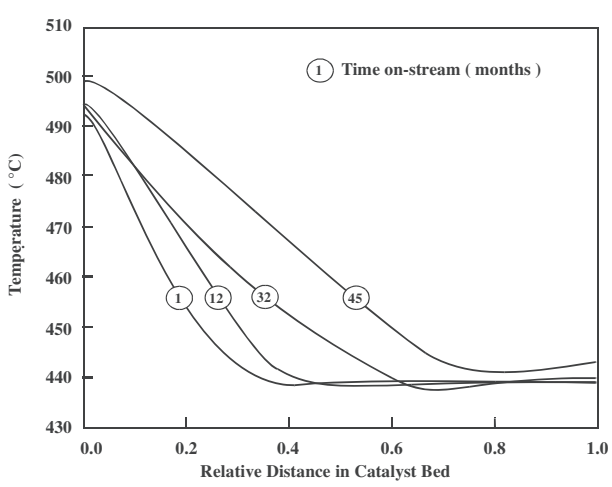

Fig. 17. Temperature profile of an adiabatic prereformer with natural gas feed in a 1600 MTPD ammonia plant (Christensen, 1996). $H_2O/C = 2.8$, $P = 35$ bar. The movement of the temperature profile with time is due to catalyst poisoning by sulphur.

3.3.2. Adiabatic prereformers at low S/C ratio

In some cases, notably in production of synthesis gas for GTL plants, operation at very low H_2O/C ratio is desirable to optimise process economics. Operation at the very low H_2O/C ratio involves the risk of formation of carbon on the catalyst in the adiabatic prereformer. Carbon formation on reforming catalysts is discussed in detail in Section 3.2.4. In prereformers, carbon may form either from methane or higher hydrocarbons (reactions (3) and (4) in Table 3).

The selection of the catalyst and the operating conditions of an adiabatic prereformer in a GTL plant are often dictated by the limits of the above reactions. The limits for carbon formation from methane (reaction (3) in Table 3) may in principle be determined from thermodynamics. Carbon may form if the gas shows affinity for carbon formation after establishment of chemical equilibrium of the methane steam reforming and shift reactions (Christensen, 1996). The risk of carbon formation from methane is most pronounced in the reaction zone where the temperature is highest.

A temperature profile for an adiabatic prereformer operating at low H_2O/C ratio is given in Fig. 19 (Aasberg-Petersen et al., 2003).

Carbon formation from higher hydrocarbons (reaction (4) in Table 3) is an irreversible reaction that can only take place in the first part of the reactor with the highest concentration of C_2^+ compounds. The criterion for carbon formation can be described as a kinetic competition between the carbon forming and steam reforming reactions. A thorough kinetic analysis, both with fresh catalyst, and towards end-of-run at each point in the reactor, is required to accurately evaluate this criterion. In general the limits for carbon formation from higher hydrocarbons are approached with reduced ratio of steam to higher hydrocarbons and with increased temperature (Rostrup-Nielsen, 1994; Christensen, 1996).

The knowledge of the carbon limits is imperative for optimal design. Examples of pilot plant experiments at low pressure performed to gather information about these limits are given in Table 4.

3.3.3. Modelling of adiabatic prereformers

The use of mathematical models is an invaluable tool in the design and optimisation of adiabatic prereformers. The chemical conversion versus time can be determined by combining reaction kinetics, pore diffusion, pressure drop and the effects of catalyst deactivation and poisoning (Christensen, 1996).

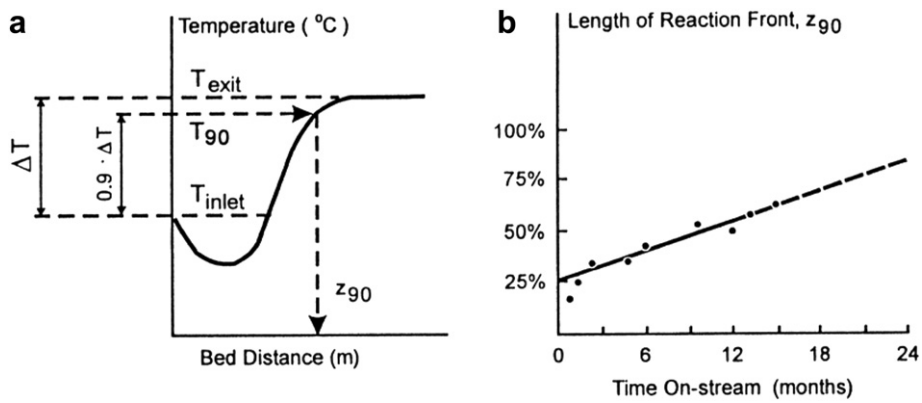

Fig. 18. Graphical deactivation plot for performance prediction: (a) Estimation of length of reaction front, z_{90} from temperature profile, (b) deactivation plot.

No radial concentration gradient exists in a prereformer due to its adiabatic nature. A one-dimensional axial model is thus sufficient to simulate the temperature and concentration profile. Simulation of (pre)reformers may be carried out by heterogeneous and pseudo-homogeneous models. The heterogeneous model is based on intrinsic kinetics. This model takes into account the pore diffusion inside the catalyst particle and the transport restrictions across the film on the external surface. Accurate representations of the conditions inside the catalyst particle may be obtained. However, these models are mostly used for development of novel catalysts and catalytic systems and for detailed investigations of deactivation phenomena (Christensen, 1996). For design purposes, pseudo-homogenous models are often used.

The prereformers often operate in the diffusion-controlled regime, which validates the use of pseudo-homogenous models. The pseudo-homogeneous model does not take into account the difference in temperature and concentration between the catalyst particle and the bulk gas phase. The transport restrictions are implicitly taken into account by the use of effective reaction rate expressions.

Details of one pseudo-homogeneous model are given (for one reaction) in (Christensen, 1996).

3.4. Tubular fired reformers

Steam reforming is, in industrial practice, mainly carried out in reactors referred to as tubular fired reformers, which are essentially fired heaters with catalyst-filled tubes placed in the radiant part of the heater. The process may also be carried out in reactors referred to as heat exchange reformers. These are essentially heat exchangers with catalyst-filled tubes and/or with catalyst in the space between tubes. Heat exchange reformer design is discussed in Section 3.5. The catalysts used in tubular fired reformers and heat exchange reformers are discussed in Section 3.2. Abundant literature is available on steam reforming and design of steam reformers. Examples are Rostrup-Nielsen (1994, 2002), Dybkjær (1995b), Rostrup-Nielsen (1984), Slack and James (1973), Kawai et al. (1984), Rostrup-Nielsen et al. (1992, 2002), Nitrogen (1995), Rostrup-Nielsen and Christiansen (1997). A detailed discussion may be found in Aasberg-Petersen et al. (2004). Reference to older literature may be found in Dybkjær (1995a).

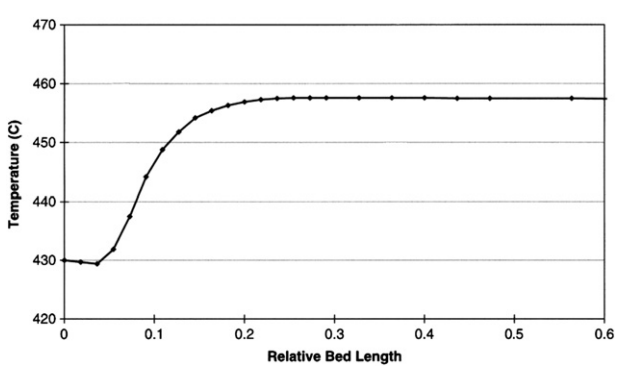

Fig. 19. Temperature profile in adiabatic prereformer during pilot plant operation. $H_2O/C = 0.4$.

3.4.1. Modelling of the reformer

3.4.1.1. Simulation of furnace chamber. Tubular steam reforming is a complex interaction of heat transfer and coupled chemical reactions (Rostrup-Nielsen et al., 1992). The heat released by the burners is transferred via radiation and convection to the reformer tubes. The heat passes through the tube walls by conduction and is transferred to the catalyst bed by convection and radiation. At the same time, a network of chemical reactions creates radial temperature and concentration gradients in the tube and around and within the porous catalyst particles.

An ideal model should be able to simulate the reformer performance on the basis of the individual burner duties, the feed stream characteristics, the properties of the catalyst and the reformer geometry.

Early simulations of the process gas side in tubular reformers were generally uncoupled from the furnace box by assuming an outer tube wall temperature profile or a heat flux profile. These profiles were established or checked by feedback from measurements in industrial plants and monotube pilot plants. It should be pointed out, however, that measurement of tube wall temperatures is difficult (Cromarty and Beedle, 1993). Pyrometric methods involve complex corrections because of reflections from furnace walls and flames. The correction is largest at the coldest position of the tube at the reformer inlet, where reaction conditions at the same time are most complex. Thermocouples welded into the tube wall give more exact information but their life may be limited. Shadowing effects in the tube row cause another uncertainty. The extent of this distortion increases with decreasing tube pitch.

3.4.1.2. Simulation of reformer tube side. One-dimensional pseudo-homogeneous models are adequate for studying reformers under non-critical conditions and for simulation of the overall performance.

Table 4
Adiabatic prereforming at low H_2O/C ratio (Christensen, 1996).

Experiment	A	B	C	D
H_2O/C	0.40	0.25	0.13	0.25
Inlet temperature, °C	455	395	400	430
Pressure, MPa	0.8	1.0	1.0	0.9

They are, however, insufficient for reformers of tight design or reformers operating close to carbon limits. For such cases a more detailed analysis of the local phenomena in the reformer is required.

Radial temperature and concentration profiles are included in two-dimensional pseudo-homogeneous models, whereas the gradients in and around the catalyst pellets are neglected.

Such models are generally plug flow reactor models with detailed kinetic schemes considering two-dimensional axi-symmetric radial temperature and concentration gradients within the tube. Heat transfer is calculated as an effective radial conductivity within the bed and a film heat transfer coefficient at the tube wall. The main parameters are the reaction kinetics and parameters in the heat transfer and the pressure drop equations. Such data are proprietary parameters, and generally quite difficult and costly to establish. However, it must be remembered that the usefulness of even the most sophisticated models is not better than the accuracy by which the relevant parameters are known.

A proprietary, in-house process model is described in Jakobsen et al. (2010), Rostrup-Nielsen et al. (1988). The parameters in this model were determined by experiments in a full-size monotube reformer process demonstration unit (PDU) (Fig. 20) (Dybkjær, 1995b; Rostrup-Nielsen et al., 1988) and validated against a large amount of industrial data.

An application of this model is shown in Fig. 21 (Rostrup-Nielsen et al., 1988), which shows a comparison between calculated and measured axial catalyst bed temperatures at measured outer tube wall temperatures.

The data are from an experiment carried out on the monotube PDU at a low steam-to-carbon ratio of 1.18 but also with a low average heat flux of 50,500 kcal/m^2/h on the inner tube surface. It is seen that there is good agreement with the measured temperature data. Similar agreement has been obtained in simulations of a large number of data sets.

Fig. 20. Tubular reformer PDU.

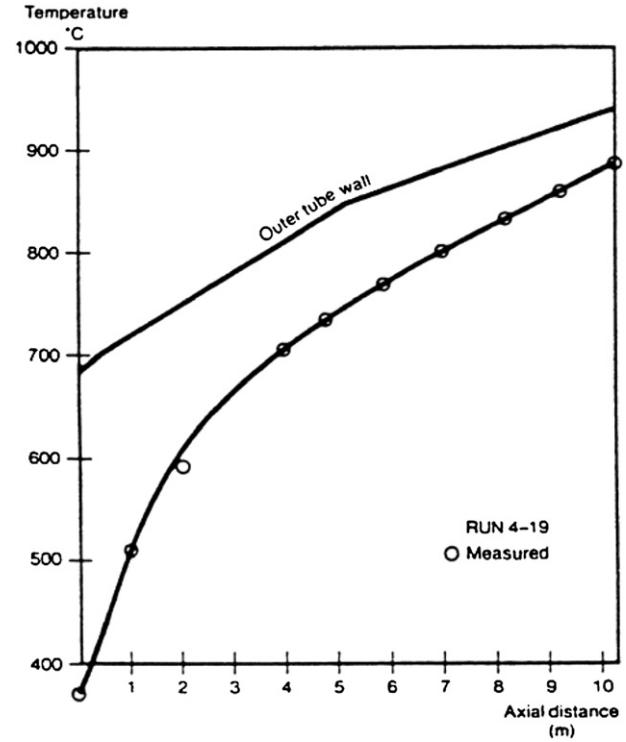

Fig. 21. Measured and calculated axial temperature profiles from run in PDU.

3.4.1.3. Modelling by CFD. CFD (Computational Fluid Dynamics) is an efficient tool for modelling and simulation of steam reformers. Results obtained by simulation of top fired furnaces have been reported in e.g. Barnett and Wu (2001), Cotton and Fisher (2002) of a terrace fired furnace in Mehrota et al. (2002) and of a side fired furnace in Nielsen and Christiansen (2002). Most attention has been on the furnace side and studies of the effects of flue gas flow and temperature maldistribution, but in order to obtain the full picture, it is necessary to couple the process gas side and the flue gas side.

In reference Taskin et al. (2008) it is described how a coupled CFD model is verified against numerous experiments performed on a full size PDU. This PDU contains a single full size catalyst-filled tube located in the centre of the side fired furnace containing five rows of burners.

Qualitatively the behaviour of the pilot reformer resembles industrial reformers. However, the temperature field on the furnace side is more homogeneous in the pilot reforming furnace. This is due to the smaller number of tubes per unit volume. Furthermore, there are no shadowing effects due to the presence of other tubes. All the CFD simulations show that the outer tube wall temperature and the tube heat flux do not vary on the perimeter of the tube. This is in accordance with what has been observed experimentally.

Fig. 22 compares the calculated outer tube wall temperature to the measured temperature. The outer tube wall temperature agrees well with the measured temperature. The small deviation (less than 10°) is well within the measurement accuracy.

The efficient heat transmission from the tube wall of the reformer tube to the gas and the catalyst pellets is of major importance in the strongly endothermic steam reforming process. An example of a detailed study of the effect of catalyst pellet morphology is given in Taskin et al. (2008). By means of CFD

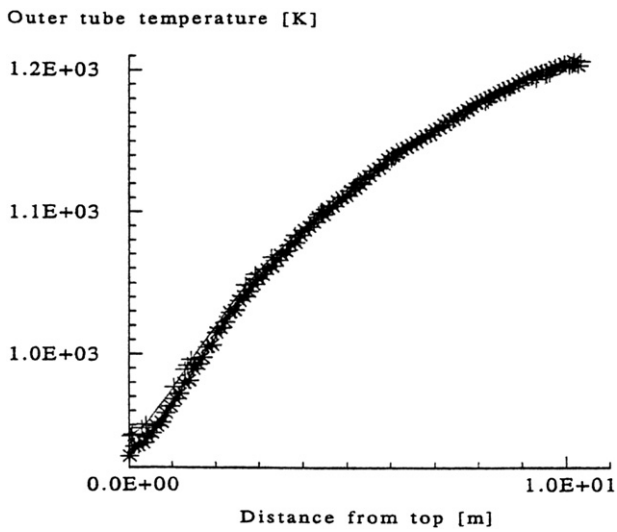

Fig. 22. Calculated and measured outer tube wall temperature.

simulations, the importance of the pellet shape is demonstrated and it is confirmed that a pellet shape with holes is advantageous relative to a ring shaped pellet in terms of efficient heat transfer.

3.5. Heat exchange reformers

Basically, a heat exchange reformer is a steam reformer where the heat required for the reaction is supplied predominantly by convective heat exchange. The heat can be supplied from a flue gas or a process gas – or in principle by any other available hot gas.

When the heat and mass balance on the process (catalyst) side only is considered, there is no difference between heat exchange reforming and fired tubular reforming, where the heat transfer is predominantly by radiation. This means that all process schemes using heat exchange reforming will have alternatives where the function of the heat exchange reformer is performed in a fired reformer. The process schemes differ 'only', in the amount of latent heat in flue gas and/or process gas and in the way this heat is utilised.

Models for design and simulation of heat exchange reformers are combinations of models for steam reformer catalyst tubes (as described in Section 3.4.1) and models for convective heat transfer (as used in design and simulation of normal gas/gas heat exchangers).

3.5.1. Types of heat exchange reformers

Three different concepts for heat exchange reformer design have been commercialised by various companies. The three concepts are illustrated in Fig. 23.

Types A and B in Fig. 23 can be used with all types of heating gas, whereas type C can only be used when the desired product gas is a mixture of the heating gas and the product gas from the catalyst in the heat exchange reformer.

3.5.1.1. Flue gas heated heat exchange reformers. These heat exchange reformers are stand-alone reformers, and their function is similar to normal fired reformers. Two designs HER (Stahl et al., 1985; Udengaard et al., 1988) and HTCR (Dybkjær et al., 1997; Dybkjær and Madsen, 1997/98) are examples of this category. As seen in Fig. 24, the HER consists of a number of concentric cylinder shells around a centrally placed burner, while the HTCR as shown in Fig. 25 features a bundle of bayonet tubes and a burner in a separate chamber. Especially the HTCR has been developed into a successful commercial product for production of hydrogen (Dybkjær, 2005; Andersen, 2006; Broman and Carstensen, 2009; Carstensen, 2011).

It may be argued that reformer concepts with bayonet tubes are partly gas heated reformers (see below) since the process gas is cooled by heat exchange with the catalyst bed, thus providing part of the heat required for the reforming reaction. However, bayonet tubes and similar concepts are in this context only considered as special reformer tube designs.

3.5.1.2. Heat exchange reformers heated by process gas. Reformers heated by process gas are normally called Gas Heated Reformers. They may be classified in two types depending on the process concept, see Fig. 23. One type, which may be referred to as HTER-s, GHR or 'two-in, two-out' (both types A and B in Fig. 23 are of this type), can in principle be used in both series and parallel arrangements (see below under Process concepts). The other type (type C in Fig. 23), which is called HTER-p, GHHER or 'two-in, one-out', can only be used in the parallel arrangement. Several types of GHR have been commercialised (Elkins et al., 1992; Farnell, 2000; Mii and Hirotani, 2001; Nitrogen, 1989; Madsen and Dybkjær, 2003). Also the design of the HTER-p or GHHER has been commercialised (Ratan and Vales, 2002; Malhotra and Hackemesser, 2002; Schneider and Joshi, 1997; Carstensen, 2005; Winter-Madsen and Olsson, 2007).

3.5.2. Process concepts

Heat exchange reformers heated by process gas are of course always installed in combination with another reformer, which may be a fired tubular reformer or an air or O_2-blown secondary or autothermal reformer. Evidently, there is a significant number of possible combinations. If there is more than one feedstock, as e.g. in GTL plants, where recycled tail gas from the synthesis may be used as additional feed to adjust the gas composition, the number of possible process concepts increases further. The use of a prereformer may also be considered, also increasing the number of possible process concepts. In the following, the possible combinations of heat

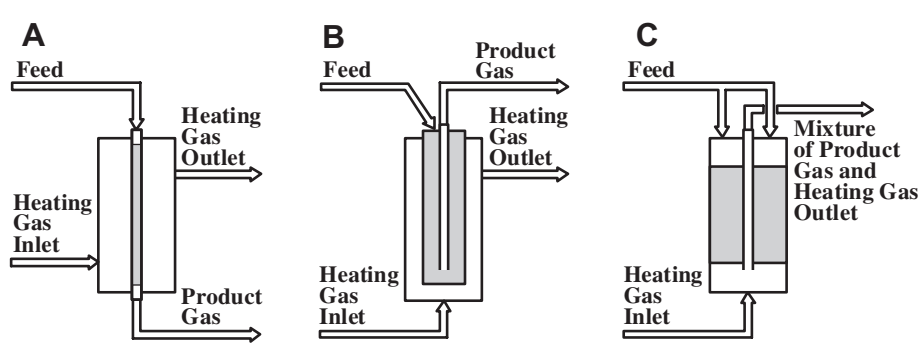

Fig. 23. (A) Concept with 'straight-through' tubes; (B) Concept with bayonet tubes; (C) Concept with mixing of heating gas and product gas before heat exchange.

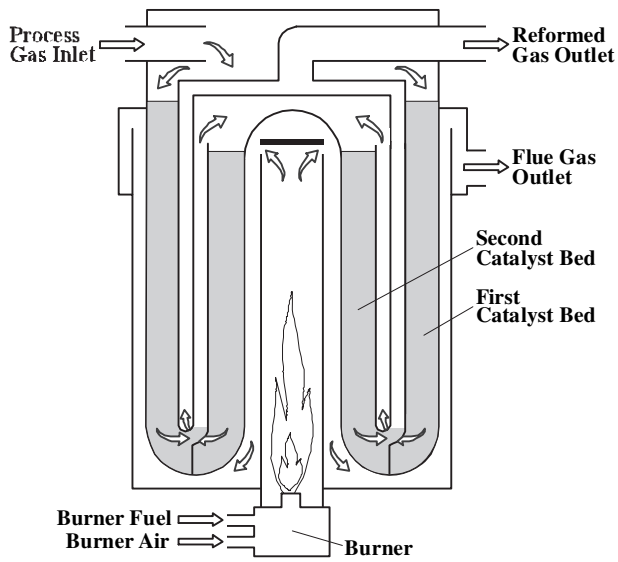

Fig. 24. Heat exchange reformer (HER).

exchange reformers with either a fired tubular reformer or a secondary or autothermal reformer are described. Only cases with one feed are considered. This feed will most often be natural gas or prereformed natural gas. The cases may be divided into two main types, series and parallel arrangements.

3.5.2.1. Series arrangements. In series arrangements, all the process feed gas passes through first a heat exchange reformer and then through a second reformer, and the product gas from the second reformer supplies heat to the heat exchange reformer. The second reformer in the series arrangement may be a fired tubular reformer (Fig. 26). This process concept has been referred to as 'Gas Heated Prereforming'.

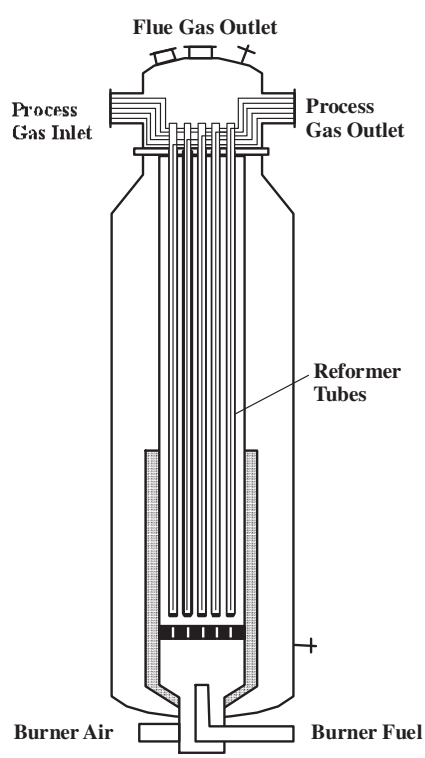

Fig. 25. Convection reformer (HTCR).

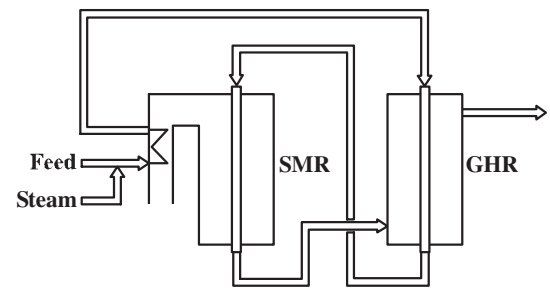

Fig. 26. Gas heated prereforming: fired tubular reforming (SMR) and GHR in series arrangement.

Alternatively, the second reformer may be an air or O_2-blown secondary reformer (Fig. 27). This concept, which is often referred to as GHR, is equivalent to two-step reforming and could be called 'two-step reforming with GHR'. (In two-step reforming, a fired tubular reformer is operated in a similar way in series with an air-fired secondary reformer for production of NH_3 synthesis gas or with an O_2-blown secondary reformer for production of synthesis gas for methanol or FT synthesis.)

There is an alternative where only part of the feed passes through the GHR, while the rest is bypassed direct to the secondary reformer (Fig. 28). This could be called 'Combined reforming with GHR'.

The operating conditions (e.g. S/C ratio) may in these concepts be limited by the steam reforming in the GHR, whereas the final gas composition will be determined by the exit conditions from the secondary reforming.

3.5.2.2. Parallel arrangements. For obvious reasons, the 'two-in, one-out' concept can only be used in parallel arrangements, i.e. process arrangements, where the feed gas is split into two streams. One goes direct to a conventional reformer, while the other goes to a gas heated reformer heated by the outlet gas from the conventional reformer or by the mixed outlet gases from the two reformers. In parallel arrangements, either the GHR or 'two-in, two-out' design or the GHHER or 'two-in, one-out' design can be used. With a GHR, it is in principle possible to produce two different product gases, whereas the GHHER for obvious reasons allows only production of one product gas, the mixture of product gases from the two reformers. The heat exchange reformer may be coupled with a tubular reformer or with an air or O_2-blown autothermal reformer. Operating conditions (S/C ratio) in the two reformers may

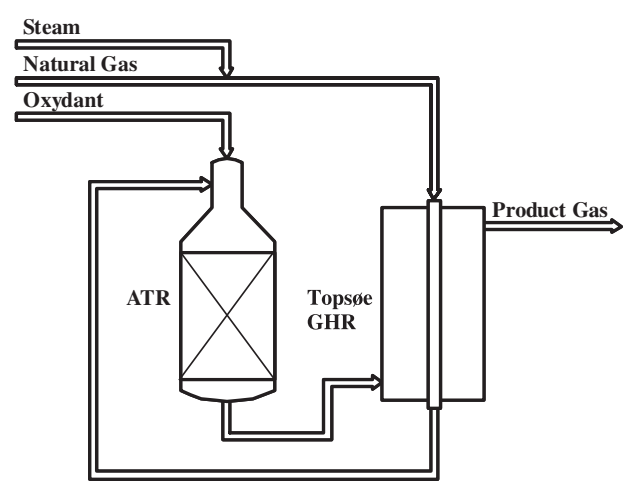

Fig. 27. Two-step reforming with GHR: ATR and GHR in series arrangement.

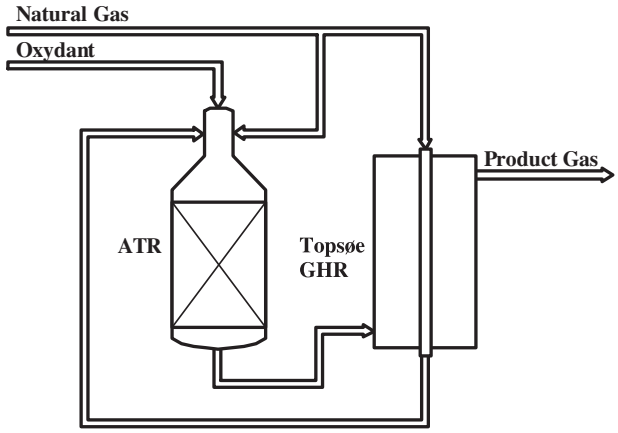

Fig. 28. Combined reforming with GHR: ATR and GHR in series arrangement with partial by-pass of feed over the GHR.

be different; final gas composition is determined by the exit conditions from the two reforming catalyst beds. The four possible schemes are shown in Figs. 29–32.

3.6. Metal dusting

Metal dusting corrosion can be a challenge in all process equipment involving synthesis gas operating with metal temperatures in the range of 400–800 °C. In particular, in all process concepts using heat exchangers heated by process gas, e.g. gas heated reformer applications, the problem of avoiding metal dusting corrosion on the heat transfer surfaces is a significant challenge. Metal dusting corrosion results in loss of material, in some cases as 'metal dust', a mixture of metal, carbides, and/or carbon. In severe cases the material wastage can be very fast, leading to catastrophic failure of equipment as well as plugging of downstream equipment.

The attack is most often seen as shallow pits, but in other cases the attack is over the entire surface. The corrosion product is a mixture of carbon, metal oxides and metal particles. Figs. 33 and 34 show examples of metal dusting attack.

The mechanism behind metal dusting involves the formation of carbon from CO and, more rarely, hydrocarbons. The carbon forming reactions are the Boudouard reaction, the CO reduction reaction and the methane cracking reactions (see Table 3). Carbon atoms are believed to adsorb on the metal surface, dissolve in the base metal and form carbides (iron carbides if the base metal is carbon steel, chromium carbides if the base metal is stainless steel or a nickel alloy). Carbides decompose into solid carbon and metal particles that on one hand further catalyse the formation of carbon

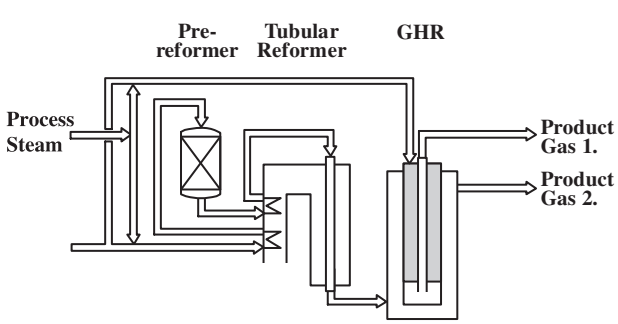

Fig. 29. Tubular reformer (SMR) and gas heated reformer ('two-in, two-out', GHR) in parallel arrangement.

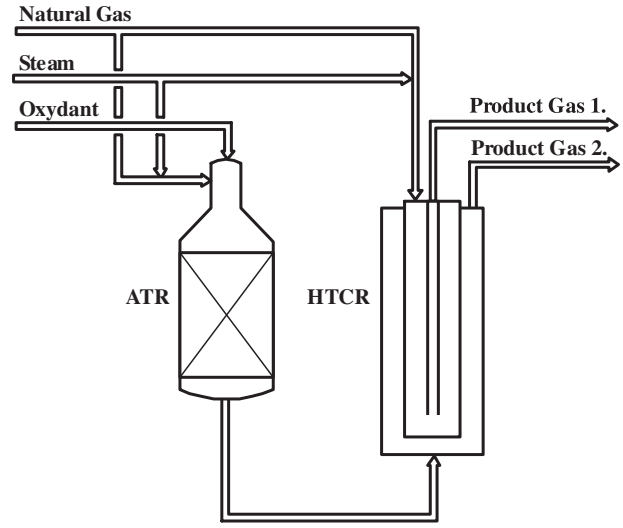

Fig. 30. Autothermal reformer (ATR) and gas heated reformer ('two-in, two-out', GHR) in parallel arrangement.

and on the other hand oxidise to inhomogeneous scales on the surface. The most current theories of the mechanisms behind metal dusting are described in Agüero et al. (in press).

It is well known that some alloys are more prone to attack by metal dusting than others. This is ascribed to the fact that some alloys are better at forming and maintaining sound and stable chromium oxide scales (alternatively alumina scale) that restrict the carbon diffusion into the material. Industrial experience has demonstrated that commercial alloys like Inconel 690, Alloy 602 CA, Inconel 693 and most recently Sumitomo 696 all have significant resistance to metal dusting attack (Baker et al., 2002; Agarwal et al., 2001; Nishiyama and Otsuka, 2009). In severe synthesis gas environments, the afore-mentioned alloys are not immune but do exhibit longer incubation times (for the first pits to appear) and low rates of material wastage compared to other materials.

Apart from alloy composition, many factors impact whether metal dusting will be seen or not in a specific synthesis gas environment. The pre-treatment of the alloy is of the utmost importance. A surface with a mixed oxide or a surface depleted of Cr will tend to corrode rapidly. The severity of the gas composition is critical. Some efforts have been put into getting an understanding of the gas severity of a certain gas composition in terms of its potential for attacking metals, but so far, no precise understanding has been achieved. It is, however, clear that the partial pressure of CO plays a major role but also the presence of steam and hydrogen is determining for the gas aggressivity.

Carbon penetration into the material can also be prevented by application of a coating on the metal surface. Various coating

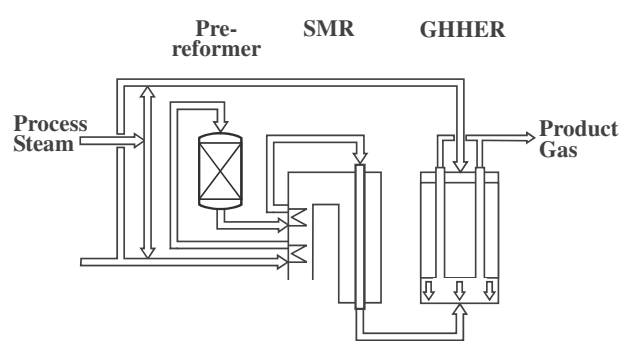

Fig. 31. Tubular reformer (SMR) and Gas heated reformer ('two-in, one-out', GHHER) in parallel arrangement.

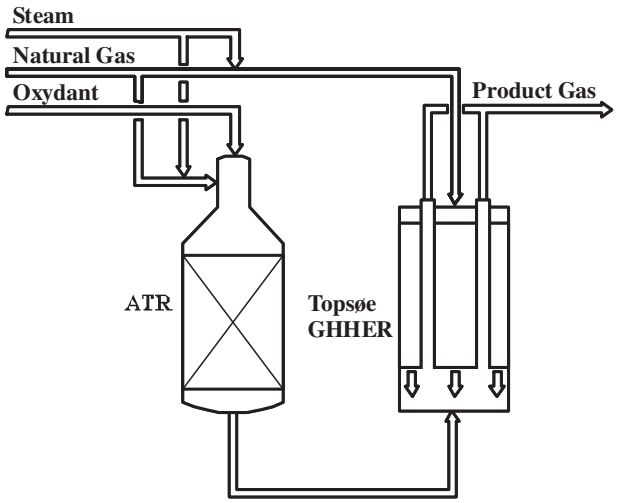

Fig. 32. Autothermal reformer (ATR) and gas heated reformer ('two-in, one-out', GHHER) in parallel arrangement.

systems have been proposed and investigated (Agüero et al., in press). Coating systems based on nickel-aluminides (NiAl) do have the most promising properties in terms of industrial application and lifetime. The foolproof coating system against metal dusting does, however, not exist as of today, but as described in Agüero et al. (in press), a significant research effort goes into this area.

Another way of mitigating the risk of metal dusting is by addition of sulphur (or phosphor) to the process. Sulphur inhibits or slows down the catalytic formation of carbon and at the same time it covers the active sites of the alloy crystal structure in which carbon would otherwise adsorb.

4. Adiabatic oxidative reforming

In adiabatic oxidative reforming the heat for the reforming reactions is supplied internally by combustion of part of the reactants. This is in contrast to fired tubular reforming (Section 3.4) and heat exchange reforming (Section 3.5), where the heat is supplied by heat exchange from an external source.

In steam reforming, where the hydrocarbon feed is reacted with steam alone, the composition of the raw synthesis gas is governed by the steam reforming reaction and the shift reaction only. In

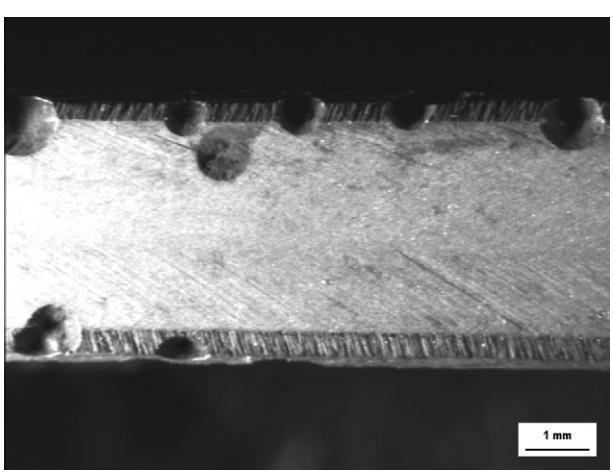

Fig. 33. Typical pitting attack caused by metal dusting.

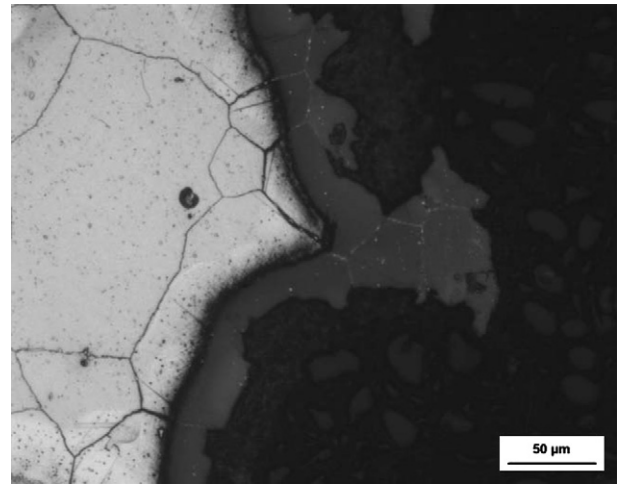

Fig. 34. Micrograph showing a typical (severe) metal dusting attack.

adiabatic oxidative reforming, additional reactions are introduced. The overall reaction is adiabatic, meaning that there is no exchange of heat with the surroundings (except a very limited heat loss). The composition of the raw synthesis gas can be predicted by a heat and mass balance over the reactor. It should be noted that the combustion reactions are all irreversible. For production of synthesis gas a sub-stoichiometric amount of oxidant is added. All oxygen will thus be consumed because this is the limiting reactant.

4.1. Process concepts

The process concepts for adiabatic oxidative reforming may be split into three categories considering the type of chemical reactions taking place in the reactor:

- homogeneous reactions
- heterogeneous reactions
- combination of homogeneous and heterogeneous reaction

Furthermore, adiabatic oxidative reforming processes may be characterised by the type of feed. If the feed comes directly from a desulphurisation unit or from a prereformer, and the reactions are carried out homogeneously without the aid of a reforming catalyst, then the oxidative adiabatic reforming is referred to as gasification or non-catalytic partial oxidation (POX). If the reactions are carried out heterogeneously on one or several catalysts, they are referred to as catalytic partial oxidation (CPO). If they are initiated by homogeneous reactions, e.g. in a burner, and completed by heterogeneous catalysis, then the reactor is called an autothermal reformer (ATR). If the feed has been partly reformed in a fired tubular reformer, the ATR reactor is most often called a secondary reformer.

A survey is shown in Table 5.

4.2. Autothermal reforming

Autothermal reforming (ATR) has been used to produce hydrogen-rich and carbon monoxide-rich synthesis gas for decades. In the 1950s and 1960s autothermal reformers where used to produce synthesis gas for ammonia production and methanol (Topsoe-SBA, 1962; ChemEng, 1962). In ammonia plants, hydrogen production was maximised by operating at high steam-to-carbon ratios ranging from 2.5 to 3.5 on a molar basis, while in the methanol units carbon dioxide recycle adjusted the synthesis gas composition. In the early 1990s, the technology was improved and

Table 5
Survey of process concepts and characteristics.

	Secondary reformer (Air)	Secondary reformer (O_2)	Autothermal reformer (O_2)	CPO (O_2)	CPO (Air)	POX (O_2)
Burner/mixer type	Burner	Burner	Burner	Mixer	Mixer	Burner
Hydrocarbon feed	Process gas[a]	Process gas[a]	Natural gas	Natural gas	Natural gas	Natural gas
Feed temp. °C	700–850	750–810	350–650	<200	<AIT[b]	<
H_2O/C ratio, mole/mole	2.0–3.5	1.2–2.5	0.5–3.5	0–2	<2.0	0–0.2
O_2/C in feed, mole/mole	0.25–0.3	0.3–0.4	0.4–0.6	0.5–0.65	0.5–0.75	0.5–0.7
Flame peak temp. °C	Up to 2000	Up to 2500	2500–3500	–	–	2500–3500
Exit temp. °C	850–1020	950–1050	850–1100	750–1300	750–1200	<450
Typical products	Ammonia synthesis gas	Methanol synthesis gas	Syngas for FT synt.		Fuel cells/Syngas for FT synt.	

[a] Partly converted process gas from primary reformer.
[b] Preheat depends on the auto-ignition temperature of the fuel.

operation at much lower steam-to-carbon ratios was achieved (Christensen and Primdahl, 1994).

For the production of CO-rich synthesis gas as feed for e.g. methanol or FT synthesis, operation at low steam-to-carbon ratio is beneficial. Operation at an H_2O/C ratio of 0.6 has been demonstrated in pilot scale (Christensen and Primdahl, 1994; Christensen et al., 1998, 2001) and industrial scale (Ernst et al., 2000; Dybkjær, 2006; Topsoe, 2010).

ATR is a combined combustion and catalytic process carried out in an adiabatic reactor as illustrated in Fig. 35. The ATR reactor consists of a burner, a combustion chamber and a catalyst bed, all of which are contained in a refractory lined pressure shell.

A mixture of natural gas and steam is partially converted by pressurised combustion under fuel-rich conditions in the combustion chamber. The temperature in the combustion chamber is in the range of about 1100–1300 °C near the catalyst bed and up to more than 2500 °C in the flame core depending upon the process conditions. In the combustion chamber also the steam reforming and water gas shift reactions take place non-catalytically due to the high temperature. In reality a very large number of chemical reactions take place in the combustion chamber involving radicals and a number of combustion reactions. For simplicity, the reactions shown in Table 6 are often used to represent the combustion chamber:

The oxygen is quantitatively consumed by the combustion reactions. However, the methane conversion is not complete in the combustion chamber. The final conversion of methane takes place in the catalyst bed according to reactions (2) and (3) in Table 6. The synthesis gas leaving the ATR reactor is at chemical equilibrium typically between 850 and 1100 °C.

The reactor can be divided into three zones;

- Combustion zone
- Thermal zone
- Catalytic zone

The combustion zone is a turbulent diffusion flame, where hydrocarbon molecules and oxygen are gradually mixed and combusted. The combustion reactions are exothermic and very fast, and from a global point of view it can be assumed progressing as 'mixed is burnt'. Combustion in an ATR is sub-stoichiometric with an overall oxygen to hydrocarbon ratio of 0.55–0.6 but, when simplified as a one-step model. The flame zone can be described as a single reaction of CH_4 to CO and H_2O with an O_2/CH_4 ratio of 1.5 (reaction (1) in Table 6). The local stoichiometry in the flame zone will vary from very fuel-lean to very fuel-rich.

In the thermal zone further conversion occurs by homogeneous gas-phase-reactions. These reactions are slower reactions like CO oxidation and pyrolysis reactions involving higher hydrocarbons. The main overall reactions in the thermal zone are the homogeneous gas-phase steam methane reforming and shift reaction (reactions (2) and (3) in Table 6). As indicated above the methane steam reforming reaction (2) does not proceed to equilibrium in the thermal zone.

In the catalytic zone the final conversion of hydrocarbons takes place through heterogeneous catalytic reactions including steam methane reforming (2) and shift reaction (3).

Fuel-rich combustion in partial oxidation processes involves the risk of incomplete combustion. Methane combustion under fuel-rich conditions is mainly proceeding through reaction steps with C_2-radicals as intermediates, which may react to soot precursors like poly-aromatic hydrocarbons (PAH) and further to soot particles (Philipson, 1970; Warnatz et al., 1996).

ATR operation is soot-free under normal circumstances. The fuel rich combustion takes place in a turbulent diffusion flame and intensive mixing is required to prevent soot formation. The exit gas contains no other hydrocarbons than methane. Soot formation is unwanted and would reduce the carbon efficiency of the process, and soot particles would need to be removed from the synthesis gas.

Careful design of the process burner and combustion chamber and selection of optimal process conditions are required in order to

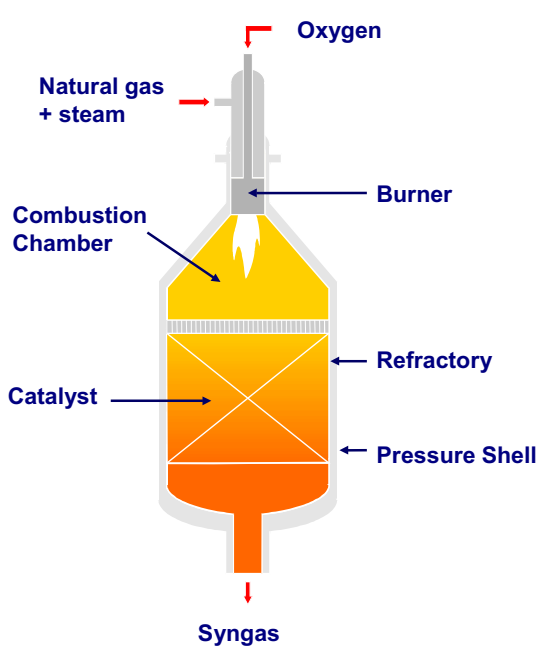

Fig. 35. Illustration of an ATR reactor (Christensen et al., 2001).

Table 6
Simplified reactions in the combustion chamber.

Combustion	$CH_4 + {}^3/_2\,O_2 \rightarrow CO + 2\,H_2O$, $\Delta H_{298}{}^o = +519$ kJ/mole	(1)
Reforming	$CH_4 + H_2O \rightleftarrows CO + 3H_2$, $\Delta H_{298}{}^o = -206$ kJ/mole	(2)
Shift	$CO + H_2O \rightleftarrows CO_2 + H_2$, $\Delta H_{298}{}^o = +41$ kJ/mole	(3)

avoid excessive temperatures and to avoid soot formation. Further, the detail design and construction of the whole ATR reactor including refractory and catalyst bed is of the utmost importance for ensuring safe design and operation of the syngas unit. Predictions and design are facilitated by reactor models based on fluid flow by use of computational fluid dynamics (CFD) and on chemical kinetics.

4.2.1. ATR reactor design

The ATR process burner is a key element of the technology. The burner provides the mixing between the hydrocarbon feed and the oxidant in a turbulent diffusion flame. The flame core may exceed 2500 °C. It is essential to minimise heat transfer by thermal radiation or hot gas recirculation to the burner parts.

In the design of the burner and the combustion chamber, the following reaction-engineering aspects must be considered in order to ensure optimal reactor performance, safe operation and satisfactory equipment lifetime:

- Effective mixing at the burner nozzles
- Low-metal temperature of the burner
- Soot-free combustion
- Homogeneous gas and temperature distribution at the catalyst bed entrance
- Protection of the refractory from the hot flame core

Recirculation of the reacted gas from the thermal zone to the burner can protect the refractory and the burner from the hot flame core and gases from the combustion zone. Efficient external re-circulation will enhance the position of the flame core along the centreline of the combustion chamber and protect the refractory from the hot flame core. The temperature of the gas circulating along the walls and into the catalyst bed is reduced to the range of 1100–1300 °C by the endothermic reactions proceeding in the thermal zone.

Sufficient re-circulation will also ensure homogeneous distribution of gas and temperature at the entrance to the catalyst bed. Inhomogeneity will result in larger distance to equilibrium, and the methane concentration in the exit gas will increase. Even distribution of gas to the catalyst bed will maximise the utilisation of the catalyst activity. Even flow and temperature distribution of the gas entering the catalyst bed is obtained by proper design of the combustion chamber.

The flow velocities in the burner nozzles can be selected within wide ranges. Highly turbulent mixing intensity of the diffusion flame is obtained with high velocities in the nozzle gaps. For applications with oxygen or enriched air as oxidant, the flame speed will be faster than for similar air flames (Baukal, 1998). The position of an oxygen flame will be very close to the burner nozzles especially at highly turbulent mixing intensities. A turbulent diffusion flame is in steady-state seen over a certain time period. However, an inherent feature of the turbulent flame is that the flame is dynamic and changes position within short time frames.

Operation of burners in secondary reformers and autothermal reformers in the industry has from time to time faced problems. The problems may range from catastrophic failure to burner wear without serious process complication.

Catastrophic failures of process burners include situations where the defective burner causes damage to the refractory and pressure vessel resulting in unscheduled shut-down and production loss. Further, a necessary repair of the reactor vessel and replacement of the refractory lining are consequences. Such an example of a catastrophic failure of an oxygen-blown secondary reformer refractory and reactor shell following a burner related incident is described in (Shaw et al., 1994). Burners for high temperature reformers can be designed with a focus on mechanical and thermal integrity in combination with the combustion chamber design (Christensen et al., 1994). CFD (Computational Fluid Dynamics) can be used to predict the flow pattern and avoid unwanted behaviour.

It is more common that burners are subject to wear of a local character. Burner wear may appear and develop slowly, but maintenance or replacement of critical parts can be done at scheduled shutdowns.

The reactor vessel is lined with refractory. The refractory insulates the steel wall of the pressure vessel from the high temperature reaction environment. The refractory is commonly constructed of several layers with different materials and insulation properties. Efficient refractory design ensures that reasonably low mechanical temperatures can be applied. Typically the temperature of the reactor wall is reduced to 100–200 °C at normal operation.

In air-blown secondary reformers it is common practice today to use a design with two refractory layers. In older designs only one layer was applied, but such a design was sensitive to cracks in the refractory layers, which resulted in gas flow and transfer of heat to the shell and thereby in hot spots on the pressure shell (Sterling and Moon, 1974). In oxygen-blown secondary reformers and ATR reactors the operating conditions are more severe including a higher operating temperature in the combustion zone. In ATR reactors, a refractory design with three layers of refractory is commonly used today. The inner layer has high thermal resistance and stability and is typically a high density alumina brick layer. The installation of the refractory lining is important and involves skilled craftsmen.

Circulation of hot gas from the high temperature combustion chamber and the catalyst bed through the refractory layers to the reactor wall does not occur with a proper refractory design and installation. However, it must be considered a potential risk and may lead to increased temperatures at the reactor walls. These could in some cases develop into so-called 'hot spots' where the design temperature of the vessel is approached or exceeded. The risk of gas bypass through the refractory is most pronounced in the combustion chamber where the temperature is highest.

The catalyst equilibrates the synthesis gas and destroys soot precursors. The catalyst particle size and shape is optimised to achieve high activity and low pressure drop in order to obtain a compact reactor design.

The hydrocarbons are only partly converted in the combustion chamber. The gas leaving the combustion chamber contains methane and a minor content of other hydrocarbons in some cases formed in the combustion chamber. In the catalytic zone the final conversion of methane and other hydrocarbons takes place.

The methane steam reforming reaction is endothermic and the temperature will decrease from typically 1100–1300 °C at the inlet to the catalyst bed to typically 900–1100 °C at the exit of the catalyst bed. The catalyst bed operates adiabatically.

A layer of protecting tiles is often placed on top of the catalyst bed for protection from the very intense turbulent flow in the combustion chamber. The radiation from the flame and the circulation velocities in the combustion chamber require that the tiles have a high thermal stability and are able to resist the thermal shocks during start-up and trips.

Sintering proceeds as in all steam reforming catalysts, see Section 3.2.2. However, the activity of the catalyst in ATR service is rapidly reduced due to the high operating temperatures, and after this initial sintering only minor further deactivation is expected due to sintering.

The requirements for the catalyst include:

- high thermal stability
- sufficient activity to reach equilibrium
- low pressure drop to avoid bypass of gas through the refractory

The support for the nickel catalyst must have a high thermal stability to achieve sufficient strength at the high operating temperatures. In ATR and secondary reformers supports of both alumina (α-Al_2O_3) and magnesium alumina spinel ($MgAl_2O_4$) are used. Spinel has a higher melting point and it generally has a higher thermal strength and stability than the alumina based catalysts.

The shape of the catalyst pellet is an important design parameter for the catalyst bed. The pressure drop should be kept low in order to reduce the risk of bypass around the catalyst bed through the refractory. Gas bypass into the refractory could lead to increased temperature on the pressure shell as described above. A shape optimised catalyst with low pressure drop and high resistance to ruby deposition (see below) should be used. One example is a catalyst with seven axial holes, as described in Christensen et al. (1994). The optimal loading of the catalytic fixed bed in the ATR reactor may consist of several layers of different types of catalysts.

Catalysts in an ATR are usually not deactivated substantially by poisons due to the high operating temperature. As in other reformer types, sulphur also reduces the catalyst activity in an ATR. However, the sulphur coverage under ATR operating conditions is relatively low and can be estimated at around 30% under typical operating conditions. The removal of sulphur upstream of the ATR for protection of the catalyst may not be required. However, this is done in most cases anyway to protect downstream shift or synthesis catalysts.

In ATR and secondary reformers, it is common to observe a deposition of white and pink crystals on the catalyst outer pellet surface. The crystals are mixtures of alumina and chromium-alumina spinel. The latter is also known as the ruby with a purple colour. Ruby formation is not poisoning as such, but it reduces the run time between shutdowns because the pressure drop over the catalyst increases and may lead to hot spots on the reactor wall. Ruby formation and deposition are well known to industry, but the knowledge about the mechanism of ruby formation is very empirical. A case story is described in Pasaribu et al. (2002) supported by some more theoretical viewpoints. The primary process leading to fouling seems to be transport of 'rubies' from the refractory and deposition in the catalyst bed. The 'ruby' formation is caused by evaporation of aluminium species, probably AlOOH, from the high-alumina bricks in the refractory. When the gas in the catalyst bed is cooled because of the reforming reaction, AlOOH will condense and together with impurities of chromium and iron deposit as rubies. The chromium and the iron come from construction materials upstream of the combustion chamber and the ATR reactor. Often ruby deposition is seen in a narrow section in the upper part of the catalyst bed. In such cases, only 'skimming' of the layer with rubies may be sufficient to solve pressure drop problems.

4.2.2. ATR process performance tests at low S/C ratio

Numerous tests with varying operating parameters were performed in the ATR PDU in order to establish the design background and limits of operation at very low H_2O/C ratio (0.6 and below). This included the influence of variations in H_2O/C ratio, temperatures and pressure as well as the effect of feed composition such as content of higher hydrocarbons, CO_2, and H_2 on the limits for soot-free operation.

The limits for formation of poly-aromatic hydrocarbons and soot were determined in pilot-scale in an ATR PDU reactor representing real-environment operation including operation with prereformed natural gas, variations in feed gas composition with different levels of C_2^+ in natural gas, and variations in recycle gas composition including CO_2 and hydrocarbons both in the form of paraffins and olefins. The experiments with prereformed natural gas showed a larger margin to the onset of soot formation than with a natural gas containing higher hydrocarbons under similar operating conditions. Even though the prereformed natural gas implies an improvement with regard to the risk of soot formation in the ATR, it is still prone to form soot under certain operating conditions, which made it necessary to establish the limits and extend the design knowledge to include a wider range of feedstocks.

Explorative tests as well as demonstration runs of longer duration with steam-to-carbon ratios in the range of 0.2–0.6 are described in Christensen et al. (1998). The tests were made with the purpose of reducing the H_2O/C ratio as much as possible without reaching the range of soot formation. Results from various pilot programs are collected in Fig. 36 (Christensen and Primdahl, 1994; Christensen et al., 1998) and Table 7.

All data represent operating conditions without soot formation, but they do not represent the limits of the technology. The ATR can produce synthesis gas within a wide H_2/CO-ratio range, when the H_2O/C ratio, recycle with CO_2-containing gas and exit temperatures are optimised.

4.2.3. Modelling the ATR reactor

As to the modelling, the ATR can be separated into two parts: the burner and the combustion chamber as one part and the fixed adiabatic catalyst bed as the second part. One model could capture the behaviour of the reactants in both parts, but it is often advantageous to split the models at the entrance to the catalyst bed. The nature of the flow, the combustion and the reforming reactions in the combustion chamber are very complex and therefore the modelling of this part is heavily relying on Computational Fluid Dynamics. More simple models would, on the other hand, suffice for the fixed catalyst bed.

4.2.3.1. Computational fluid dynamics. Computational Fluid Dynamics (CFD) is a significant tool for design and performance prediction of the autothermal reformer, the oxygen fired secondary reformer or the secondary reformer. For severe applications at for instance low steam-to-carbon ratios, CFD simulations are mandatory to fully understand the conditions prevailing around the burner, in the combustion chamber and gas entry into the catalyst bed.

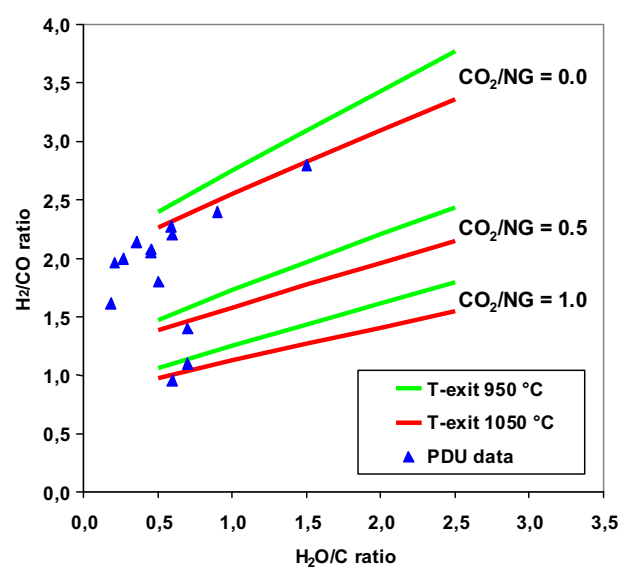

Fig. 36. Syngas equilibrium; experimental data from soot-free ATR-operation (Christensen and Primdahl, 1994; Christensen et al., 1998).

Table 7
ATR pilot plant demonstration runs (Christensen and Primdahl, 1994; Christensen et al., 1998).

Test	A	B	C	D	E
Feed ratios[a] *(mole/mole)*					
H_2O/C	0.59	0.21	0.51	0.60	0.36
CO_2/C	0.01	0.01	0.19	0.01	0.01
O_2/C[b]	0.62	0.59	0.62	0.58	0.57
Product gas					
Temperature (°C)	1065	1065	1025	1020	1022
Pressure (bar)	24.5	24.5	27.5	28.5	28.5
H_2/CO (mole/mole)	2.24	1.96	1.80	2.30	2.15
CO/CO_2 (mole/mole)	5.05	9.93	4.44	4.54	6.78
CH_4-leakage (dry mole %)	0.48	1.15	0.92	1.22	1.66

[a] Mole per mole of hydrocarbon C-atoms½.
[b] The O_2/C-ratio is approximately 5% higher than truly adiabatic reactors with same exit temperature.

With CFD analyses, the behaviour of gases flowing in complex geometries undergoing chemical reactions may be simulated. The simulations give us detailed information on the variables: three-dimensional velocity field, the turbulence level and the distribution of temperature, pressure and chemical composition.

In order to achieve these results, the reactor geometry is divided into a mesh of millions of computational volumes, each holding information on the local variables and their derivatives in time and space. The overall equations of momentum and energy conservation are solved in an iterative manner.

CFD modelling involves a number of choices that will have a significant impact on the quality of the simulation result:

- the computational mesh and the resolution in time
- choice of turbulence model
- method of modelling chemical reactions

The simulation accuracy is very dependent on the computational mesh. The mesh needs to be very fine in areas where large gradients in any of the variables are expected and could be coarser in low gradient areas or areas of lesser interest. For large ATR simulations where the interest is both in the fluid behaviour in the burner zone and in the physically much larger flame and reaction zones, the need for accuracy can lead to very large simulation models. Sometimes, a steady state solution is sufficiently accurate to capture the physical behaviour, but in most simulations related to autothermal reforming, it is required to perform transient simulations with very small time steps. All in all, this puts heavy requirements on the computer hardware and often, only by means of High Performance Computer clusters with massive parallelisation of the simulation, will it be possible to achieve good and reliable results within an acceptable time frame (i.e. days or weeks).

The correct choice of turbulence model is similarly important but this choice is by no means straightforward. Turbulence modelling is used to predict how small-scale fluctuations in the turbulent flow will affect the average flow field. Different models attack this problem in different ways and encompass different levels of complexity – and yield for those reasons different results. Therefore, in order to put some trust into the CFD simulations, validation of the CFD models is of the utmost importance.

In Fig. 37 from Gyde Thomsen et al. (2007), a set of experimental data is compared with simulation results for two different simulation approaches on an ATR burner – one turbulence model used in steady-state mode and transient mode respectively. It is seen that, while the more advanced model captures the fact that there is a (possibly detrimental) central back flow in the burner, the steady state model does not.

The modelling of chemical reactions in the flowing media adds another level of complexity to the problem. The time scales of the chemical reactions are often many orders of magnitude smaller than those of the fluid flow and therefore direct implementation of chemical reaction schemes leads to numerical instability of the CFD simulation.

Different approaches exist to overcome this problem (Poinsot and Veynante, 2005). For simulations of combustion processes it often suffices to assume that the reaction rates are infinitely high whereby combustion is controlled by turbulent mixing. If studies of emissions are involved or focus is on local chemical composition, more sophisticated models are required. These typically involve some kind of statistical approach (probability density functions) and are linked to assumptions of local transport being controlled by diffusion. In some cases complete chemistry is modelled (typically though, adopting reduced skeleton mechanisms to minimise computational effort) using dedicated stiff chemistry equation solvers to ensure robustness of the simulation process.

Because of the complex nature of the interaction of the turbulence and reaction kinetics, it is difficult to obtain very accurate

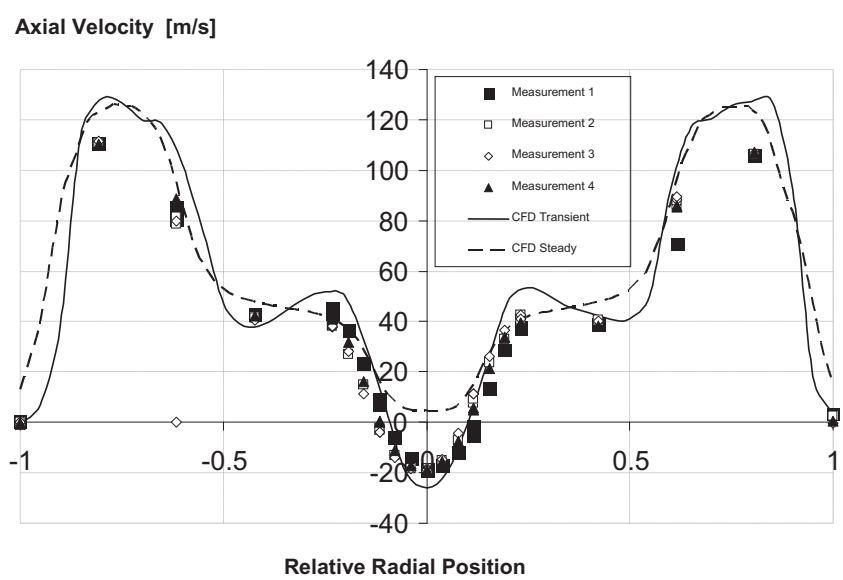

Fig. 37. Example of verification of CFD simulations against measurements.

results even with the most advanced models. Experience shows that the models often either overestimate or underestimate the chemical reaction. It is therefore, again, necessary to validate the results against pilot data and industrial experience and introduce appropriate corrections in the modelling. Also, as a supplement to the CFD based calculation, general chemical kinetic modelling is used to predict the conversion in the combustion zone of the ATR, see for instance (Christensen et al., 2001).

An example of a CFD simulation results for an ATR burner and combustion chamber is shown in Christensen et al. (1994). This simulation was made with a commercial computer program (CFX-4) using a 2D model assuming rotational symmetry in the combustion chamber. The results of a more state-of-the-art simulation are shown in Fig. 38. Here, a full 3D model has been adopted and the simulation has been run for a large number of time steps in transient mode. A Reynolds-Stress type of turbulence model is used, and both the combustion and reforming reactions have been accounted for in the simulation. Although the simulation has been carried out in transient mode to capture the inherently fluctuating nature of the pressure and flow field, the figure depicts time-averaged results. It is noted that the flow pattern in the combustion chamber exhibits a centrally positioned flame with good re-circulation or back-mixing that ensures that the refractory is kept cool. Likewise, the mixing ensures a homogeneous composition and temperature field at the inlet to the catalyst bed.

4.2.3.2. Fixed bed simulation of the catalyst bed. Simulation of the catalyst bed includes radial distribution of gas and temperature, gas diffusion in the gas film and catalyst pore system, heterogeneous catalysis reactors and pressure drop. The catalyst bed is simulated by fixed bed reactor models using input from the CFD simulation with respect to the gas and temperature distribution profiles into the fixed bed. Although the pressure drop is the simplest part, it may nevertheless be the most important, since a catalyst with too high pressure drop will result in gas bypass through the refractory leading to hot-spots on the pressure shell.

Fixed-bed reactor models are divided into two groups: pseudo-homogeneous and heterogeneous models (Froment and Bischoff, 1990). The catalyst performance is controlled by a combination of both film diffusion and pore diffusion, and relatively successful simulations were achieved with both a heterogeneous model (Christiansen and Jarvan, 1986) and with a pseudo-homogeneous model (Rostrup-Nielsen et al., 1988). A key parameter in determining the necessary catalyst volume is the gas distribution at the entrance to the catalyst layer. Burners of poor design and damaged burners may cause an increased average methane leakage from the catalyst bed as a result of inefficient mixing in the combustion chamber leading to uneven flow and temperature distribution at the entrance to the catalyst bed (Christensen et al., 1994). Even with an optimal burner design, some gradients in temperature and concentrations are observed along the radius of the reactor as a result of the mixing efficiency. Variations in the O/C and H/C atomic ratios along the inlet to the catalyst bed will result in different adiabatic equilibrium states at the exit of the catalyst bed, which may be seen as an overall approach to equilibrium which is caused more by mixing and gas distribution than by catalyst activity.

5. Other technologies

Most or all of the technologies described in the previous section are in commercial use today for production of synthesis gas. However, substantial efforts to develop new technologies are undertaken due to the fact that the most capital intensive part of large-scale plants is the Syngas Generation Unit (SGU). The focus of many of these developments is to reduce or eliminate the use of oxygen and/or reduce the size of the primary reactor in the SGU. In the following text the production of synthesis gas by CPO and Oxygen Membrane Reforming (OMR) will be briefly described.

5.1. Catalytic partial oxidation

The principle of CPO is illustrated in Fig. 39. The hydrocarbon feed and the oxidant are mixed in an inlet zone upstream of the catalyst bed. In the catalytic section, the mixture reacts by heterogeneous reactions (partial and total combustion along with the methane steam reforming and shift reactions). The catalyst is normally based on noble metals and the space velocity is in many cases very high. Catalysts in the form of pellets, monoliths, and foams have been used to perform the reaction.

The methane steam reforming and shift reactions are typically at or close to equilibrium at the reactor exit. It has been claimed (Choudhary et al., 1992) that methane reacts by partial oxidation according to reaction (15) below and that methane conversions above those corresponding to thermodynamic equilibrium of the methane steam reforming reaction can be obtained.

$$CH_4 + ½O_2 \rightarrow CO + 2H_2 \quad (15)$$

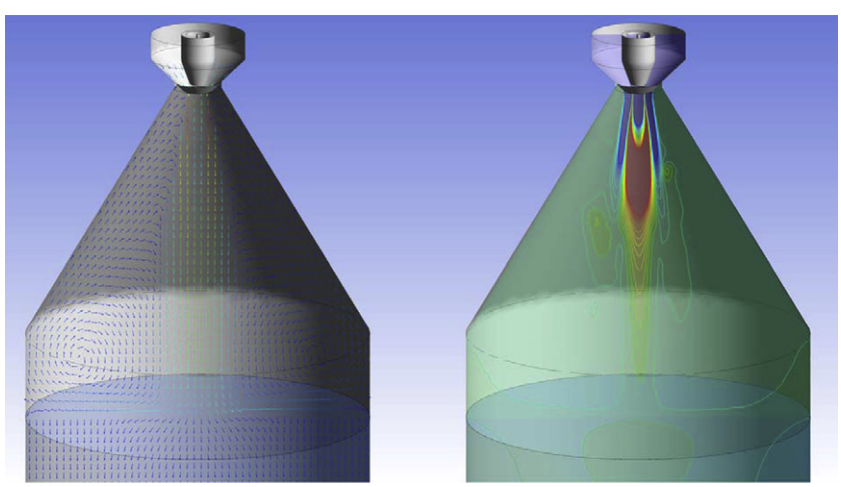

Fig. 38. Example of CFD modelling results for the combustion chamber in an ATR reactor. The left part shows time averaged velocity vectors and the right side shows averaged temperatures.

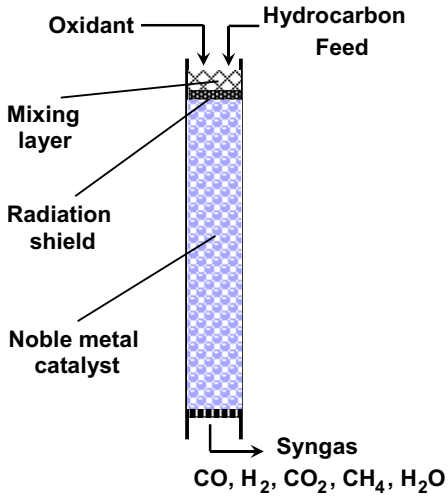

Fig. 39. CPO principle.

However, in practice the products of reaction (15) will further oxidise, and fundamental studies have shown that partial oxidation is only kinetically favoured at temperatures above 900 °C (Schmidt, 2001). Gas compositions indicating higher conversions than thermodynamic equilibrium most likely reflect the temperature of the catalyst (Rostrup-Nielsen, 1993).

CPO differs from ATR especially by the fact that no burner is used. Instead all the chemical reactions take place in the catalytic zone. Total combustion takes place to some extent in the first part of the catalyst layers making the catalyst very hot in this region. Laboratory measurements have indicated that this temperature may be higher than 1100 °C (Basini et al., 2001). In order to avoid overheating of the gas upstream of the catalyst, a thermal shield is often employed as indicated in Fig. 39. It should be noted that the gas temperature remains comparatively low as compared to the catalyst surface temperature in the inlet zone (Basini et al., 2001).

CPO has been investigated extensively for many years. Before 1992 most studies were carried out at moderate or low space velocities at a residence time of 1 s or above (Basini et al., 2001). However, later CPO has been carried out at least in the laboratory at very short contact times between 0.1 and 10 ms in some cases without preheating the feedstock and with no steam addition. Additional information regarding research, mainly of a fundamental nature, can be found for example in a series of papers by L.D. Schmidt and co-workers (Schmidt, 2001; Hickman and Schmidt, 1992, 1993; Hickman et al., 1993; Torniainen et al., 1994; Dietz and Schmidt, 1995).

Both air and oxygen may in principle be used as oxidant in a CPO reactor. An example of the use of oxygen in a CPO reactor in the laboratory is given in Fig. 40, illustrating that stable conversion may be obtained at elevated pressure. Experiments with CPO and air as oxidant have been conducted at the Topsøe pilot plant in Houston, Texas. Selected results at various pressures with and without steam in the feed are presented in Fig. 41. In all cases, the methane conversion corresponds closely to the equilibrium of the methane steam reforming reaction.

The presence of a flammable mixture in the inlet zone upstream of the catalyst may in some cases make use of CPO at high inlet temperatures difficult, especially at elevated pressures. In Table 8 the auto-ignition temperature is given for natural gas in air as a function of pressure. The auto-ignition temperatures are lower with oxygen as oxidant. For safety reasons, the inlet feed temperatures of the hydrocarbon feedstock and oxidant must be kept low. This increases both the oxygen consumption and the natural gas

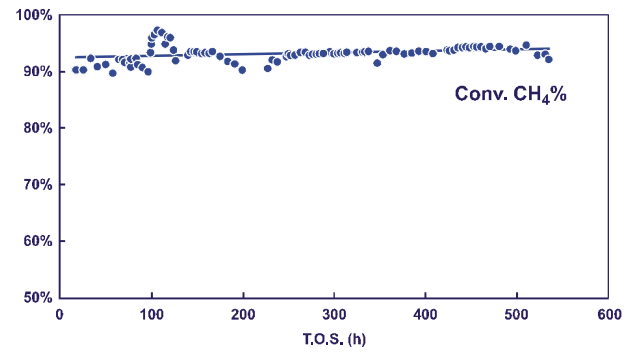

Fig. 40. CPO with methane feed and oxygen as oxidant (Basini et al., 2001). $P = 1.5$ MPa. $H_2O/CH_4 = 0.26$; $CO_2/CH_4 = 0.11$; $O_2/CH_4 = 0.56$.

consumption as shown in Table 9. A higher oxygen consumption increases the air separation unit investment.

The increased oxygen consumption and the potential safety problems related to the premixing of oxygen and hydrocarbon feed make it unlikely that CPO will ever be competitive for large scale production of synthesis gas.

5.2. Oxygen membrane reforming

The principle of Oxygen Membrane Reforming (OMR) is indicated in Fig. 42.

Very significant efforts have been undertaken to develop OMR, see eg. Shen et al. (2003). Air is introduced at one side of a membrane through which oxygen in the form of ions is transported selectively to the other side of the ceramic membrane. On the other side of the membrane, the oxygen ions react with the hydrocarbon feedstock to produce synthesis gas. The concept simultaneously avoids the capital cost of the air separation unit and a high content of inert nitrogen in the synthesis gas. The catalyst on the synthesis side of the membrane may be in the form of pellets or directly attached to the membrane itself.

The membrane itself is made out of a ceramic material often in the form of a perovskite or a brownmillerite. The driving force across the membrane is proportional to the logarithm of the ratio of the partial pressures of oxygen on the two sides. Hence, in principle air may be introduced at ambient pressure to supply oxygen to the other side at elevated pressure because the oxygen partial pressure on the process side is extremely low. The temperature should probably be above 750–800 °C for sufficient oxygen flux.

The membrane material must enable a high flux probably in the range of more than 10 N m^3 O_2/m^2 h. The membrane should also

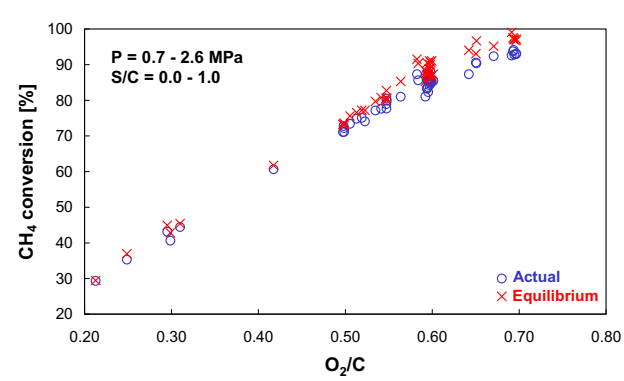

Fig. 41. Methane conversion in CPO pilot plant experiments with air as oxidant.

Table 8
Auto-ignition temperatures for natural gas in air (Groningen, 1988).

Pressure (bar)	Auto-ignition temp. (°C)
1	465
4	313
20	267
40	259

withstand reducing gas on one side and air on the other. Various types of composite membranes have been proposed and research is also undertaken to place a thin membrane on a stronger porous support.

A key challenge in the development of OMR is the absolute pressure difference across the membrane. It may render the process non-economical if air must be compressed to ensure similar pressures on the two sides of the membrane. It puts great demands on the mechanical integrity of the membrane if ambient pressure air is used. In any case, the process may be best suited for small or medium scale applications as the scaling factor of the membrane unit will be close to unity.

At the present stage of development of OMR it is not possible to predict when (if ever) it will be ready for commercial use. Essential issues still remain to be solved, and OMR is not considered to be a competitor for large scale production of synthesis gas within the foreseeable future.

6. Synthesis gas conversion and purification

Synthesis gas prepared by any of the reforming processes described in the preceding paragraphs contains as its main components hydrogen, carbon oxides, nitrogen, argon, and residual methane in concentrations which depend on the properties and amounts of feed materials and on the operating conditions in the reforming section.

Depending on the final use of the synthesis gas, it may be necessary to change its composition, either by changing the ratio between hydrogen and carbon oxides (in plants producing methanol and similar products) or by complete removal of carbon oxides (in ammonia plants). In such cases, the shift conversion technology is important, see Section 6.1. Partial or complete removal of carbon dioxide may be required in these cases. Technology for carbon dioxide removal is not considered within the scope of this paper. Descriptions may be found in Dybkjær (1995a). Finally, it may be desirable to remove nitrogen compounds and other impurities, especially if they are poisons for the catalysts in the synthesis section. Such final purification is discussed in Section 6.2. Final removal of the traces of carbon oxides present after removal of carbon dioxide in ammonia and hydrogen plants by methanation is discussed in Section 6.2.1.

Table 9
Relative oxygen and natural gas consumption for CPO- and ATR-based GTL front-ends for production of hydrogen and carbon monoxide (Zeppieri et al., 2010).

Reactor	S/C ratio	Hydrocarbon feed temperature, reactor inlet (°C)	Oxygen consumption (relative)	Natural gas consumption (relative)
ATR	0.6	650	100	100
CPO	0.6	200	121	109
ATR	0.3	650	97	102
CPO	0.3	200	114	109

An adiabatic pre-reformer is located upstream of the ATR. CO_2 is introduced before the partial oxidation reactor at 200 °C in an amount to give $H_2/CO = 2.00$. Pressure: 25 bar abs. Oxygen temperature: 200 °C. Exit temperature: 1050 °C.

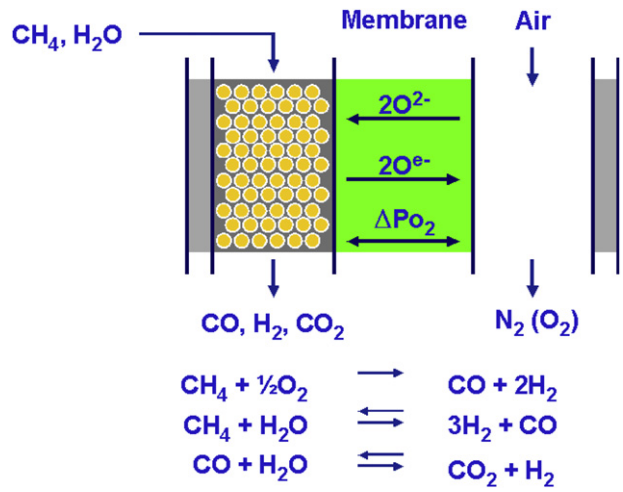

Fig. 42. Principle of oxygen membrane reforming.

6.1. Shift conversion

6.1.1. Introduction

To optimise the yield of hydrogen and to remove carbon monoxide, the water gas shift (WGS) reaction, often referred to as the shift reaction (reaction (3) in Table 2), is carried out:

$$CO + H_2O = CO_2 + H_2$$

The shift reaction is an exothermic, equilibrium limited reaction with $\Delta H^o = -41$ kJ/mol. Since the number of moles is the same on both sides of the equation the WGS equilibrium constant is independent of the total pressure:

$$K_p = \frac{P_{CO_2} \cdot P_{H_2}}{P_{CO} \cdot P_{H_2O}} \tag{16}$$

The temperature dependence of the equilibrium constant can be expressed (Newsome, 1980) as

$$K_p = e^{\left(\frac{4577.8}{T} - 4.33\right)} \tag{17}$$

A typical gas composition equilibrated in the steam reforming reaction is 10.4% CO, 6.3% CO_2, 41.2% H_2 and 42.0% H_2O excluding minor amounts of methane. The calculated equilibrium composition of such gas as a function of temperature is depicted in Fig. 43 (Outokompu, 2002). The above gas composition corresponds to an equilibrium temperature of 1000 °C, which is in the typical range of the exit temperature of a secondary reformer. The exothermic nature of the shift reaction is reflected in the fact that the equilibrium concentrations of CO and H_2O decrease at decreasing temperature while the equilibrium concentrations of CO_2 and H_2 increase.

The shift reaction is almost always operated adiabatically. In such a case the exothermicity of the reaction imposes a restriction on the process. As the reaction proceeds, the temperature increases until equilibrium is reached. The gas is thus equilibrated at a higher temperature than the inlet temperature resulting in a higher CO leakage than if the reaction were carried out isothermally. In most hydrogen plants a PSA unit is used for hydrogen clean-up, and the off-gas from the PSA containing unreacted CH_4 and CO is recycled to the fired reformer as fuel. It is therefore not so important whether the CO leakage is 3% or 0.3%. Accordingly, a single adiabatic shift reactor is most often used, either high temperature shift (HTS) or medium temperature shift (MTS). In ammonia plants, however, the synthesis

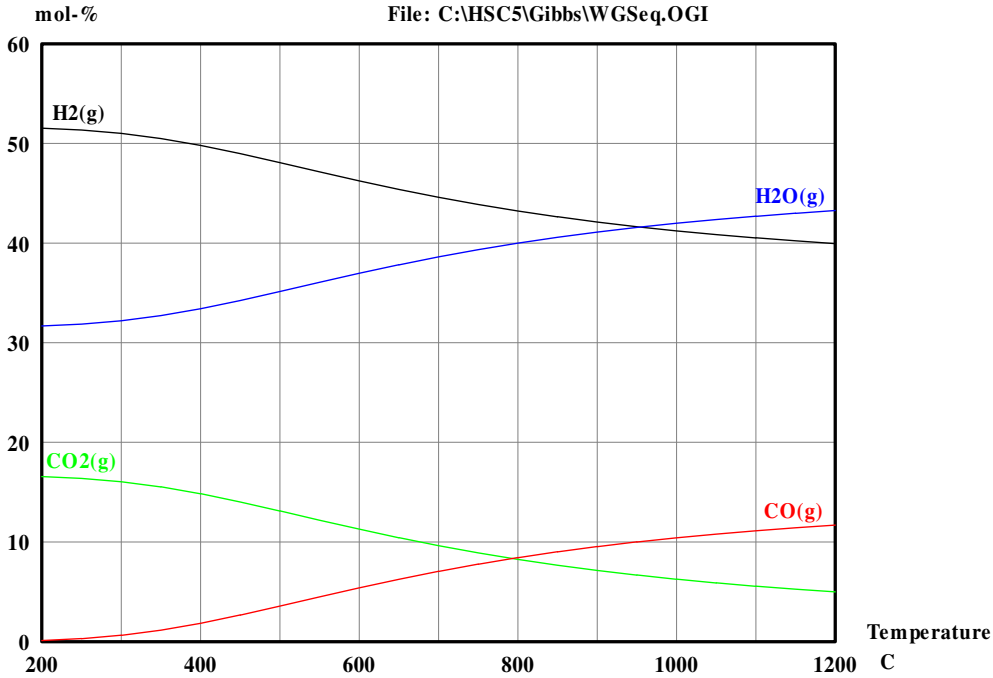

Fig. 43. Equilibrium composition of a synthesis gas as function of temperature.

gas must be completely free of oxygen containing species, including CO, and it is important that the CO leakage should be as low as possible. It is therefore customary to use two serially connected shift reactors with inter-stage cooling, designated high and low temperature shift. Typical operating temperatures are 350–450 °C and 190–235 °C, respectively. Fig. 44 shows the WGS equilibrium curve and a typical operating line for a two-stage adiabatic shift reactor system. The inlet temperatures are chosen to be 380 °C for the HTS and 190 °C for the low temperature shift (LTS) unit. The two-stage operation mode is advantageous because the high reaction rate at high temperatures is exploited in the HTS unit.

Various types of catalysts used industrially for the WGS reaction are listed in Table 10. The above-mentioned MTS is typically operated in the temperature range of 190–330 °C. The catalysts used for this process are Cu based like LTS catalysts but, due to the elevated temperatures in the MTS, the requirements for thermostability with regard to both activity and mechanical strength are much higher than for LTS catalysts. In order to achieve optimum MTS performance, a composite loading, consisting of different types of MTS catalysts at the top and the bottom of the reactor can be used. This allows the use of catalyst types that are tailor-made for the conditions prevailing in different parts of the reactor, resulting in significantly increased lifetimes of such composite charges.

The present chapter will discuss various aspects of the HTS and LTS catalysts with emphasis on the most recent developments and understanding. The CoMoS catalysts used in the so-called sour gas shift, which is widely used in coal gasification plants, will not be discussed. Likewise, the large effort during the past ten years on developing shift catalysts for use in fuel cell applications is considered to be outside the scope of this article. Although exciting new catalysts have emerged, almost all studies have been carried out at or near atmospheric pressure, thus far from the conditions of industrial practice regarding natural gas and coal conversion.

A number of excellent reviews on the water gas shift reaction exist. For practical purposes, Catalyst Handbook is very serviceable (Lloyd et al., 1996). A recent comprehensive review by Ratnasamy and Wagner (Ratnasamy and Wagner, 2009) emphasises developments within WGS catalysts through the past decade – not least the large amount of work carried out on WGS catalysts for fuel cell applications. This review also discusses mechanistic aspects of the WGS reaction. A succinct account for WGS catalysis is given by Kochloefl in Handbook of Heterogeneous Catalysis (Kochloefl, 1997). A discussion of the reaction mechanisms over Cu-based as well as Fe-based catalysts is given in Catalysis Today (Rhodes et al., 1995). Of older date is the review by Newsome (1980). A synopsis of the literature on low temperature WGS catalysis is given by Jacobs and Davis (2007) including a section on homogeneous WGS. A review of the WGS reaction kinetics has recently been published (Byron Smith et al., 2010).

The intention of the present contribution is to discuss selected topics of relevance to the WGS reaction and in particular WGS catalysts in the context of natural gas conversion.

6.1.2. High temperature shift

6.1.2.1. Fe–Cr based catalysts. Iron–chromium based catalysts are used for the high-temperature WGS reaction. These catalysts usually contain promoters, especially Cu. The active phase of the catalyst is magnetite Fe_3O_4 which has an inverse spinel structure with Fe(II) and half of the Fe(III) in octahedral sites and the remaining Fe(III) in tetrahedral positions, thus $Fe(II)^{O}Fe(III)^{O}Fe(III)^{T}O_4$. Pure magnetite deactivates relatively fast due to sintering and loss of surface area. It is plausible that sintering of Fe_3O_4 is facilitated by the ease of change of coordination number and coordination geometry of Fe(III) since there is no ligand field stabilisation of this d^5 ion. Chromium is used as stabiliser and is very efficient for this purpose. This may be rationalised by the strong ligand field stabilisation of the d^3 Cr(III) ion in octahedral environment which inhibits its change in coordination geometry, which is necessary for particle migration. In industrial HTS catalysts, chromium is added in a concentration of 8–14%. If it is added in higher amounts, Cr_2O_3 segregates as a separate phase (Newsome, 1980).

Regarding the mechanism of stabilisation of Cr in Fe_3O_4 it was originally proposed by Chinchen et al. (1984) that Cr – also in low

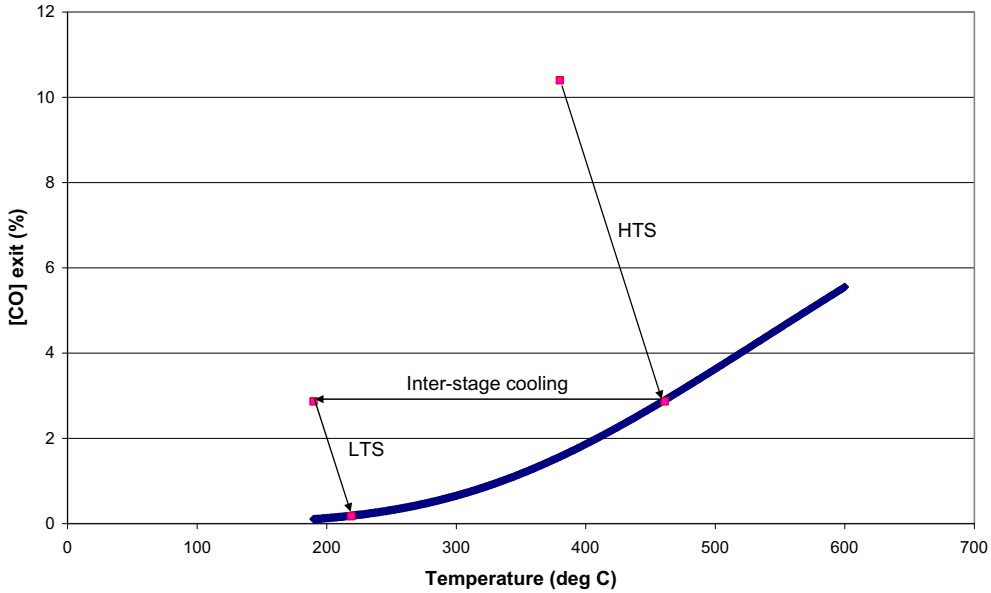

Fig. 44. Equilibrium curve and operating line for a two-stage adiabatic WGS reactor system.

concentration – forms a separate Cr_2O_3 phase, which acts as a physical barrier for migration of Fe_3O_4 particles. This group observed that thermal deactivation of an Fe/Cr catalyst proceeds in two steps; an initial fast deactivation and a following slow deactivation. Deactivation was followed by a concomitant loss of surface area. The fast deactivation, it was proposed, was due to sintering of neighbouring Fe_3O_4 particles, which would proceed until all Fe_3O_4 particles were separated by the more refractory Cr_2O_3 particles. However, the evolution of modern techniques has shed a new light on this matter. Using a combination of XPS, XRD and high-resolution electron microscopy (Edwards et al., 2002) it was recently shown that Cr forms a solid solution in magnetite. In a freshly reduced Fe/Cr catalyst containing 8% Cr, only a single spinel phase was detected by XRD and by high-resolution electron microscopy (HREM). Moreover, the sample was analysed by STEM-EDX and no Cr_2O_3 particles were found. By this method, 100 single crystallites (10–60 nm) were analysed by STEM-EDX using a 1 nm probe. Furthermore, it was found that on average the centre of the particles contained 6.3% Cr whereas at the edge of the particles the Cr content was 10.7%. The more sensitive and less destructive XPS method actually revealed a surface Cr concentration of 23%. This result has later been reproduced by another group (Scariot et al., 2008) who found by XPS analysis a Cr/Fe ratio of 0.25 corresponding to 20% Cr in the surface of a freshly reduced catalyst. A Cu and Cr-promoted Fe_3O_4 catalyst was also analysed. The freshly reduced sample showed significant surface enrichment in both Cr and Cu. The initial fast deactivation observed by Chinchen et al. (1984) was proposed to be a consequence of the inhomogeneous distribution of Cr in the magnetite particles. Thus, particles with a low Cr-content will grow fast until eventually all particles contain sufficient Cr to prevent this steep decay.

Not exactly in accordance with this, DFT calculations on Cr-substituted magnetite have indicated (Koy et al., 1995) that Cr segregation to the surface costs energy relative to having Cr in the bulk. Further calculations show that the Cr dopant tends to form Cr–Cr pairs and actually forms a superstructure in the magnetite lattice. This discrepancy between experiments and calculations may be resolved in at least two ways. The experimentally determined Cr-enrichment of the surface was found in the freshly reduced catalyst. Although aged samples were prepared in the study of Edwards et al. (2002) they were not subject to analysis of element distribution within the separate particles. Therefore it cannot be excluded that Cr migrates to the interior of the Fe_3O_4 particles during WGS operation. Another explanation relates to the DFT study in which no details were given on how the surface was terminated. Seemingly the particles were considered in vacuo, which is in contrast to the H_2O-rich atmosphere of the WGS reaction.

Current Fe-Cr HTS catalysts are promoted with Cu in the range of 1–3%. The copper promoter has two important effects. Fe/Cr/Cu catalysts produce much less methane and virtually no higher hydrocarbons compared to unpromoted Fe/Cr catalysts (Ratnasamy and Wagner, 2009). The other effect is that it lowers the activation energy significantly. In a recent study (Rhodes and Hutchings, 2003) the activation energy was determined to be 118 ± 9 kJ/mol for the pristine Fe/Cr catalyst while the activation energy is only 80 ± 10 kJ/mol for a Cu/Fe/Cr catalyst. These activation energies were valid within the pressure range of 1–27 bar and were measured in the intrinsic regime (no diffusion limitations).

Although Cu is the main component in the LTS Cu/Zn/Al catalysts, it is debated whether its effect on the activity of the HTS

Table 10
Types of WGS catalysts.

	Active phase	Support	Promoters
High-temperature	Fe/Cr oxide	None	Cu, Ca, Mg, Zn, Al
Medium-temperature	Cu	ZnO/Al_2O_3 or ZnO/Cr_2O_3	
Low-temperature	Cu	ZnO/Al_2O_3	Alkali metals
Sour gas shift	CoMoS	Al_2O_3, MgO, ZnO and combinations	Alkali metals
Fuel cell applications	Noble metals	CeO_2, ZrO_2, TiO_2 and combinations	

catalyst is merely additional or if it acts as a true promoter for the Cr-substituted magnetite. Several studies point towards copper being present as metallic Cu particles during HTS operation. Using the inverse spinel $CuFe_2O_4$ as starting material, XRD and XAFS were used to characterise the structural changes during reduction (Estrella et al., 2009). Although this mixed metal oxide was much more difficult to reduce than the parent oxides CuO and Fe_2O_3, the results showed that from 350 to 450 °C the $CuFe_2O_4$ was reduced to Cu and Fe_3O_4 with concurrent onset of catalytic activity for the WGS reaction.

According to an in situ fluorescence XAFS study on Cu-promoted Fe/Cr oxide catalysts (Kappen et al., 2001), Cu is in the metallic phase during operation. Furthermore, a sample containing 1% Cu was extracted several times with aqueous ammonia and analysed again. After the extraction, the sample contained 0.17% Cu. Surprisingly, the two samples – before and after extraction – had the same WGS activity, indicating that only a fraction of the added Cu is active. This result has recently been corroborated by further in situ XAFS studies (Puig-Molina et al., 2010) where it was estimated that less than 0.1% Cu is responsible for the full promotional effect. Again, only metallic Cu was observed under typical high-temperature shift reaction conditions, whereas oxidic copper was below the detection limit. This limit was, however, also estimated to be 0.1% and therefore it cannot conclusively be rejected that the part of the Cu responsible for the promotion is actually in an oxidic form such as $CuFe_2O_4$.

In the paper of Edwards et al. (2002) it is described how an Fe/Cr/Cu catalyst sample was aged for 1000 h at 370 °C with a foreseeable loss of surface area from 50 to 17 m^2/g. Nonetheless the sample occasionally displayed 7–12 nm particles of CuO (the sample must have become oxidised) in contact with magnetite particles as evidenced by HREM. This is a surprisingly small particle size when taking into consideration the low Tammann and Hüttig temperatures of Cu.

On the basis of the above findings, one interpretation of the role of Cu in Fe/Cr/Cu catalysts for HTS is that a fraction of the Cu is trapped as nano-particles, which are somehow stabilised by the surrounding metal oxide framework. Another is simply that some Cu ions are trapped in the magnetite structure in such low concentration that their presence is not easily measured.

The reaction mechanism over the HTS Fe/Cr/Cu catalyst is still debated. The most widely accepted theory is that it is a regenerative (also called redox) type with consecutive CO reduction and H_2O oxidation of the catalyst surface. The feasibility of this mechanism is indicated by the fact that both of the following reactions are down-hill energetically:

$$Fe_3O_4 + 4CO = 3Fe + 4CO_2, \qquad \Delta G^\circ = -14 \text{ kJ/mol}$$

$$3Fe + 4H_2O = Fe_3O_4 + 4H_2, \qquad \Delta G^\circ = -101 \text{ kJ/mol}$$

The first of these reactions is well known to cause problems. If the steam-to-carbon ratio of the gas during operation is too low, the catalyst may become over-reduced with formation of iron carbides and/or elemental iron. This results in hydrocarbon formation and severe loss of strength resulting in increasing pressure drop over the reactor. This is also the reason why the catalyst should not be activated (reduced from Fe_2O_3 to Fe_3O_4) in H_2 or H_2/N_2 but only in steam-containing reducing gas.

Recent DFT calculations from the group of Lund have contributed to the mechanistic debate. In one study (Van Natter et al., 2008), a micro-kinetic model was constructed based on the reactions

$$CO + O^* = CO_2 + {}^* \text{ and}$$

$$H_2O + {}^* = H_2 + O^*$$

which is the simplest form of the regenerative model. The model was found to provide a good fit to published kinetic data. In a later publication (Coleman et al., 2010), however, it was claimed impossible to distinguish between a regenerative and an associative mechanism.

The HTS catalyst has the advantage that it is quite tolerant towards poisons. Sulphur acts as a reversible poison. At sulphur concentrations higher than typically 150 ppm there is potential for transformation to bulk FeS but even when bulk sulphidation occurs the catalyst has about half the activity of the unsulphided catalyst.

6.1.2.2. Cr-free HTS catalysts. Appreciable concern is directed towards the content of chromium in industrial HTS catalysts. While the chromium is present as Cr(III) during operation of the catalyst, part of it may be present as Cr(VI) in the non-reduced catalyst, and it may form during unloading of the spent charge. The search for Cr-free HTS catalysts is thus the subject of many scientific papers. Most of these catalysts are iron-based. While some cobalt catalysts are actually more active for the WGS reaction and also more sulphur tolerant (e.g. Co–Cr, Co–Mn and Co-promoted Fe–Cr (Kochloefl, 1997)), they are less selective and produce more methane than the Fe-based catalysts. Combined with the relatively high cost of Co, this has prevented industrial use of these catalysts.

There are also several reports concerning replacement of Cr by Al. It was found (Araujo and Rangel, 2000) that Fe/Al and Fe/Cu catalysts were less active than a commercial Cu/Cr/Fe catalyst, while an Fe/Al/Cu catalyst showed an activity comparable to that of the commercial catalyst. Later on, the group of Rangel reported Al-doped hematite to have activity close to that of a commercial Fe/Cr-catalyst in de Souza and do Carmo Rangel (2002). The group of Ozkan has been working consistently on developing Fe/Al/Cu catalysts. Thus, such catalysts made by co-precipitation (Natesakhawat et al., 2006) and by a sol–gel method (Zhang et al., 2008) were found to be highly active. The promotional effect of Cu was found to be strongly dependent on the preparation method. Thus, co-precipitation of Fe/Al oxides followed by impregnation with copper nitrate did not give the same high activity. Recently the group of Ozkan (Gawade et al., 2010) has further improved on the sol–gel preparation method for Cu/Al/Fe catalysts. A study directed towards the effect of Cu loading (Zhang et al., 2009) points towards molar ratios of Fe/Al = 10 and Fe/Cu = 5 being close to the optimum. Although the Fe/Al/Cu catalysts appear promising, the reported activities are seemingly measured at atmospheric pressure. Furthermore, the catalytic activity has not been measured for a period of more than 100 hours' duration. In a recent study (Popa et al., 2010) it was found that aluminium alone could not effectively stabilise magnetite in co-precipitated catalysts. On the other hand, addition of Al to the Fe/Cr/Cu catalyst resulted in a higher surface area of the spent catalyst than without addition.

Replacement of Cr in Fe-based HTS catalysts was attempted with a combination of Al_2O_3 and one of the oxides ZrO_2, MnO_2, La_2O_3 and CeO_2 (Ladebeck and Kochloefl, 1995). All catalysts were promoted with 2.5% Cu. The best result was obtained with a catalyst promoted with 5% Al_2O_3 and 2.5% CeO_2. This catalyst had an initial activity which was 3.8 times higher than that of a comparative Cu–Fe–Cr catalyst and it showed fairly high thermal stability during thermal cycles at 500 °C. Another catalyst, composed by Fe/Al/Ce oxides was claimed to have comparable activity to that of an Fe/Cr oxide catalyst (Liu et al., 2005). Vanadium was claimed to be a promoter for iron oxide (Junior et al., 2005) but as in Liu et al. (2005), only Cu-free catalysts were considered. Substitution of thorium for chromium has been reported to result in improved catalyst properties (Costa

et al., 2002) although the benefit of this replacement may be arguable. Gadolinium ferrites of the Gd–Fe garnet ($Gd_3Fe_5O_{12}$) and the Gd–Fe perovskite ($GdFeO_3$) types were reported to have activities approaching that of magnetite Fe_3O_4 and of a commercial catalyst K 6–10 with an optimal calcination temperature of 800 °C (Tsagaroyannis et al., 1996). In the patent literature a few examples of composite catalysts have emerged, mainly Fe/Cu/Al/Ce and Fe/Cu/Al/Zr (Schneider et al., 1998) and Fe/Al/Si/Mg/V/Ni/K (Wei et al., 2003).

None of the above catalysts have found any widespread use in industry. Lack of sufficient thermal stability for years of operation may well be the most common reason for failure of these alternative catalysts.

While the above catalysts are all iron-based, a completely different HTS catalyst has recently been developed. The catalyst is based on $ZnO/ZnAl_2O_4$, which has been known for decades to have (low) WGS activity. Recently a study of reverse WGS activity over $ZnO–Al_2O_3$ catalysts has been published (Joo and Jung, 2003). Surprisingly, it has been found that this oxide system is strongly promoted by alkali metals in the order $Cs \approx K > Na \gg Li$. The catalyst has the advantages that it is chromium-free, it may be operated at very low steam-to-carbon ratio, and it has a high thermal stability. In a patent application (Schjødt) it is shown that the WGS rate of reaction of K-promoted $ZnO/ZnAl_2O_4$ is up to 6 times higher than that of unpromoted $ZnO/ZnAl_2O_4$ and up to 9 times higher than that of K-impregnated alumina. Under the same set of conditions the $K/ZnO/ZnAl_2O_4$ catalyst is even slightly more active than a typical Cu/Fe/Cr catalyst. Interestingly, K-promoted $MgO/MgAl_2O_4$ is almost without activity.

6.1.3. Low temperature shift

6.1.3.1. Cu–Zn–Al catalysts. Copper-based catalysts have excellent low-temperature activity for the WGS reaction. At the present time Cu–Zn–Al catalysts are used almost exclusively in industry. The catalyst is usually formulated as pellets of the mixed oxides and must be reduced (with great caution) to transform the catalyst to its active form, which is metallic Cu suspended in a mixed zinc oxide and aluminium oxide matrix. There is wide agreement that the metallic Cu particles constitute the active phase but a complex interplay with the oxidic components has also been suggested.

The role of ZnO in copper catalysts has been discussed by Saito and Murata (2004). It was shown that ZnO has a strong positive effect on the Cu-surface specific activity with regard to methanol synthesis and the reverse WGS reaction, but no effect on the specific activity for methanol steam reforming and the WGS reaction. This may be rationalised in the way that ZnO becomes partly reduced under the strongly reducing conditions of the former two reactions while in the latter two reactions the high water partial pressure keeps the ZnO oxidised. This observation was valid for Cu catalysts supported on alumina, zirconia as well as silica. Although in the WGS reaction zinc oxide does not increase the surface-specific activity, it may promote the catalyst by increasing the Cu dispersion. This is exactly what happens when Cu and Zn salts are co-precipitated due to the formation of partly zinc-substituted copper hydroxycarbonate. Impregnation of zinc nitrate does not result in an increase in dispersion (Saito and Murata, 2004). A similar effect is reported by Spencer (1999).

Contradicting results on the possible structure sensitivity of Cu/Zn/Al catalysts exist. Chinchen and Spencer (1991) found a high degree of structure sensitivity for the WGS reaction within a group of 16 catalysts differing by composition and preparation parameters. They found that the relative activity for the WGS reaction varied by more than an order of magnitude for these catalysts, and that there was no significant dependence on the specific copper surface area. On the other hand, Ginès et al. (1995) found that a group of 18 Cu/Zn/Al catalysts differing by composition and calcination temperature displayed an almost constant TOF independent of Cu surface area. This discrepancy has seemingly not been resolved, but a possible reason may be the different test conditions used. While the former group measured the WGS activity at 30 bar and an H_2O/C ratio of 0.4, the latter group examined the activity at 1 bar total pressure and an H_2O/C ratio of 3.0. In their work on modelling the kinetics of the WGS reaction, Ovesen et al. (1992) pointed towards two possible rate limiting steps, namely CO oxidation and water scission. The actual rate limiting step, they claimed, would depend on the conditions. It was previously shown (Nakamura et al., 1990) that over a clean single crystal Cu surface, the WGS reaction is highly structure sensitive. The Cu (110) surface had a specific activity of 4–10 times (depending on temperature) that of a Cu (111) surface. For both surfaces the WGS reaction was shown to be 1st order in H_2O and 0th order in CO. Thus, under the applied conditions water scission was the rate determining step. A possible resolution of the issue of structure sensitivity of Cu/Zn/Al catalysts for the WGS reaction could be that water scission is structure sensitive while CO oxidation is not, and the observed overall structural dependence of the WGS activity therefore depends on the conditions and in particular on the steam-to-CO ratio. For example, it was found (Ovesen et al., 1996) that Cu catalysts supported on SiO_2, Al_2O_3 or ZnO/Al_2O_3 display the same copper surface specific activity under the specified conditions. The reaction order of CO and H_2O were both close to unity indicating that CO oxidation was rate limiting in this case.

The activity of Cu/Zn/Al catalysts is known to depend on the preparation history of the catalyst. This is sometimes referred to as the chemical memory of the catalyst (Bems et al., 2003; Behrens et al., 2009). The principles of modern LTS catalyst preparation are accounted for by Chinchen and Spencer (1991). A mixture of the nitrates is precipitated with Na_2CO_3 to form an initial phase. This phase is recrystallised to a Cu–Zn hydroxycarbonate phase by ripening of the precipitate. In a study of the activity of Cu/Zn catalysts in relation to precursor structure and morphology, Waller et al. (1989) demonstrated the importance of the ripening of the catalyst precursor. Thus un-aged catalyst precursors resulted in catalysts with much lower activity for the reverse WGS reaction than catalysts resulting from aged precursors. The group of Behrens has been very active within the study of Cu/Zn catalyst preparation and the effect of precursor on the final catalyst. The importance of the meso- and nano-structure of the catalysts has been emphasised by this group (Behrens, 2009; Behrens and Girgsdies, 2010; Behrens et al., 2010a,b).

6.1.3.2. Reaction mechanism. The reaction mechanism and the kinetics have been the subject of many publications since Armstrong and Hilditch published their pioneering paper on the water gas shift reaction in 1920 (Armstrong and Hilditch, 1920). The reaction mechanisms have traditionally been divided into (surface) redox or regenerative mechanisms and associative mechanisms (Rhodes et al., 1995). The redox mechanism contains a catalyst (surface) oxidation and reduction step. Typically, the Cu surface is firstly oxidised by water under formation of hydrogen and surface Cu–O followed by reduction of the latter species (regeneration) by reaction with CO to form CO_2. The activities of Cu based WGS catalysts supported on ZnO/Al_2O_3, Al_2O_3 or SiO_2 were modelled using a microkinetic model based on the redox mechanism (Ovesen et al., 1996). The rate determining steps in this mechanism are dissociation of water and reaction of CO with oxygen atoms (Ovesen et al., 1992). It was found that water dissociation is slightly faster than CO oxidation at industrial pressures. To improve the predictive power of the model especially at high pressure, formation of formate had to be included as a spectator species. By fitting a power law model to the experimental data the following reaction

orders were found: CO: 1 (fixed), H_2O: 1.4–1.9, CO_2: −0.7–(−1.4) and H_2: −0.7–(−0.9). Schumacher et al. (2005) used the redox model and linear energy scaling relationships to obtain a general description of WGS activities of transition metals. It was established that the activity is described well by the oxygen and the CO adsorption energies. Reactivity trends are well predicted by the model while the model fails to describe experimental data quantitatively. Cu is found to be close to the optimum of the volcano curve but the model predicts that improved activity may be obtained with stronger bindings of CO and oxygen to the metal surface than observed for Cu.

The "associative" reaction mechanism has been suggested as an alternative to the redox mechanism. In this mechanism, the reaction proceeds via a reactive intermediate species such as formate species (Herwijnen and van and De Jong, 1980; Herwijnen et al., 1980) or carboxyl (Gokhale et al., 2008). Many articles have been devoted to studies of the presence of and decomposition of formate (Rhodes et al., 1995). Experimental and theoretical studies indicate significant coverage of formate under WGS conditions (Ovesen et al., 1992; Armstrong and Hilditch, 1920; Herwijnen and van and De Jong, 1980; Gokhale et al., 2008) and it has been suggested that decomposition of formate is the rate determining step in WGS (Herwijnen and van and De Jong, 1980). However, it still remains unclear whether formate is a reaction intermediate or a spectator species. Most recently, new insight into the WGS reaction was gained by extensive DFT calculations of the thermodynamics of all intermediates and energy barriers and pre-factors for the most relevant species at Cu(111) (Gokhale et al., 2008). Using these values as input to a microkinetic model, it was concluded that the WGS reaction proceeds via a carboxyl species, COOH, formed from the reaction of an OH radical with CO. The carboxyl species reacts with OH to form CO_2 and H_2O and this latter step is rate determining. The surface redox mechanism as well as reaction via a formate intermediate was found to be insignificant. However, formate was found to be an important spectator species. The model reproduced the reaction orders and activation energy well but the model data was only compared to experimental data obtained at ambient pressure.

Finally, some authors have discussed the influence of the support. Grenoble et al. (1981) considered dissociation and adsorption of water by the support and suggested that formate may be formed by insertion of CO adsorbed on the metal into an OH bond of water adsorbed on the support. Subsequently, the intermediate may decompose after transfer to the metal. In this case the reactivity of the catalyst will depend on the length of the periphery of the metal particles. More recently, Boisen et al. (2010) prepared a series of catalysts with 12 transition metals on $Ce_{0.75}Zr_{0.25}O_2$ and $MgAl_2O_4$ supports. In general the activities were highest when the $Ce_{0.75}Zr_{0.25}O_2$ support was used, but for Cu and Au the highest activities were obtained using $MgAl_2O_4$ support. For the catalysts on the latter support, the activities form a volcano curve when plotted as a function of the adsorption energy of oxygen atoms while the best descriptor for the $Ce_{0.75}Zr_{0.25}O_2$ supported catalysts was the CO binding energy. This behaviour was explained by fast water dissociation on the $Ce_{0.75}Zr_{0.25}O_2$ support making the effect on the reaction rate of the O binding energy small while the effect of the CO binding energy is dominating. Since water is not expected to dissociate on the $MgAl_2O_4$ support, water splitting may be the rate limiting step of this support and hence the binding energy of O is the best descriptor for the activity.

6.1.3.3. Deactivation. Cu-based LTS catalysts normally last several years when operated under standard industrial WGS conditions. The main loss of activity is due to one or more of the following three deactivation mechanisms: (i) thermal sintering, (ii) S poisoning and (iii) Cl poisoning. Other poisons exist such as Na, K, As, Si, Ni, Fe and P, but these are less common. One of the main reasons for loss of activity of a shift catalyst is loss of the active Cu surface area by Cu particle growth. The melting point of Cu is relatively low, 1083 °C, and therefore surface transport of Cu becomes important at fairly low temperatures. This can for example be seen by the low Hüttig and Tammann temperatures of 134 °C and 405 °C, respectively. Growth of the ZnO particle is also important and comparable to that of Cu. At a first sight this is peculiar as ZnO has much higher stability than Cu towards high temperatures since it is a stable solid up to 1975 °C. However, the reason for the growth of ZnO particles under WGS conditions is that the growth of ZnO particles is mediated by more mobile species such as surface $Zn(OH)_2$ or $ZnCO_3$ rather than ZnO species. ZnO may also react with Al_2O_3, which is a common component in industrial WGS catalysts, under the formation of $ZnAl_2O_4$. Al_2O_3 is added to minimise sintering and is acting as a structural promoter.

Chlorine is a severe poison for Cu-based WGS catalysts. Cl forms the mobile species CuCl and $ZnCl_2$ with Cu and ZnO, and these components have very low melting points (430 and 283 °C for CuCl and $ZnCl_2$, respectively) (Carnell, 1989, p. 78). Therefore chlorine poisoning leads to fast sintering of the catalysts and hence loss of activity and in some cases even strength. The tolerance in the feed is low – of the order of 1 ppb (Ratnasamy and Wagner, 2009).

Another severe poison for WGS catalysts is sulphur. Sulphur containing compounds form sulphur on the Cu surface under WGS conditions and hence block the surface reaction. Sulphur is a more common poison than chlorine. Sulphur may be introduced with the process steam, and even in plants with a well-functioning desulphurisation section, sulphur levels in the low-ppb range at the inlet of the LTS reactor are not uncommon. The presence of ZnO makes the catalyst self-guarding to a certain extent. This is because the potential for the formation of ZnS is even larger than the potential for formation of Cu_2S. Thus at 220 °C

$$2Cu + H_2S = Cu_2S + H_2, \qquad \Delta G = -51.7 \text{ kJ/mol}$$

$$ZnO + H_2S = ZnS + H_2O, \qquad \Delta G = -73.3 \text{ kJ/mol}$$

the equilibrium H_2S concentration over ZnO is approximately 5 ppb under typical LTS reaction conditions. This means that all sulphur above 5 ppb will be absorbed at the top of the LTS reactor. In practice a dead-zone without activity will evolve during the catalyst lifetime. Fig. 45 shows simulated temperature profiles in an LTS reactor through the lifetime of a catalyst with a steadily evolving dead-zone and a simultaneous loss of activity in the rest of the bed. Catalyst deactivation is compensated for by increasing the inlet temperature.

6.1.3.4. Alternative LTS catalysts. During the past decade so-called bi-functional catalysts have been intensely studied. These catalysts are comprised of a metal component (usually a noble metal e.g. Pt, Au, Pd, Rh, Ru) and a metal oxide component (e.g. CeO_2, TiO_2, ZrO_2, Fe_3O_4). The role of the metal component is to bind CO, which is then oxidised by the metal oxide. The metal oxide becomes reoxidised by steam and releases hydrogen, thus completing the WGS cycle. The reason for the interest in these catalysts is the use of the WGS reaction to purify hydrogen streams to be used in proteon exchange (PEM) fuel cells, especially for automotive purposes. Traditional Cu/Zn/Al catalysts are not regarded as optimal in automotive operation since a) they are pyrophoric in their active state, b) they deactivate fast at temperatures above 300 °C and c) the rate of reaction is close to first order in P_{CO} resulting in excessive catalyst volumes in order to reach equilibrium conversion at the low pressure available. Contrary, the use of noble metals for WGS catalysts in traditional

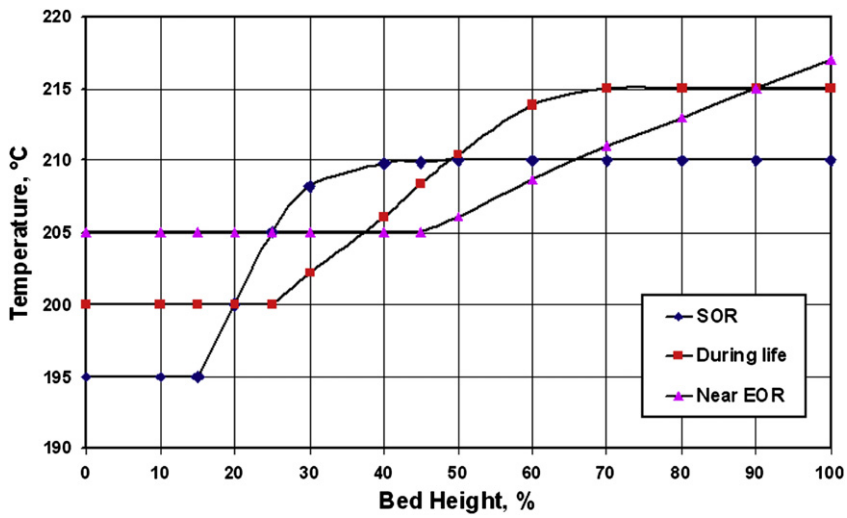

Fig. 45. Simulated temperature profiles for a typical LTS reactor.

applications for hydrogen and ammonia production suffers from several obstacles of which the high noble metal price is just one. The noble metals – apart from Au – have much higher adsorption enthalpies of CO than Cu. While this is an advantage for low-pressure applications it is disadvantageous when operating at high pressure. Another problem relates to the long-term stability of these catalysts. It has been claimed that ceria may suffer from over-reduction (Zalc et al., 2002) when operated in a hydrogen-rich atmosphere. This claim has been countered experimentally (Wang et al., 2002) by stability studies of Pt/CeO_2 and Pd/CeO_2 where deactivation was caused by loss of metal surface area, especially when treated with pure CO. Over-reduction of the support will, however, be a concern when operating at high pressure. Noble metal catalysts on reducible and non-reducible oxides have been thoroughly reviewed (Ratnasamy and Wagner, 2009).

A number of explorative catalyst systems have also been found to be active for the LTS reaction albeit they have only been tested at ambient pressure. This is so for Cu/Mn catalysts (Tanaka et al., 2003, 2005), Mo_2C (Moon and Ryu, 2004) and Co/Mo_2C (Nagai and Matsuda, 2006), Cu/ZrO_2 (Ko et al., 2005) and Cu/TiO_2 catalysts (Bocuzzi et al., 2002).

The Cu/CeO_2 system is much less costly than the noble metal catalysts. Focus has been on low-pressure applications for hydrogen purification in connection with PEM fuel cells for which a number of papers claim high WGS activity; see e.g. (Djinovic et al., 2008). A single high-pressure study exists on methanol synthesis (Shen et al., 2005). The authors found very high activity for this reaction over a 10% Cu/CeO_2 catalyst compared to a traditional $Cu/ZnO/Al_2O_3$ methanol synthesis catalyst, particularly at low temperature (195 °C). Some deactivation was observed within the duration of the activity tests (24.5 h) but no sign of over-reduction of the ceria was observed by XRD analysis of the spent catalysts. On the contrary, copper was found to be at least partially oxidised.

Raney copper catalysts have been explored in a number of works and have been reviewed with emphasis on preparation, structure and activity for methanol synthesis and the WGS reaction (Wainwright and Trimm, 1995). Andreev et al. (1991) found that the catalyst was characterised by a hydrotalcite-like phase in contact with a metallic (partly unleached) phase. The surface area specific activity measured at 2.2 MPa was reported to be an order of magnitude higher than in a co-precipitated Cu–Zn–Al catalyst. This result is corroborated by the work of Mellor et al. (1997). The latter work includes testing of Raney copper catalysts for the LTS reaction for prolonged reaction times (850 h). An important conclusion was the need for the presence of zinc oxide in the catalyst to prevent excessive sintering of Cu particles. This may be done by impregnation or, preferably, by increasing the zinc content in the Raney copper alloy (Mellor et al., 1997).

6.2. Final purification

In addition to the main components, the product gas from the reforming section may contain traces of nitrogen compounds (NH_3 and HCN). Methanol and other alcohols as well as other organic compounds except formic acid are not present in the gas from the reforming section but may be formed in trace amounts in downstream processes. The nitrogen compounds are formed together with trace amounts of formic acid at high temperature, especially in adiabatic, oxidative reformers. The chemistry behind the formation of the nitrogen compounds is described in Aasberg-Petersen et al. (2004). In special cases, other compounds may be present e.g. sulphur added to avoid carbon formation in tubular fired reformers in the SPARG process (Rostrup-Nielsen, 1984) or to mitigate the risk for metal dusting in downstream equipment (Grabke, 2000). The concentration of ammonia may be significant (several hundred ppm) depending on the operating conditions and especially on the partial pressure of nitrogen in the high temperature reactor. Formic acid and HCN will normally only be present in single-digit ppm concentrations. In air-blown processes such as processes for production of synthesis gas for ammonia production, more ammonia and hydrogen cyanide will be formed than in oxygen-blown processes.

The content of ammonia, hydrogen cyanide and formic acid in both the synthesis gas and the process condensate may cause problems in downstream process steps. In synthesis of methanol, ammonia and hydrogen cyanide will be converted to methyl amines, which are undesired in the products and must be removed, e.g. by ion exchange. A more serious effect is seen in hydrocarbon synthesis by FT reactions, especially when catalysts based on Co are used US Patent. Sulphur is a severe poison and must be removed to a very low level (NREL, 2006).

If the synthesis gas passes a shift reactor, hydrogen cyanide will be converted by hydrolysis to very low levels. Hydrogen cyanide is also removed by most carbon dioxide removal processes. But in cases where the synthesis gas is used direct without adjustment of the composition (as in GTL plants and most methanol plants),

special process steps are required if the impurities must be removed. This may be done by catalytic processes (Patent EP 1476246; Patent EP 07724334.3; Patent EP 08841696.1).

In the normal case, the synthesis gas is cooled, condensate is separated and the synthesis gas is sent to the synthesis section. The condensate will contain dissolved gases including carbon oxides, most of the ammonia, and almost all of the formic acid. The pH of the condensate will typically be around 7.

Hydrogen cyanide will at this pH not be dissociated in the water and will, together with other non-dissociated gases, be distributed between gas and condensate according to the relevant vapour/liquid equilibria. The synthesis gas will thus, in addition to the main components hydrogen, carbon monoxide, carbon dioxide and methane, contain traces of ammonia and hydrogen cyanide. The condensate will contain the dissolved gases comprising ammonia, hydrogen cyanide and formic acid.

The condensate is most often purified by flashing and/or stripping with steam followed by final purification by ion exchange. Hydrogen cyanide may be removed by flashing or low temperature steam stripping (with low pressure steam at 100–120 °C) together with other dissolved gases including ammonia and carbon dioxide. However, hydrogen cyanide may cause corrosion in the equipment, even when this is made from stainless steel. If the stripping is done at a higher temperature, e.g. by stripping with medium pressure steam at 230–250 °C, hydrogen cyanide will be converted to formic acid by the following reactions:

$$HCN + H_2O = HCONH_2 \tag{18}$$

$$HCONH_2 + H_2O = HCOOH + NH_3 \tag{19}$$

Ammonia will, after condensate separation, mainly be in the process condensate. Traces remaining in the synthesis gas may easily be removed by washing with cold water.

Formic acid remains in the condensate in the stripping process. It must be removed in the final purification of the stripped condensate by ion exchange and constitutes a major part of the load on this process step and thus of the consumption of chemicals required for regeneration of the ion exchange resin.

6.2.1. Methanation

Trace amounts of CO from the shift conversion and CO_2 ($\sim$1%) from the carbon dioxide removal unit may have to be removed, especially in ammonia plants, since these compounds are very poisonous for the synthesis catalysts. This final removal of carbon oxides is in most cases done by methanation. Methanation is the reverse of the steam reforming reactions:

$$CO + 3H_2 \leftrightarrow CH_4 + H_2O, \quad -\Delta H_{298} = 206 \text{ kJ/mol}$$

$$CO + 4H_2 \leftrightarrow CH_4 + 2H_2O, \quad -\Delta H_{298} = 165 \text{ kJ/mol}$$

The reactions are exothermic and the gas contracts during reaction. This means that the reaction is favoured at low temperature and high pressure. In practice the process is operated at relatively low water pressure, which means that the reaction is not thermodynamically controlled and the trace amounts of carbon oxides can without difficulty be converted down to single-digit ppm concentrations. The methanation reactions are accompanied by the WGS reaction. This means that remaining carbon oxides are essentially only carbon dioxide.

Group VIII metals are active in the methanation reaction. Ni is the preferred choice for industrial methanation catalyst, since it features both high activity and moderate price. The support materials are oxides, typically alumina (Vannice, 1976), but silica, lime, magnesia and calcium aluminates have also been reported as support material (Pearce et al., 1989). An understanding of the nature of the active site and the reaction mechanism and kinetics for the methanation reaction is important for optimal catalyst formulation. This has over the years been a subject for discussion in which focus has been on the structure sensitiveness of the reaction and the nature of the rate limiting step (Pearce et al., 1989; Vannice, 1982; Anderson et al., 2008). Recent studies have emphasised the importance of highly under-coordinated sites, i.e. step/kink sites for the methanation reaction, where the methanation reaction rate in CO methanation was found to be inversely proportional with the Ni-crystallite size for a series of nickel catalysts (Anderson et al., 2008). CO dissociation through a COH intermediate was suggested as the rate limiting step supported by DFT calculations. Catalyst formulation should therefore aim at obtaining small nickel crystallites. Poisons such as sulphur and potassium having a high affinity for adsorption at the under-coordinated sites should be avoided. The support material is chosen for high catalyst strength and long lifetime under operating conditions.

The physical properties of the catalyst are important to minimise mass transport restrictions, assuring low pressure drop over the reactor, and maintain catalyst strength under operating conditions. The reaction is to some extent diffusion controlled at the highest operating temperatures, and a geometric shape of the catalyst pellet with maximised external surface area is an advantage. The catalyst is offered in different shapes, for instance as solid or hollow tubular extrudates or cylindrical pellets. The size of the catalyst pellets is typically about 5 mm.

7. Complete production processes

As explained in previous sections, various forms of steam reforming and adiabatic oxidative reforming are the most important technologies in the production of synthesis gas.

Synthesis gas is often characterised by the H_2/N_2 ratio (ammonia synthesis), the H_2/CO ratio (LTFT), or by the so-called stoichiometric number (SN) or module $M = (H_2 - CO_2)/(CO + CO_2)$ (methanol and derivatives). For HTFT, the so-called Ribblett ratio $R = H_2/(2CO + 3CO_2)$ is often used. For stoichiometric gas for methanol synthesis, $M = 2R = 2.0$.

With CH_4 as the reactant, steam reforming alone will produce a gas with a module of 3.0. This makes it possible, by full recycle of CO_2 from the raw synthesis gas back to the steam reformer, to produce hydrogen and carbon monoxide in a ratio of 3. This concept is often used in so-called HYCO plants, where both H_2 and CO are products (Vannby et al., 1993). Alternatively, CO may be converted to CO_2 utilising the WGS reaction, producing a 4 to 1 mixture of H_2 and CO_2. By removal of CO_2 (and other undesired components in e.g. a PSA unit), pure H_2 may then be produced. This is the dominating process in H_2 production (Dybkjær and Madsen, 1997/98).

Adiabatic oxidative reforming will produce raw synthesis gas with a different composition. Fig. 46 (Christensen et al., 1998) shows as an illustration the values of the module M and the H_2/CO ratios, which can be obtained by autothermal reforming of CH_4 using O_2 as the oxidant.

Much larger single-stream units are possible with adiabatic oxidative reforming than with steam reforming, and adiabatic oxidative reformers are very compact units compared to fired reformers. Furthermore, reformer tube materials limit the outlet temperature from fired reformers to a maximum of about 950 °C, while the adiabatic oxidative reforming processes easily exceed 1000 °C. This makes higher conversion of the feed possible, even at low steam-to-carbon ratio.

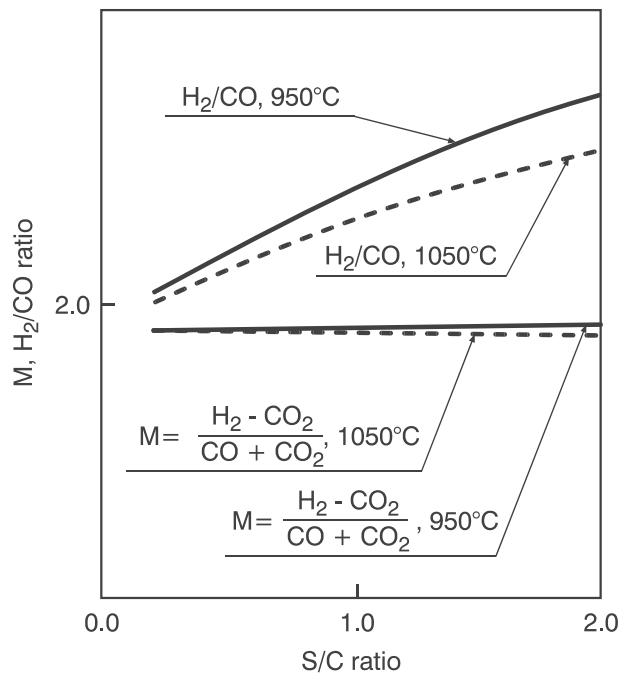

Fig. 46. M and H_2/CO in raw gas from ATR.

Steam reforming and adiabatic oxidative reforming may be used in combination. In such cases it is, as explained below, possible to adjust the synthesis gas composition to the desired compositions between the extremes offered by steam reforming and adiabatic oxidative reforming alone.

With respect to desirable synthesis gas characteristics, three situations exist:

- Ammonia: the synthesis is a reaction between hydrogen and nitrogen. Oxygen in all forms (also as water or carbon oxides) is a poison for the synthesis catalyst and therefore all oxygen containing compounds must be removed before the synthesis. The final synthesis gas is a 3 to 1 mixture of hydrogen and nitrogen, preferably with a low content of inerts (mainly methane and argon).
- Methanol and derivatives such as DME, olefins (MTO) and hydrocarbons (MTG and TIGAS), and high-temperature Fischer Tropsch (HTFT) synthesis: The synthesis reaction is between hydrogen and carbon oxides. The synthesis catalyst has, in addition to the synthesis reactions as such, also activity for the shift reaction. Carbon dioxide is thus a reactant, and the desired synthesis gas composition is similar to methanol synthesis gas. It is, as mentioned above, characterised by the module M or the Ribblett ratio R.
- Low-temperature Fischer Tropsch (LTFT) synthesis: The synthesis catalyst has no or very low activity for the shift reaction. Carbon dioxide is essentially inert, and the synthesis gas composition is best characterised by the H_2/CO ratio, which should ideally be somewhere between 2.0 and 2.2 depending on the overall H/C ratio in the product. However, the H_2/CO ratio actually required depends on the characteristics of the synthesis process and may differ from the ideal value.

In the following, complete process schemes for production of ammonia, methanol, and synthesis gas for low-temperature FT synthesis (GTL) will be described as illustrations of industrial applications of the technologies discussed in the foregoing sections.

7.1. Ammonia

Two-step reforming with air-blown secondary reforming is the dominating process for manufacture of synthesis gas for NH_3 production from natural gas (Dybkjær, 1995a). A typical process scheme is shown in Fig. 47 (Nielsen, 2002).

The process concept is used by all important suppliers of technology for NH_3 production. Natural gas is desulphurised, mixed with process steam, and passed to a fired tubular reformer, the 'primary reformer'. The product gas from the primary reformer is reacted with air in the secondary reformer to produce the raw synthesis gas, which is processed further by shift conversion, removal of CO_2, and methanation to give the final synthesis gas, a 3 to 1 mixture of H_2 and N_2 with small amounts of inerts, mainly CH_4 and Ar. The amount of air added to the secondary reformer is adjusted to give the correct ratio of H_2 and N_2 in the synthesis gas. Variations of the process scheme exist, see Dybkjær (1995a).

The secondary reformer is a refractory lined vessel with a mixer/burner (normally a multi-nozzle design), a combustion chamber, where homogeneous reactions take place, and a bed of Ni-based reforming catalyst, where the shift and reforming reactions are equilibrated by heterogeneous reaction on the catalyst.

In a modern NH_3 plant, the steam-to-carbon ratio at the inlet of the primary reformer is in the range of 2.5–3.5, the pressure at the

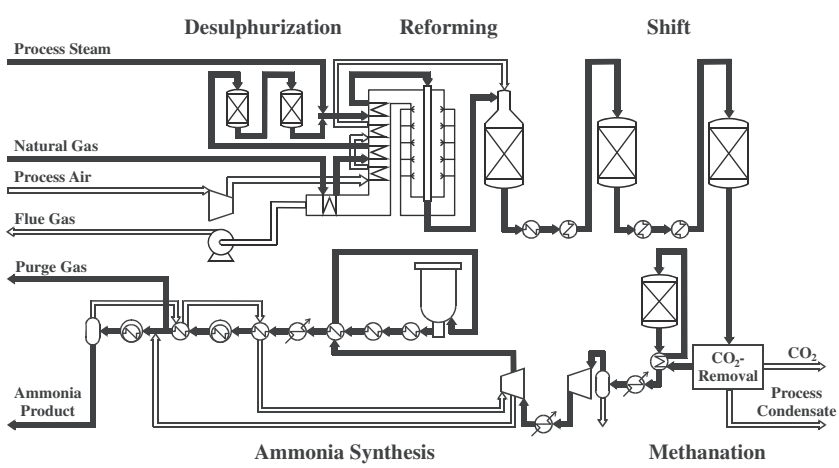

Fig. 47. Complete ammonia plant.

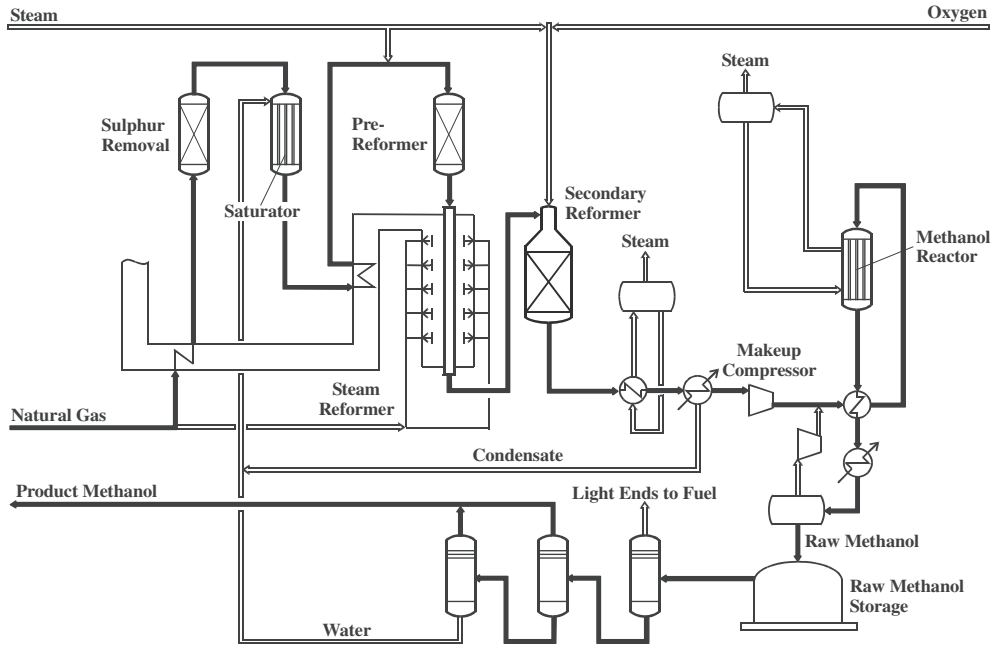

Fig. 48. Methanol production by two-step reforming.

outlet of the secondary reformer is 25–35 bar g, and the outlet temperatures from the primary and secondary reformers are 750–850 °C and 950–1050 °C, respectively.

Use of enriched air as oxidant in the secondary reformer has been suggested as a revamp option (Koenig et al., 1998) in combination with a fired reformer.

Also combinations with heat exchange reformers are known and used in industry. Both concepts with air and enriched air are described in Dybkjær (1995a), Thomsen et al. (2006). Production of ammonia synthesis gas using ATR as the only reforming technology is described in Dybkjær (2005).

7.2. Methanol

A process scheme for production of methanol synthesis gas by so-called 'two-step reforming', using prereforming, fired tubular reforming, and O_2-blown secondary reforming is illustrated in Fig. 48 (Topsoe, 2000).

The natural gas feed is desulphurised, and process steam is added in a saturator. The mixture of feed and steam is passed to a prereformer, a primary reformer and an O_2-blown secondary reformer. The steam-to-carbon ratio at the inlet to the prereformer is 1.5–2.0, the outlet pressure from the secondary reformer is about 35 bar g, and the outlet temperatures from the three reformers are about 450 °C, 750–800 °C, and 1000–1050 °C, respectively.

The design of the secondary reformer is very similar to the design used in air-blown processes. However, the operating conditions in the secondary reformer are more severe than in the air fired concept, and multi-nozzle burner design cannot be used. Instead, a design similar to the design of burners for autothermal reformers (see Section 2.5) is used.

In a variation of the concept, the natural gas feed is split into two parts. One is added to the primary reformer, whereas the other part is sent directly to the secondary reformer. This concept is normally referred to as 'combined reforming'. It has also been used in a HTFT synthesis plant (De Wet et al., 1998).

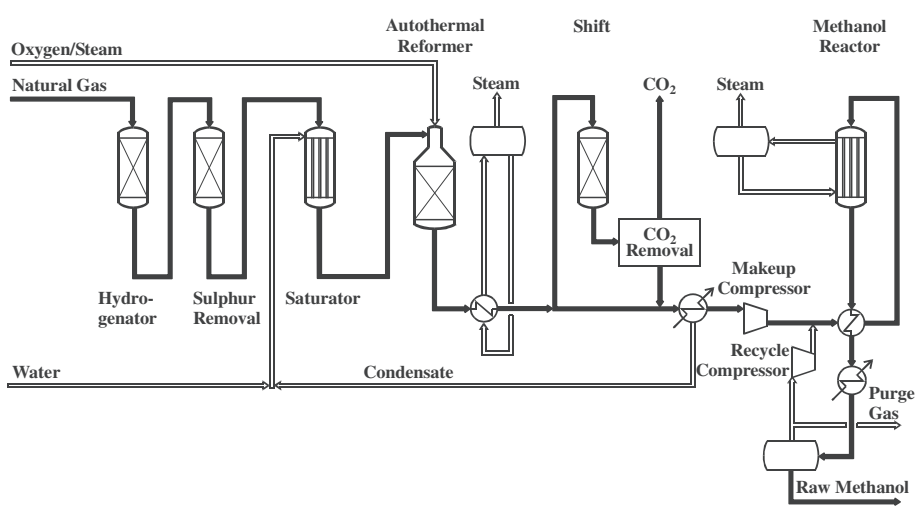

Fig. 49. Methanol production by ATR and CO_2 removal.

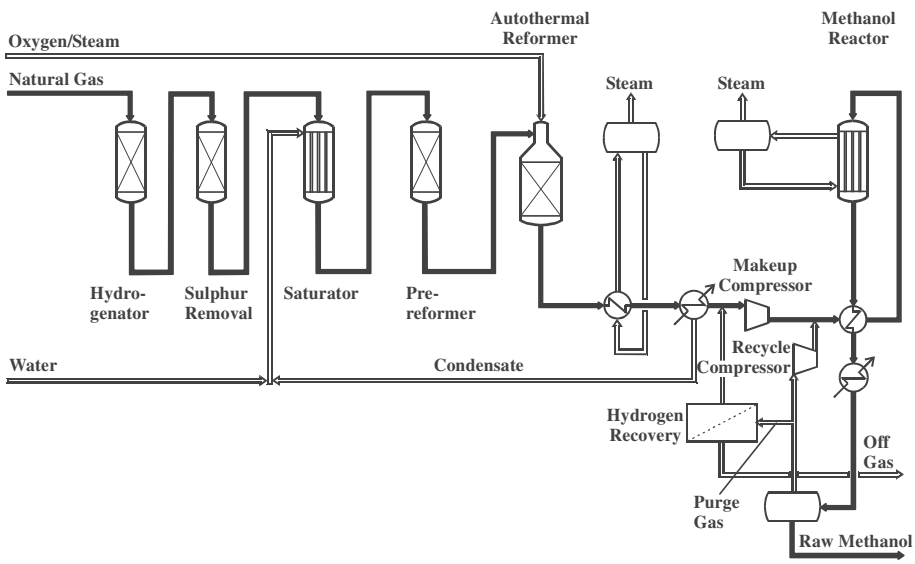

Fig. 50. Methanol production by ATR and H_2 recovery and recycle.

The advantage of using O_2 instead of air as oxidant is obvious. The presence of N_2 as an inert in the final synthesis gas is avoided. Use of air as oxidant has been suggested in production of synthesis gas for methanol (Hydrocarbon, 1999) and FT synthesis (Christensen et al., 1998; Jess et al., 1999). However, this is not economically feasible (Dybkjær and Christensen, 2001) since the presence of large amounts of N_2 – about 50 vol % in the dry synthesis gas – makes recycle concepts in the synthesis gas impossible, leading to low overall efficiency. Furthermore, compression of the large amounts of air required consumes more power than required for production and compression of O_2 in O_2-blown concepts.

Two concepts for large-scale production of methanol with synthesis gas production by ATR are shown in Figs. 49 and 50 (Haugaard and Holm-Larsen, 1999; Topsoe, 2000).

The two process concepts differ mainly in the way the composition of the raw synthesis gas is adjusted in order to match the requirements of the methanol synthesis. As mentioned above and shown in Fig. 47, the raw synthesis gas from an ATR is lean in H_2. Typical values of the module M are 1.7–1.8, whereas a value slightly above 2.0 is preferred for methanol (and HTFT) synthesis.

In Fig. 49, the module is adjusted by removal of CO_2. The natural gas feedstock is desulphurised and saturated with steam to a steam-to-carbon ratio of 0.6–1.0. The mixed feed is passed to a prereformer and, after preheating to a high temperature, to the ATR, which operates at an outlet temperature of typically 1050 °C and an outlet pressure of 30–40 bar g. Higher outlet pressure is possible (Olsvik and Hansen, 1998), but not advantageous at a very low steam-to-carbon ratio due to the resulting increase in CH_4 leakage in the synthesis gas.

In Fig. 50, the adjustment of the gas composition is done by addition of hydrogen. The hydrogen is recovered from the tail gas from the methanol (or HTFT) synthesis loop. Apart from this, the process scheme and the operating conditions are similar to the scheme and conditions in Fig. 49. The use of heat exchange reforming in combination with ATR for very large scale production of synthesis gas for methanol is described in Aasberg-Petersen, K., et al. (2007).

7.3. Low temperature FT (GTL)

Production of synthesis gas for low temperature FT synthesis by ATR is illustrated in Fig. 51 (Aasberg-Petersen et al., 2003). This process is generally accepted as the most economically attractive process for this purpose (Bonneau, 2010).

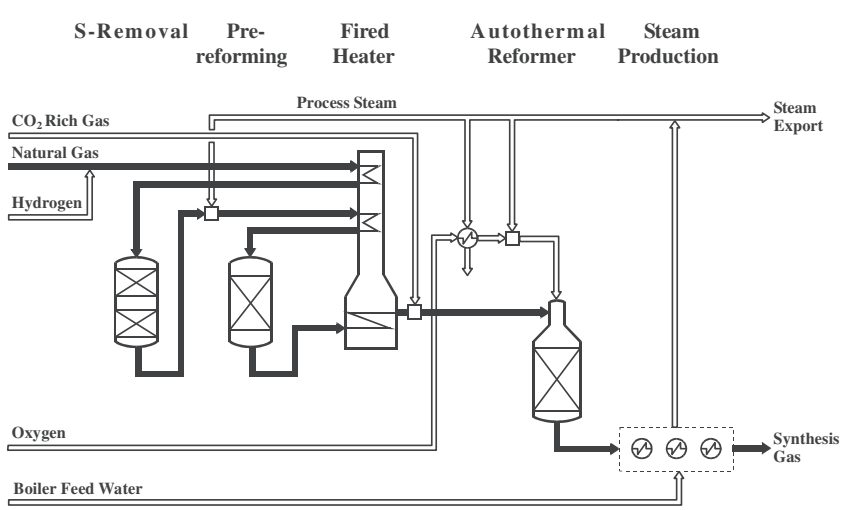

Fig. 51. Typical process flow diagram for synthesis gas production for GTL.

The process scheme is relatively simple. The natural gas feedstock is desulphurised, and process steam is added to a low steam-to-carbon ratio. The mixture of feed and steam is passed to a pre-reformer and further, after mixing with carbon-rich tail gas from the FT synthesis and preheating, to the ATR. Here it reacts with O_2 to form a synthesis gas with the desired composition. Heat is recovered from the synthesis gas by production of high pressure steam, and the gas is cooled for removal of H_2O before it is passed without compression to the synthesis section.

Although simple in principle, the process offers significant challenges. One is the sheer capacity. For production of 34,000 bbl/d of FT products, just two ATR reactors are needed. For future projects, an even larger scale is contemplated. Another challenge is the risk for metal dusting corrosion in downstream equipment, see Section 3.6.

ATR may, as fired tubular reforming, be combined with heat exchange reformers in a number of process schemes. Such schemes are described in Section 3.5.2.

8. Conclusions and future trends

Synthesis gas may be defined as a mixture containing mainly hydrogen, carbon monoxide, and carbon dioxide. Synthesis gas may be seen as an intermediate in the use of natural gas for production of a variety of bulk chemicals such as ammonia and methanol as well as for production of synthetic fuels, e.g. by the FT technology (GTL). Several attempts have been made to produce the desired end product, especially methanol, directly without using synthesis gas as an intermediate. However, these attempts have up to now been unsuccessful (Rostrup-Nielsen, 2004) and it is expected that synthesis gas will remain a key intermediate in the chemical industry for years to come.

Technologies required for the conversion of natural gas to synthesis gas are well established and important elements in a wide range of chemical process units. It may be noted that almost all ammonia (world production in 2008: 133 million tons, average annual increase in 2004–2008: 2.6% (Ammonia)) and methanol (annual production in 2010: 45 million tons, average annual increase in 2005–2010: 4.8% (MMSA)) are made from synthesis gas based on natural gas. The total amount of natural gas required for production of these two chemicals alone amounts to about 100 billion N m^3/y. It may further be expected that the consumption of natural gas in GTL plants for production of synthetic fuel, which is today only about 5 billion N m^3/y, may increase rapidly as new, large units come on stream (Velasco et al., 2010). Finally, it may be mentioned that production of hydrogen, which is not described specifically in this paper, but which is essentially based on the technologies described, consumes an estimated further 100 billion N m^3/y of natural gas. Hydrogen has several applications but is mainly used in refineries for production of various types of fuel such as gasoline, kerosene and diesel. The environmental regulations have in recent years become more stringent with the result that the use of hydrogen in refineries is increasing. All in all, it is clear that the technologies for production of synthesis gas are a very important part of the petrochemical industry and the energy industry, and that they will continue to be so for decades to come.

Several of the technologies described in the preceding sections are mature and have been in use for many years. However, even for these technologies improvements to reduce capital cost and/or increase the plant efficiency are continuously being identified. It is expected that the increased focus on environmentally benign technical solutions and sustainability will further push development towards more efficient plant design.

One good example is the use of heat exchange reformers. Heat exchange reformers have the potential to significantly boost the plant carbon and energy efficiency. The use of heat exchange reformers is not widespread at this point in time although a number of plants with these technologies are in operation. One of the main reasons is that in most cases, the plants should be designed for operation at low steam-to-carbon ratio in order to maximise the economical and environmental benefits. Under such conditions, heat exchange reformers face a serious challenge due to the risk of metal dusting corrosion. It is expected that the technical challenge of metal dusting will be resolved within the next 10 years, allowing more efficient and economical designs with heat exchange reformers. Finally, it should be mentioned that in some parts of the world limits may be imposed politically on the quantity of carbon dioxide that may be emitted to the atmosphere as a greenhouse gas. This may lead the way towards conceptual changes in plant design to optimise the layout incorporating carbon dioxide capture and sequestration. This will be yet a significant challenge to catalyst and technology developers.

References

Aasberg-Petersen, K., Hansen, J.H.B., Christensen, T.S., Dybkjær, I., Seier Petersen, P., Stub Nielsen, C., Winter-Madsen, S., Rostrup-Nielsen, J.R., 2001. Appl. Catal. A: Gen. 221, 379.

Aasberg-Petersen, K., Christensen, T.S., Nielsen, C.S., Dybkjær, I., 2003. Fuel Process. Technol. 83, 253.

Aasberg-Petersen, K., Christensen, T.S., Dybkjær, I., Sehested, J., Østberg, M., Coetzen, R.M., Keyser, M.J., Steynberg, A.P., 2004. Fischer–Tropsch Technology. Elsevier (Chapter 4), p. 258.

Aasberg-Petersen, K., Nielsen, C.S., Dybkjær, I., 2007. Very Large Scale Synthesis Gas Production and Conversion to Methanol or Multiple Products, National Gas Conversion VIII. In: Noronha, F.B., Schmal, M., Sousa-Aguiar, E.F. (Eds.). Elsevier B.V., p. 243–248.

Abild-Pedersen, F., Nørskov, J.K., Rostrup-Nielsen, J.R., Sehested, J., Helveg, S., 2006. Phys. Rev. B 73, 115419. 309 (2006) 237.

Agüero, A., Marcos Gutiérrez, L., Korcakova, T.T.M., Nguyen, B., Hinnemann, S., Saadi. Metal Dusting Protective Coatings. A Literature Review, Oxidation of Metals. in press.

Agarwal, D.C., Brill, U., Kloewer, J., 2001. Corrosion, recent results on metal dusting of nickel base alloys and some applications. NACE Conference Paper No. 01382.

Ammonia: World Production, By Country. http://indexmundi.com/en/commodities/minerals/nitrogen/nitrogen_t12.html.

Andersen, K.H., Nov. 2006. Hydrogen agenda. Hydrocarb. Eng..

Anderson, M.P., Abild-Pedersen, F., Remediakes, I.N., Bligaard, T., Jones, G., Engbæk, J., Lytken, O., Horch, S., Nielsen, J.H., Sehested, J., Rostrup-Nielsen, J.R., Nørskov, J.K., Chorkendorff, I., 2008. J. Catal. 255, 6.

Andreev, A., Kafedjiiski, V., Halachev, T., Kunev, B., Kaltchev, M., 1991. Appl. Catal. 78, 199–211.

Araujo, G.C., Rangel, M.C., 2000. Catal. Today 62, 201–207.

Armstrong, E.F., Hilditch, T.P., 1920. Proc. Roy. Soc. A97, 265–272.

Avetisov, A.K., Rostrup-Nielsen, J.R., Kuchaev, V.L., Hansen, J.B.H., Zyskin, A.G., Shapatina, E.N., 2010. J. Mol. Catal. A 315 (8), 155.

Baker, B.A., Smith, G.D., Hartmann, V.W., Shoemaker, L.E., McCoy, S.A., 2002. Nickel-base material solutions to metal dusting problems. Corrosion NACE Conference NACE 2002, Paper No 02394.

Barnett, D., Wu, D., 2001. Ammonia Plant Saf. 41, 9.

Bartholomew, C.H., 2001. Appl. Catal. A 212, 17.

Basini, G., Aasberg-Petersen, K., Guarinoni, A., Oestberg, M., 2001. Catal. Today 64, 9.

Baukal Jr., C.E. (Ed.), 1998. Oxygen-Enhanced Combustion. CRC Press, Boca Raton.

Behrens, M., Girgsdies, F., 2010. Z. Anorg. Allg. Chem. 636, 919–927.

Behrens, M., 2009. J. Catal. 267, 24–29.

Behrens, M., Girgsdies, F., Trunschke, A., Schlögl, R., 2009. Eur. J. Inorg. Chem., 1347–1357.

Behrens, M., Kasatkin, I., Kühl, S., Weinberg, G., 2010a. Chem. Mater. 22, 386–397.

Behrens, M., Furche, A., Kasatkin, I., Trunschke, A., Busser, W., Muhler, M., Kniep, B., Fischer, R., Schlögl, R., 2010b. ChemCatChem 2, 816–818.

Bems, B., Schur, M., Dassenoy, A., Junkes, H., Herein, D., Schlögl, R., 2003. Chem. Eur. J. 9, 2039–2052.

Bengaard, H.S., Nørskov, J.K., Sehested, J., Clausen, B.S., Nielsen, L.P., Molenbroek, A.M., Rostrup-Nielsen, J., 2002. J. Catal. 209 (2), 365.

Bocuzzi, F., Chiorino, A., Manzoli, M., Andreeva, D., Tabakova, T., Ilieva, L., Iadakiev, V., 2002. Catal. Today 75, 169–175.

Boisen, A., Janssens, T.V.W., Schumacher, N., Chorkendorff, I., Dahl, S., 2010. J. Catal. 315, 163–170.

Bonneau, R., 2010. Upgrade syngas production. Hydrocarb. Process, April.

Broman, E., Carstensen, J.H., 2009. Convection reformer technology. Hydrocarb. Eng. February.

Byron Smith, R.J., Muruganandam, L., Shekar, S.M., 2010. Int. J. Chem. Reactor Eng. 8 (R4), 1–32.

Carnell, J.H., 1989. In: Twiggs, M.V. (Ed.), Catalyst Handbook, second ed. Wolfe Publishing Ltd., London, p. 199.
Carnell, P.J.H., Denny, P.J., 1985. Ammonia Plant Saf. 25, 99.
Carstensen, J.H., 2005. Options for revamp of hydrogen plants. National Petrochemical & Refineries Association. Annual Meeting, March 13–15, 2005.
Carstensen, J.H., 2010, NPRA, Annual Meeting, Phoenix, Arizona, USA, March. Additional hydrogen production by heat exchange steam reforming. AM-10-141 1.
Chem. Eng. July, 1962, 88.
Chinchen, G.C., Spencer, M.S., 1991. Catal. Today 10, 293–301.
Chinchen, G.C., Logan, R.H., Spencer, M.S., 1984. Appl. Catal. 12, 89–96.
Choudhary, V.R., Rajput, A.M., Prabhakar, B., 1992. Catal. Lett. 15, 363.
Christensen, T.S., Primdahl, I.I., 1994. Hydcar. Proc. 73, 39.
Christensen, T.S., Rostrup-Nielsen, J.R., 1996. Deactivation and testing of hydrocarbon processing catalysts. In: ACS Symposium Series, vol. 634. ACS, Washington.
Christensen, T.S., Dybkjær, I., Hansen, L., Primdahl, I.I., 1994. Ammonia Plant Saf. 35, 205.
Christensen, T.S., Hansen, J.H.B., Christensen, P.S., Primdahl, I.I., Dybkjær, I., 1998. Synthesis gas preparation by autothermal reforming for conversion of natural gas to liquid products (GTL). Second Annual Conference "Monetizing Stranded Gas Reserves", San Francisco, December 14–16, 1998.
Christensen, T.S., Christensen, P.S., Dybkjær, I., Hansen, J.H.B., Primdahl, I.I., 1998. Stud. Surf. Sci. Catal. 119, 883.
Christensen, T.S., Østberg, M., Hansen, J.H.B., 2001. Process demonstration of autothermal reforming at low steam-to-carbon ratios for production of synthesis gas. AIChE Annual Meeting, Reno, Nevada, USA, November 4–9, 2001.
Christensen, T.S., 1996. Appl. Catal. A: Gen. 138, 285.
Christiansen, L.J., Jarvan, J.E., 1986. NATO ASI Ser. E 110, 35.
Clausen, B.S., Knudsen, K.G., Højlund Nielsen, P.E., Nørskov, J.K., 2006. Catal. Today 111 (1) 1 f.f.
Coleman, J.S., Zhang, M., Van Natter, R.M., Lund, C.R.F., 2010. Catal. Today. doi:10.1016/j.cattod.2010.05.006.
Costa, J.L.R., Marchetti, G.S., Rangel, M.C., 2002. Catal. Today 77, 205–213.
Cotton, B., Fisher, B., 2002. Ammonia Plant Saf. 43, 106.
Craciun, R., Shereck, B., Gorte, R.J., 1998. Catal. Lett. 51 (3–4), 149.
Creemer, J.F., Helveg, S., Hoveling, G.H., Ullmann, S., Molenbroek, A.M., Sarro, P.M., Zandbergen, H.W., 2005. Ultramicroscopy 108, 993–998.
Cromarty, B.J., Beedle, S.C., 1993. Ammonia Plant Saf. 33, 63.
de Souza, J.M.T., do Carmo Rangel, M., 2002. React. Kinet. Catal. Lett. 77, 29–34.
De Wet, H., Minnie, R.O., Davids, A.J., 1998. Ammonia Plant Saf. 38, 64.
Dietz III, A.G., Schmidt, L.D., 1995. Catal. Lett. 43, 15.
Djinovic, P., Batista, J., Pintar, A., 2008. Appl. Catal. A: Gen. 347, 23–33.
Dybkjær, I., Christensen, T.S., 2001. Stud. Surf. Sci. Catal. 136, 435.
Dybkjær, I., Madsen, S.W., 1997/98. Int. J. Hydcar. Eng. 3 (1), 56.
Dybkjær, I., Gøl, J.N., Cieutat, D., Eyguessier, R., 1997. NPRA Annual Meeting, San Antonio, USA. Paper No. AM-97-18, March 16–18.
Dybkjær, I., Nørgaard, T., Perregaard, J., Joensen, F., 2006. Methanol, diemethyl ether, ammonia, urea. In: Amadei, C. (Ed.), Encyclopaedia of Hydrocarbons, pp. 501–543.
Dybkjær, I., 1995a. In: Nielsen, A. (Ed.), Ammonia. Springer-Verlag, Berlin, p. 199.
Dybkjær, I., 1995b. Fuel Process. Technol. 42, 85–107.
Dybkjær, I., 2003Fundamentals of Gas to Liquids. Petrol. Econ., 16.
Dybkjær, I., Sept 2005. New reforming concepts for large scale NH_3 plants. In: 50th Annual Safety in Ammonia Plants and Related Facilities Symposium, Toronto, Canada.
Dybkjær, I., 2005. Increasing hydrogen production. PTQ Winter.
Dybkjær, I., 2006. Synthesis gas technology. Hydrocarb. Eng. July.
Edwards, M.A., Whittle, D.M., Rhodes, C., Ward, A.M., Rohan, D., Shannon, M.D., Hutchings, G.J., Kiely, C.J., 2002. Phys. Chem. Chem. Phys. 4, 3902–3908.
Elkins, K.J., Gow, A.J., Kitchen, D., Pinto, A., 1992. Proceedings No. 319. The Fertiliser Society, London.
Ernst, W.S., Venables, S.C., Christensen, P.S., Berthelsen, A.C., 2000. Hydcarb. Proc. 79 (3), 100-C.
Economides, J., Wood, D.A., 2009. J. Nat. Gas Sci. Eng. 1, 1–13.
Estrella, M., Barrio, L., Zhou, G., Wang, X., Wang, Q., Wen, W., Hanson, J.C., Frenkel, A.I., Rodriguez, J.A., 2009. J. Phys. Chem. C 113, 14411–14417.
Fan, H., Li, C., Gno, H., Xie, K., 2003. J. Nat. Gas Chem. 12, 43.
Farnell, P.W., 2000. Ammonia Plant Saf. 40, 173.
Froment, G.F., Bischoff, K.B., 1990. Chemical Reactor Analysis and Design. Wiley, New York.
Gawade, P., Mirkelamoglu, B., Tang, B., Ozkan, U.S., 2010. J. Mol. Catal. A: Chem. 321, 61–70.
Ginès, M.J.L., Amadeo, N., Laborde, M., Apesteguia, C.R., 1995. Appl. Catal. A: Gen. 131, 283–296.
Gokhale, A.A., Dumesic, J.A., Mavrikakis, M., 2008. J. Am. Chem. Soc. 130, 1402–1414.
Grabke, H.J., 2000. Mater. High Temp. 17 (4), 483.
Grenoble, D.C., Edstadt, M.M., Ollis, D.F., 1981. J. Catal. 67, 90–102.
Physical Properties of Natural Gas, 1988. Groningen N.V., Nederlandse Gusunie.
Gyde Thomsen, S., Holm-Christensen, O., Christensen, T.S., 2007. Scale-up challenges in synthesis gas production. In: Proceedings of the 8th Natural Gas Conversion Symposium, Natal, Brazil.
Haugaard, J., Holm-Larsen, H., 1999. Recent advances in autothermal technology – reducing production cost to prosper in a depressed market. Paper Presented at the World Methanol Conference, San Diego, Cal., USA, Nov. 29–Dec 1, 1999.
Helveg, S., López-Cartes, C., Sehested, J., Hansen, P.L., Clausen, B.S., Rostrup-Nielsen, J.R., Abild-Pedersen, F., Nørskov, J.K., 2004. Nature 427, 426.
Herwijnen, T., van and De Jong, W.A., 1980. J. Catal. 63, 83–93.
Herwijnen, T., van Guczalski, R.T., De Jong, W.A., 1980. J. Catal. 63, 94–101.
Hickman, D.A., Schmidt, L.D., 1992. J. Catal. 138, 267.
Hickman, D.A., Schmidt, L.D., 1993. Science 259.
Hickman, D.A., Haupfear, E.A., Schmidt, L.D., 1993. Catal. Lett. 17, 223.
Hidalgo-Vivas, A., Cooper, B.H., 2003. In: Vielstich, W., et al. (Eds.), Handbook of Fuel Cells. John Wiley & Sons Ltd.
Hou, K., Hughes, R., 2001. Chem. Eng. J. 82, 311.
Hydrocarb. Asia Oct., 1999, 56.
Jacobs, G., Davis, B.H., 2007. In: Spivey, J.J., Dooley, K.M. (Eds.), Specialist Periodical Reports: Catalysis, vol. 20, pp. 122–285.
Jakobsen, J.G., Jørgensen, T., Chorkendorff, I., Sehested, J., 2010b. Appl. Catal. A 377, 158.
Jakobsen, J.G., Jakobsen, M., Chorkendorff, I., Sehested, J., 2010a. Catal. Lett. 140, 90.
Jensen, P.E., Søndergaard, K., 1984. Ammonia Plant Saf. 24, 47.
Jess, A., Popp, R., Hedden, K., 1999. Appl. Catal. A: Gen. 186, 321.
Jones, G., Jakobsen, J.G., Shim, S.S., Kleis, J., Andersson, M.P., Rossmeisl, J., Abildedersen, F., Bligaard, T., Helveg, S., Hinnemann, B., Rostrup-Nielsen, J.R., Chorkendorff, I., Sehested, J., Nørskov, J.K., 2008. J. Catal. 259, 147.
Joo, O.-S., Jung, K.-D., 2003. Bull. Korean Chem. Soc. 24, 86–90.
Junior, I.L., et al., 2005. Appl. Catal. A 283, 91–98.
Kappen, P., Grunwaldt, J.D., Hammershøi, B.S., Tröger, L., Clausen, B.S., 2001. J. Catal. 198, 56–65.
Kawai, T., Takermura, K., Zaghloud, M.B., 1984. Paper Presented at International Plant Engr. Conf., Bombay.
Kikuchi, E., Tanaka, S., Yamazaki, Y., Morila, Y., 1974. Bull. Jpn. Pet. Inst. 16 (2), 95.
Knözinger, H., Schüth, F., Weitkamp, J. (Eds.), 2008, Handbook of Heterogeneous Catalysis, vol. 2. Wiley-VCH, p. 803 (Chapter 3.1.3).
Ko, J.B., Bae, C.M., Jung, Y.S., Kim, D.H., 2005. Catal. Lett. 105, 157–161.
Kochloefl, K., 1997. In: Ertl, G., Knözinger, H., Weitkamp, J. (Eds.), Handbook of Heterogeneous Catalysis, vol. IV. Wiley VCH, Weinheim.
Koenig, J., Kontopoulos, A.J., Dybkjær, I., Rostrup-Nielsen, T., 1998. Ammonia Plant Saf. 38, 206.
Koy, J., Ladebeck, J., Hill, J.R., 1995. Stud. Surf. Sci. Catal. 119, 479–484.
Ladebeck, J., Kochloefl, K., 1995. In: Poncelet, G., Martens, J., Delmon, B., Jacobs, P.A., Grange, P. (Eds.), Preparation of Catalysts VI. Studies in Surface Science and Catalysis, vol. 91, pp. 1079–1083.
Liu, Q., et al., 2005. Catal. Today 106, 52–56.
Lloyd, L., Ridler, D.E., Twigg, M.V., 1996. In: Twigg, M.V. (Ed.), Catalyst Handbook, second ed. Manson Publishing, Frome, England, pp. 283–339 (Chapter 6).
Maestri, M., Vlachos, D.G., Beretta, A., Groppi, G., Tronconi, E., 2009. AIChE J. 55, 993.
Makogon, Y.F., 2010. J. Nat. Gas Sci. Eng. 2, 49–59.
Malhotra, A., Hackemesser, L., 2002. Ammonia Plant Saf. 42, 223.
Mehrota, V., Rosendall, B., Heath, A., Berkoe, J., 2002. PVP-Vol 448-2, Computational Technologies for fluid/Thermal/Structural/Chemical Systems with Industrial Applications, Vol II, ASME 2002, PV 2002-1581, P. 119
Mellor, J.R., Coville, N.J., Sofianos, A.C., Copperthwaite, R.G., 1997. Appl. Catal. A: Gen. 164, 171–183.
Mellor, J.R., Coville, N.J., Sofianos, A.C., Copperthwaite, R.G., 1997. Appl. Catal. A: Gen. 164, 185–195.
Mii, T., Hirotani, K., 2001. Economic evaluation of a jumbo DME plant. Presented to WPC Asia Regional Meeting, Shanghai, Sep. 17–20.
MMSA Global Methanol Supply and Demand Balance, 2005-2010E. www.methanolmsa.com.
Molenbroek, A.M., Helveg, S., Topsøe, H., Clausen, B.S., 2009. Top. Catal. 52, 1303–1311. Springer Science Business Media, LLC.
Moon, D.J., Ryu, J.W., 2004. Catal. Lett. 92, 17–24.Patt, J., Moon, D.J., Phillips, C., Thompson, L., 2000. Catal. Lett. 65, 193–195.
Nørskov, J.K., Bligaard, T., Rossmeisl, J., Christensen, C.H., 2009. Nat. Chem. 1.
Nagai, M., Matsuda, K., 2006. J. Catal. 238, 489–496.
Nakamura, J., Campbell, J.M., Campbell, C.T., 1990. J. Chem. Soc. Faraday Trans. 86, 2725–2734.
Natesakhawat, S., Wang, X., Zhang, L., Ozkan, U.S., 2006. J. Mol. Catal. A 260, 82–94.
Unconventional Natural Gas Resources. NaturalGas.org.
Newsome, D.S., 1980. Catal. Rev. Sci. Eng. 21, 275–318.
Nielsen, S.E., 2002. Ammonia Plant Saf. 42, 304.
Nielsen, P., Christiansen, L.J., 2002. Proceedings of 4th international Symposium on Computational Technologies for Fluid/Thermal Chemical Systems with Industrial Applications, August 4–8, Vancouver, B.C., Canada.
Nishiyama, Yoshitaka, Otsuka, Nobuo, 2009. Metal dusting behaviour of new Ni-base alloy in a laboratory carbonaceous environment. Corrosion NACE Conference 2009, Paper 09157.
Nitrogen 72, 1971, 34.
Nitrogen 179 (May–June), 1989, 16.
Nitrogen 214, 1995, 38.
Nitrogen Methanol 266, 2003, 33.
Biomass Systems, Synthesis Gas Cleanup and Oxygen Separation Equipment, May 2006. National Renewable Energy Laboratory (NREL), California, USA. Also available on: http://www.nrel.gov/docs/fy06osti/39947.pdf Subcontract Report SR-510-39947, task 9, section 2.1.1.
Olsvik, O., Hansen, R., 1998. Stud. Surf. Sci. Catal. 119, 875.
Outokompu HSC Chemistry® for Windows Version 5.1. 2002.
Ovesen, C.V., Stoltze, P., Nørskov, J.K., Campbell, C.T., 1992. J. Catal. 134, 445–468.
Ovesen, C.V., Clausen, B.S., Hammershøi, B.S., Steffensen, G., Askgaard, T., Chorkendorff, I., Nørskov, J.K., Rasmussen, P.B., Stoltze, P., Taylor, P., 1996. J. Catal. 158, 170–180.
Pasaribu, D., Primdahl, I.I., Speth, C., 2002. Ammonia Plant Saf. 42, 175.
Patent application EP 07724334.3

Patent application EP 08841696.1.
Patent EP 1476246.
Pearce, B.B., Twigg, M.V., Woodward, C., 1989. In: Twigg, M.V. (Ed.), Catalyst Handbook. Wolfe, London (Chapter 7).
Philipson, J.J., 1970. In: Catalyst Handbook. Wolfe Scientific Books, London, p. 46.
Poinsot, T., Veynante, D., 2005. Theoretical and numerical combustion. Sec. Ed. Edwards.
Popa, T., Xu, G., Barton, T.F., Argyle, M.D., 2010. Appl. Catal. A: Gen. 379, 15–23.
Puig-Molina, A., Cano, F.M., Janssens, T.V.W., 2010. J. Phys. Chem. C 114, 15410–15416.
Qin, D., Lapszewicz, J., 1994. Catal. Today 21, 551.
Rasmussen, F.B., Sehested, J., Teunissen, H.T., Molenbroek, A.M., Clausen, B.S., 2004. Appl. Catal. A 267, 165.
Ratan, S., Vales, C.F., 2002. Hydcar. Proc. March, 57.
Ratnasamy, C., Wagner, J.P., 2009. Catal. Rev. 51, 325–440.
Rhodes, C., Hutchings, G.J., 2003. Phys. Chem. Chem. Phys. 5, 2719–2723.
Rhodes, C., Hutchings, G.J., Ward, A.M., 1995. Catal. Today 23, 43–58.
Richardson, J., Drucker, R., 1998. Ammonia Plant Saf. 38, 21.
Rostrup-Nielsen, J.R., Christiansen, L.J., 1997. In: Tominaga, H., Tamaki, M. (Eds.), Tubular Steam Reforming. Chemical Reaction and Reactor Design. John Wiley, Chichester (Chapter 5.2).
Rostrup-Nielsen, J.R., Hansen, J.-H.B., 1993. J. Catal. 144, 38.
Rostrup-Nielsen, J.R., Christiansen, L.J., Hansen, J.H.B., 1988. Appl. Catal. 43, 287.
Rostrup-Nielsen, J.R., Dybkjær, I., Christiansen, L.J., 1992. In: de Lasa, H.J., et al. (Eds.), NATO ASI Chemical Reactor Technology for Environmentally Safe Reactors and Products. Kluwer, Dordrecht, p. 249.
Rostrup-Nielsen, J.R., Sehested, J., Nørskov, J.K., 2002. Adv. Catal. 47, 65.
Rostrup-Nielsen, J.R., 1973. J. Catal. 31, 173.
Rostrup-Nielsen, J.R., 1984. In: Anderson, J.R., Boudart, M. (Eds.), Catalysis, Science and Technology. Springer-Verlag, Berlin, p. 1.
Rostrup-Nielsen, J.R., 2008. In: Ertl, G., Knözinger, H., Schüth, F., Weitkamp, J. (Eds.), Handbook of Heterogeneous Catalysis. Wiley, p. 2882 (Chapter 13.1).
Rostrup-Nielsen, J.R., 1984. J. Catal. 85, 31.
Rostrup-Nielsen, J.R., 1993. Catal. Today 18, 305.
Rostrup-Nielsen, J.R., 1994. Catal. Today 21, 257.
Rostrup-Nielsen, J.R., 2002. Catal. Today 71, 243.
Rostrup-Nielsen, T., 2002. Hydcarb. Eng. August, 51.
Rostrup-Nielsen, J.R., 2004. Fuels and Energy for the Future: The Role of Catalysis. Catal Rev Sci Eng 46 (3–4), 247–270.
Saadi, S., Abild-Pedersen, F., Helveg, S., Sehested, J., Hinnemann, B., Appel, C.C., Nørskov, J.K., 2010. J. Phys. Chem. C 114, 11221.
Saito, M., Murata, K., 2004. Catal. Surv. Asia 8, 285–294.
Scariot, M., Francisco, M.S.P., Jordao, M.H., Zanchet, D., Logli, M.A., Vicentini, V.P., 2008. Catal. Today 133–135, 174–180.
Schädel, B.T., Duisberg, M., Deutschmann, O., 2009. Catal. Today 142, 42.
Schjødt, N.C. Chromium-free water gas shift catalyst. US Patent application 20100000155 A1.
Schmidt, L.D., 2001. Stud. Surf. Sci. Catal. 1.
Schneider III, R.V., Joshi, G., 1997. PTQ summer, 85.
Schneider, M., et al., 1998. Chromium-free catalyst based on iron oxide for the conversion of carbon monoxide. US patent 5.830.425.
Schumacher, N., Boisen, A., Dahl, S., Gokhale, A.A., Kandoi, S., Grabow, L.C., Dumesic, J.A., Mavrikakis, M., Chorkendorff, I., 2005. J. Catal. 229, 265–275.
Sehested, J., Carlsson, A., Janssens, T.V.W., Hansen, P.L., Datye, A.K., 2001. J. Catal. 197, 200.
Sehested, J., Gelten, J.A.P., Remediakis, I.N., Bengaard, H., Nørskov, J.K., 2004. J. Catal. 223, 432.
Sehested, J., Gelten, J.P., Helveg, S., 2006. Appl. Catal. A 3009, 237.
Sehested, J., 2003. J. Catal. 217, 417.
Sehested, J., 2006. Catal. Today 111, 103.
Shaw, G., de Wet, H., Hohmann, H., 1994. Ammonia Plant Saf. 35, 315.
Shen, J., Venkataramanan, V., Gray, D., 2003. Fundamentals of gas to liquids. Petrol. Econ., 24.
Shen, W.J., Ichihashi, Y., Matsumura, Y., 2005. Appl. Catal. A: Gen. 282, 221–226.
Slack, A.V., James, G.R., 1973. Ammonia, Part 1. Marcel Decker, Inc., New York, p. 145.
Spencer, M.S., 1999. Top. Catal. 8, 259–266.
Stahl, H., Rostrup-Nielsen, J., Udengaard, N.R., 1985. In: Fuel Cell Seminar 1985. Tucson, Arizona. p. 83.
Sterling, M.B., Moon, A.J., 1974. Ammonia Plant Saf. 17, 135.
Tanaka, Y., Utaka, T., Kikuchi, R., Takeguchi, T., Sasaki, K., Eguchi, K., 2003. J. Catal. 215, 271–278.
Tanaka, Y., Takeguchi, T., Kikuchi, R., Eguchi, K., 2005. Appl. Catal. A: Gen. 279, 59–66.
Taskin, M., Dixon, A., Nijemeisland, M., Sitt, E., 2008. CFD study of the influence of catalyst particle design on steam reforming reaction heat effects in narrow packed tubes. Ind. Eng. Chem. Res..
Thomsen, S.G., Han, P.A., Loock, S., Ernst, W., 2006. The first industrial experience with the Haldor Topsøe exchange reformer. Ammonia Tech. Manual, 259–266.
Topsøe, H., et al., 1996. Hydrotreating Catalysis. Springer-Verlag, Berlin, Heidelberg.
Topsøe methanol technology. Paper Presented at the Bahrain Natural Gas Conversion Seminar, Bahrain, Jan. 2000.
Topsøe autothermal reforming technology and catalysts, Nitrogen+Syngas 305, May–June 2010.
Topsoe-SBA autothermal process. J. World Nitrogen May, 1962.
Torniainen, P.M., Chu, X., Schmidt, L.D., 1994. J. Catal. 146, 1.
Tsagaroyannis, J., et al., 1996. Mater. Lett. 28, 393–400.
Udengaard, N.R., Christiansen, L.J., Summers, W.A., 1988. Endurance Testing of a High-efficiency Steam Reformer for Fuel Cell Power Plants. EPRI AP-6071, Project 2192-1. Electric Power Research Institute, California.
U.S. Patent no. 6107353.
Van Natter, R.M., Coleman, J.S., Lund, C.R.F., 2008. J. Mol. Catal. A: Chem. 292, 76–82.
Vannby, R., Nielsen, C.S., Kim, J.S., 1993. Hydcar. Tech. Int..
Vannice, M.A., 1976. J. Catal. 44, 152.
Vannice, M.A., 1982. In: Andersen, J.R., Boudart, M. (Eds.), Catalysis, Science and Technology, vol. 3. Springer, Berlin, p. 139.
Velasco, J.A., Lopez, L., Velásquez, M., Boutonnet, M., Cabrera, S., Järås, S.-, 2010. Gas to liquids: a technology for natural gas industrialization in Bolivia. JNGSE 2, 222–228.
Wainwright, M.S., Trimm, D.L., 1995. Catal. Today 23, 29–42.
Waller, D., Stirling, D., Stone, F.S., Spencer, M.S., 1989. Faraday Discuss. Chem. Soc. 87, 107–120.
Wang, X., Gorte, R.J., Wagner, J.P., 2002. J. Catal. 212, 225–230.
Warnatz, J., Maas, U., Dibble, R.W., 1996. In: Glassman, I. (Ed.), Combustion, third ed. Springer-Verlag, Heidelberg Academic Press, San Diego.
Wei, K., et al., 2003. Chromium-free Fe-based catalyst for CO high-temperature-shift reaction and its preparation. US Patent 6.569.804.
Winter-Madsen, S., Dybkjær, I., 2003. Novel revamp solutions for increased hydrogen demands. Presented to ERTC, London, Nov. 17–19, 2003.
Winter-Madsen, S., 1998. Paper Presented at the International Symposium on Large Chemical Plants, vol. 10, Antwerp.
Winter-Madsen, S., Olsson, H., 2007. Steam reforming solutions. Hydrocarb. Eng. July, 37–40.
Wise, H., McCarty, J., Oudar, J., 1985. In: Wise, H., Oudar, J. (Eds.), Deactivation and Poisoning of Catalysts. Marcel Dekker, New York, p. 1 (Chapter 1).
Xu, G.F., Froment, 1989. AIChE J. 35, 88.
Yamaguchi, A., Iglesia, E., 2010. J. Catal. 274, 52.Wei, J., Iglesia, E., 2004. Angew. Chem. Int. Ed. 43, 3685.Wei, J., Iglesia, E., 2004. Phys. Chem. Chem. Phys. 6, 3754.Wei, J., Iglesia, E., 2004. J. Catal. 225, 116.Wei, J., Iglesia, E., 2004. J. Catal. 224, 370.Wei, J., Iglesia, E., 2004. J. Phys. Chem. B 108, 7253.Wei, J., Iglesia, E., 2004. J. Phys. Chem. B 108, 4094.
Zalc, J.M., Sokolovskii, V., Löffler, D.G., 2002. J. Catal. 206, 169–171.
Zeppieri, M., Villa, P.L., Verdone, N., Scarsella, M., De Filippis, P., 2010. Appl. Catal. A 387, 147.
Zhang, L., Wang, X., Millet, J.M.M., Matter, P.H., Ozkan, U.S., 2008. Appl. Catal. A: Gen. 351, 1–8.
Zhang, L., Millet, J.M.M., Ozkan, U.S., 2009. Appl. Catal. A: Gen. 357, 66–72.

Acronyms

AIT: Autoignition temperature
ATR: Autothermal reforming
CFD: Computational fluid dynamics
CMR: Ceramic membrane reforming
CPO: Catalytic partial oxididation
DFT: Density functional theory
DME: Dimethyl ether
FT: Fischer-Tropsch
GHHER: Gas heated heat exchange reforming
GHR: Gas heated reforming
GTL: Gas to liquid
HDS: Hydrodesulphurisation
HER: Heat exchange reformer
HREM: High resolution electron microscopy
HTCR: Haldor Topsøe convection reformer
HTER: Haldor Topsøe exchange reformer
HTFT: High-temperature Fischer Tropsch
HTS:: High-temperature shift
LTFT: Low-temperature Fischer Tropsch
LTS: Low-temperature shift
MTG: Methanol to gas
MTO: Methanol to olefins
MTS: Medium-temperature shift
OMR: Oxygen membrane reforming
PAH: Polyaromatic hydrocarbons
PDU: Process demonstration unit
PEM: Proton exchange membrane
POX: Partial oxidation
PSA: Pressure swing absorption
S/C: Steam to carbon
SGU: Syngas generation unit
SMR: Steam methane reforming
SN: Stoichiometric number
SPARG: Sulphur passivated reforming
STEM-EDX: Scanning transmission electron microscopy - energy-dispersive x-ray spectroscopy
TIGAS: Topsøe integrated gasoline synthesis
TOF: Turnover frequency
WGS:: Water gas shift
XAFS: X-ray absorption fine structure spectroscopy
XPS: X-ray photoelectron spectroscopy
XRD: X-ray diffraction